ISBN 978-82-326-3270-1 (printed version)
ISBN 978-82-326-3271-8 (electronic version)
ISSN 1503-8181

Doctoral Thesis
Marshed Kassim Mohamed

Doctoral theses at NTNU, 2018:240

Marshed Kassim Mohamed

Dynamic Channel Models for Wireless Body Area Networks

NTNU
Norwegian University of
Science and Technology
Faculty of Information Technology
and Electrical Engineering
Department of Electronic Systems

NTNU
Norwegian University of
Science and Technology

Doctoral theses at NTNU, 2018:240

NTNU

NTNU
Norwegian University of
Science and Technology

Marshed Kassim Mohamed

Dynamic Channel Models for Wireless Body Area Networks

Thesis for the degree of Philosophiae Doctor

Trondheim, April 2018

Norwegian University of Science and Technology
Faculty of Information Technology
and Electrical Engineering
Department of Electronic Systems

NTNU
Norwegian University of
Science and Technology

NTNU
Norwegian University of Science and Technology

Thesis for the degree of Philosophiae Doctor

Faculty of Information Technology
and Electrical Engineering
Department of Electronic Systems

ISBN 978-82-326-3270-1 (printed version)
ISBN 978-82-326-3271-8 (electronic version)
ISSN 1503-8181

Doctoral theses at NTNU, 2018:240

Printed by Skipnes Kommunikasjon as

To my mother and sisters

Abstract

The advancements in technology have made it possible to create a network of implant and wearable nodes around the human body known as wireless body area network (WBAN). These communication systems have potentially great applications in areas such as health monitoring, sports activities, and specialized occupations such as paramedics, fire-fighters, and military personals. However, networking of these wearable devices is a challenging task due to the complex propagation mechanisms of radio frequency (RF) signals in the vicinity of the human body. The movement of the body components causes time-varying shadowing and fading effects, and signal reflection/scattering from objects around the human body result in multipath fading effects. Reliable communication in such time-variant channel conditions can only be achieved with a greater understanding of the communication channel.

In this Ph.D. project, dynamic channel models for WBANs were developed with focus on on-body, off-body, and body-to-body communication scenarios. We started with physical channel modeling by utilizing a dynamic human walking model, which provides a detailed description of the movement of the different body parts, and the uniform theory of diffraction (UTD) to accurately calculate the time-varying shadowing and scattering effects due to the movements of the body parts. A physical model for the signal affected by moving human bodies in an indoor environment was developed. Further, standard statistical distribution was added to the model to represent the multipath fading effects by the scatterers around the human body, and a physical-statistical model for off-body wireless communications channels was obtained. Both the physical and the physical-statistical models were validated in terms of first- and second-order statistics utilizing measurement data and showed good agreements.

For body-to-body communications, a measurement campaign was conducted for different scenarios of running and cycling activities. Among others, the results indicated the presence of good and bad states with each state following a specific distribution for the considered propagation scenarios. The empirical channel model developed here was based on the two-state semi-Markov model. Further, a lognormal mixture shadowing model based on a cluster concept was utilized in the modeling of the first-order statistics of the channels. The mixture model addresses the inaccuracies observed using a single distribution that may not accurately represent the measurement data set. The accuracy of the proposed mixture model was compared to other commonly utilized single distributions showing significant improvement in representing the measurement results.

The application of propagation channel fingerprints to improve the security of WBANs was also investigated. More specifically, the usage of received signal strength indicator (RSSI) as a source of gait recognition was proposed. The RSSI approach does not require additional sensors (hardware) or sampling of them but uses the RSSI values already available on all radio devices. Radio channel features were extracted from the unique signature of the RSSI in relation to the corresponding subject. The extracted features were then used together with classification learners to evaluate the method in which an accuracy of up to 98% was achieved.

Lastly, the channel characteristics during walking for on-body, off-body, and body-to-body communication were investigated together in the same conditions so that a complete picture of the overall network could be observed and compared. The finite-difference time-domain (FDTD) was used as it could separate the channel gain into propagation loss and antenna gain, which cannot be achieved through measurement since the body is within the near field of the antenna. Correlation between the channels and the application of multivariate normal distributions in the modeling of WBAN channels was also investigated.

The developed channel models and the measurement results in this Ph.D. study can be used for accurate planning and deployment of WBANs in various applications. They can be used for simulating different capacity enhancing techniques, and for exploring new methods for the air interference, multiple access, and architectural approaches.

Preface

This thesis is submitted in partial fulfillment of the requirements for the degree of Philosophiae Doctor at the Faculty of Information Technology and Electrical Engineering of the Norwegian University of Science and Technology (NTNU), Norway. The doctoral thesis concludes my research work from April 2015 to April 2018.

The majority of the research work presented in this Ph.D. thesis has been conducted at NTNU Gjøvik. I have also been a visiting researcher at the Department of Information Technology of Ghent University in Belgium from June to October 2017. The Ph.D. research was supported by the Ministry of Education and Research, Norway.

The thesis consists of two parts. The first part provides an overview of the research field I have been working on during my Ph.D. studies as well as a brief summary of the contributions to the corresponding fields. The second part includes the research papers underpinning this thesis.

List of Included Publications

Paper I
M. Mohamed, M. Cheffena, F. Perez-Fontan, and A. Moldsvor, "A dynamic channel model for indoor wireless signals: Working around interference caused by moving human bodies," *IEEE Antennas and Propagation Magazine,* vol. 60, no. 2, pp. 82-91, 2018.

Paper II
M. Mohamed, M. Cheffena, A. Moldsvor, and F. P. Fontan, "Physical-statistical channel model for off-body area network," *IEEE Antennas and Wireless Propagation Letters,* vol. 16, pp. 1516-1519, 2017.

Paper III
M. Mohamed, M. Cheffena, and A. Moldsvor, "Characterization of the body-to-body propagation channel for subjects during sports activities," *Sensors,* vol. 18, no. 2, p. 620, 2018.

Paper IV
M. Cheffena and M. Mohamed, ""The application of lognormal mixture shadowing model for B2B channels," *IEEE Sensors Letters,* vol. 2, no. 3, pp. 1-4, 2018.

Paper V
M. Mohamed and M. Cheffena, "Received signal strength based gait authentication," *IEEE Sensors Journal,* vol. 18, no. 16, pp. 6727-6734, 2018.

Paper VI
M. Mohamed, W. Joseph, G. Vermeeren, E. Tanghe, and M. Cheffena, "Characterization of dynamic wireless body area network channels during walking," *Submitted to EURASIP Journal on Wireless Communications and Networking,* 2018.

Acknowledgments

Many thanks to Professor Michael Cheffena of NTNU, who followed my studies at every step and pointed me in the right directions. I would also like to thank Associate Professor Arild Moldsvor of NTNU, and Professor Fernando Pérez Fontán of University of Vigo, for being available for assistance whenever I needed them.

Thanks to the lovely people of IVB department of NTNU, who made me feel at home, and to everyone at WAVES research group of Ghent University, who made my stay in Ghent a real pleasure. This work has been funded by the Ministry of Education and Research, Norway, which is gratefully acknowledged.

Marshed Mohamed
April 2018, Gjøvik

Contents

List of Figures

List of Abbreviations

AAL	Ambient assisted living
ACF	Auto-correlation function
AFD	Average fade duration
BLE	Bluetooth Low Energy
CA	Collision avoidance
CDF	Cumulative distribution function
CSI	Channel state information
CSMA	Carrier sense multiple access
EM	Expectation maximization algorithm
FDTD	Finite-difference time-domain
ISM	Industrial Scientific and Medical
LCR	Level crossing rate
LOS	Line-of-sight
MICS	Medical Implant Communication Service
MLE	Maximum likelihood estimate
NLOS	Non-line-of-sight
PDF	Probability density function

PSD Power spectral density

RMSE Root mean square error

RSSI Received signal strength indicator

STD Standard deviation

TNR True negative rate

TPR True positive rate

TSSMM Two-state semi-Markov model

UTD Uniform theory of diffraction

VNA Vector network analyzer

WBAN Wireless body area network

WMTS Wireless Medical Telemetry Services

Part I

Overview of Research Field

Chapter 1

Introduction

1.1 Background

The advancements in the miniaturization of hardware, signal processing techniques, software and biomedical engineering have made it possible to create a network of implant and wearable nodes around the human body known as wireless body area network (WBAN) [1]. These communication systems have potentially great applications in areas involving monitoring and transmission of human physiological data such as health monitoring, sports activities, as well as important data for specialized occupations such as paramedics, fire-fighters, and military personals [2]. For example, health monitoring may involve the on-body nodes in real-time monitoring of heart activities, blood pressure, breathing rate etc., or biomedical implant devises to fine-tune medical treatments (e.g., an artificial pancreas which regulates the dose of insulin for diabetic patients) over an extended period of time [3]. Other applications include data file transfer, video/audio streaming for specialized occupations, training aids for sports persons, gaming, and social networking applications (e.g., automatic exchange of digital profile or business card) [4]. The placement of the nodes varies considerably from one application to the other depending on the information to be transferred or the physiological attributes being monitored.

The WBANs have considerable challenges. They require a low-power communication approach due to their need for long battery life and the proximity of body surface nodes to human tissue [6]. In addition to this challenge, the networks are subjected to varying signal shadowing caused by relative human body orientation between the communicating nodes which vary with human body movement. In addition to the shadowing of the signal by moving body components, signal re-

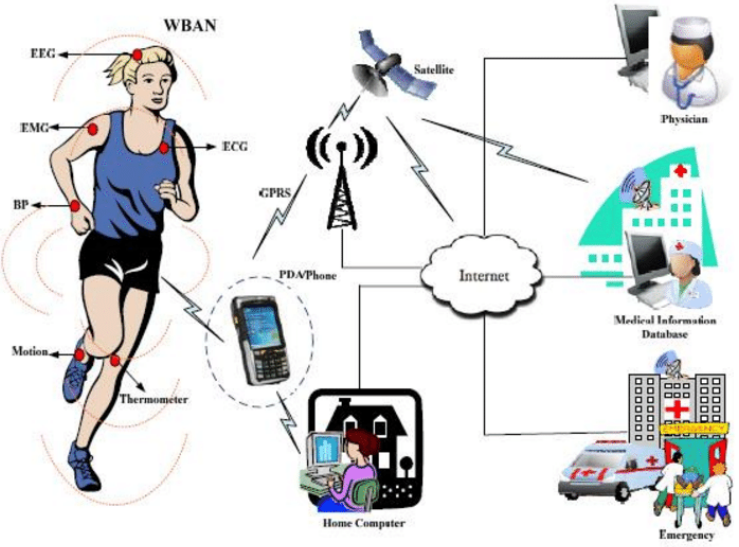

Figure 1.1: WBAN architecture of medical applications [5].

flection/scattering from objects around the human body result in multipath fading effects [7]. The body itself also affects the antenna performance by altering the radiation pattern and polarization [8], and the angular variations of the antenna gains during motion give rise to time-varying channel conditions [9].

Understanding the radio channel is a fundamental requirement for designing robust and reliable WBANs. Channel models can then be used for simulating different capacity enhancing techniques such as adaptive coding and modulation, and for exploring new methods for the air interface, multiple access, and architectural approaches that include cooperation and interference mitigation techniques.

1.2 The Scope of Thesis

The main objective of this Ph.D. work is to develop dynamic channel models for WBANs with focus on on-body, off-body, and body-to-body wireless communications. Three different approaches were utilized in the modeling of the WBANs channels.

- **Physical modeling:** This kind of modeling gives a deeper understanding of the channel characteristics. However, to achieve good accuracy with this approach, one needs a good approximation of the shapes of the obstacles, and their position in the propagation environment. In complex propagation

environments with a large number of obstacles, the method requires large computation time and resources, and hence it is limited to simple propagation scenarios.

- **Physical-statistical modeling:** This kind of modeling enables the physical models to be applied in more complex propagation environments. It combines the physical model with a statistical approximation to form a channel model which can be applied in various environments by adjusting the appropriate parameters. For example, the channel contribution from the main obstacle (the human body) could be modeled physically, while the contributions from the environment could be modeled using standard distributions (Rayleigh, Ricean, etc.) leading to a physical-statistical channel model.
- **Empirical modeling:** This kind of modeling is based on measurements. The model is derived by observing the results of the measurements conducted for a specific scenario. The load of such modeling process lies on the necessary measurement campaign, however, the resulting models are normally simple and straightforward to use in similar links under similar constraints. In addition to the model, the measurement results also provide practical channel statistics which could be used independently.

In addition to that, the developed channel models, and the measurement results were used in the following applications

- **Comparison analysis with existing models:** Comparison between models developed in this Ph.D., and models currently used in similar propagation environments were done in terms of first- and second-order statistics.
- **System performance analysis:** Channel capacity and outage probabilities of different body-to-body radio channels were compared.
- **Propagation channel fingerprinting for subject identification:** The channel characteristics observed in the measurement results were used for gait authentication method. The method does not require additional hardware or sampling of sensor data making it more energy efficient compared to the popular accelerometer based gait recognition systems.

The remaining part of this thesis is organized as follows: **Chapter 2** describes the type of WBANs considered in this Ph.D. study, **Chapter 3** focuses on the propagation channel modeling of on-body, off-body, and body-to-body channels, **Chapter 4** focuses on the application of propagation channel fingerprinting in subject identification, and **Chapter 5** concludes the thesis with a short presentation of the included papers, and future works.

Chapter 2

Wireless Body Area Network

2.1 Introduction

Wireless body area network is the interconnection of multiple intelligent, low-power, micro and nano-technology sensors and actuators, which can be placed in, on, or around the surface of the body, and are capable of wireless communication. These nodes allow simple and unobtrusive measurements of physiological parameters of a subject, or other data of the surrounding environment, and transmit the data to the remote server if needed [10]. The nodes which are located inside the body are normally called implants, and those located outside the body as wearables [11]. This research was limited to WBANs which do not involve implants.

WBANs applications span in a wide area, and they can be categorized into medical and non-medical applications [1]. The ability of WBANs nodes to continuously monitor physiological attributes such as blood pressure, heartbeat and body temperature, is the key solution in various medical application. The applications can range from early diagnosis, monitoring to the treatment of patients with diseases such as diabetes, hypertension and cardiovascular-related diseases. Further, the accompanying sensors could be set to monitor the environment for health-affecting substances such as harmful gases and smoke for specialized professionals such as firefighters, or allergic agents for patients suffering from asthma [10]. In the ambient assisted living (AAL), continuous and often real-time monitoring of the living environment, and the human body, enables people with disabilities and elderly to maintain a more independent lifestyle. It facilitates assistance which is triggered by events, and user-specific support within the home environment [12, 13]. In sports training, the monitoring can be extended to capture motion, which enables the athletes to fine-tune their technique and hence improve their performance. The

monitoring could also be used in rehabilitation and injury prevention to the athletes.

In addition to medical applications, WBANs have a great potential in the entertainment area. It can enable avid video game players to have a total immersion, and make the gaming experience more natural. Instead of traditional interfaces such as joysticks, keyboards, and mice, video games could be controlled with a hand gesture, and body motion [14]. WBANs also find its use in mobile real-time audio/video streaming. Audio/Video streaming is used in team sports such as cycling, search and rescue in army and emergency personnel, tour guidance in museum and many other areas. WBANs has also found application in the area of secure authentication. They can be used in providing both physiological and behavioral biometrics of the human body in a noninvasive way and without the subject intervention [15].

2.2 Communication Architecture

The independent devices with communication capabilities present in a WBAN are known as nodes. The nodes can be classified into three different groups based on their role in the network [16].

- **Coordinator:** The coordinator node is in charge of collecting information from sensors and actuators, and acts as body gateway to the outside world, or another WBAN.

- **End Nodes:** The end nodes are the sensors and actuators, limited to performing their embedded application. They are neither capable of performing the duties of coordinator nor relay messages from one node to another.

- **Relay:** Relay nodes are capable of relaying messages from one node to the other. The relay nodes are necessary when the distance between the coordinator and the end node is too large for reliable communication. They can be sensors or actuators, at critical locations with capabilities of acting as a relay for those nodes in extreme locations.

These nodes operate in either a one-hop or two-hop star topology with the node in the center of the star as the coordinator [17]. The use of multi-hop assists in reducing the concentration of the transmission power from the source to its destination which is important considering the proximity of the nodes to the human tissue. The coordinator could control the communication by transmitting periodic beacons enabling device synchronization. In asynchronous WBANs a node in the

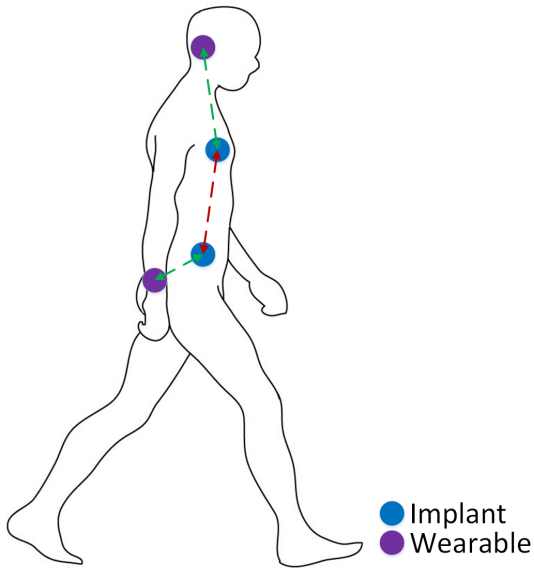

Figure 2.1: WBANs implants communication channels.

network is capable of sending data to the coordinator using carrier sense multiple access with collision avoidance (CSMA/CA) when required [18].

The communication channels of WBANs can be divided into two categories, those which involve implants, and those which do not. Implant communication channels are shown in Figure 2.1. They can either be implant-to-implant or implant-to-wearable radio channels. These channels were not the focus of this Ph.D. project. As for those which do not involve implants, the communication architecture can be separated into three communication channels as shown in Figure 2.2.

- **On-body communication:** The communication between the end nodes, relays and the coordinator present on the body, is known as on-body communication see Figure 2.2(a).
- **Off-body communication:** The communication between the coordinator present on the body, and the access point present away from the body is known as off-body communication see Figure 2.2(b).
- **Body-to-body communication:** The communication between two coordinators of different WBANs present on different bodies is known as body-to-body communication see Figure 2.2(c).

These channels were the focus of this Ph.D. project, and hence in the rest of this

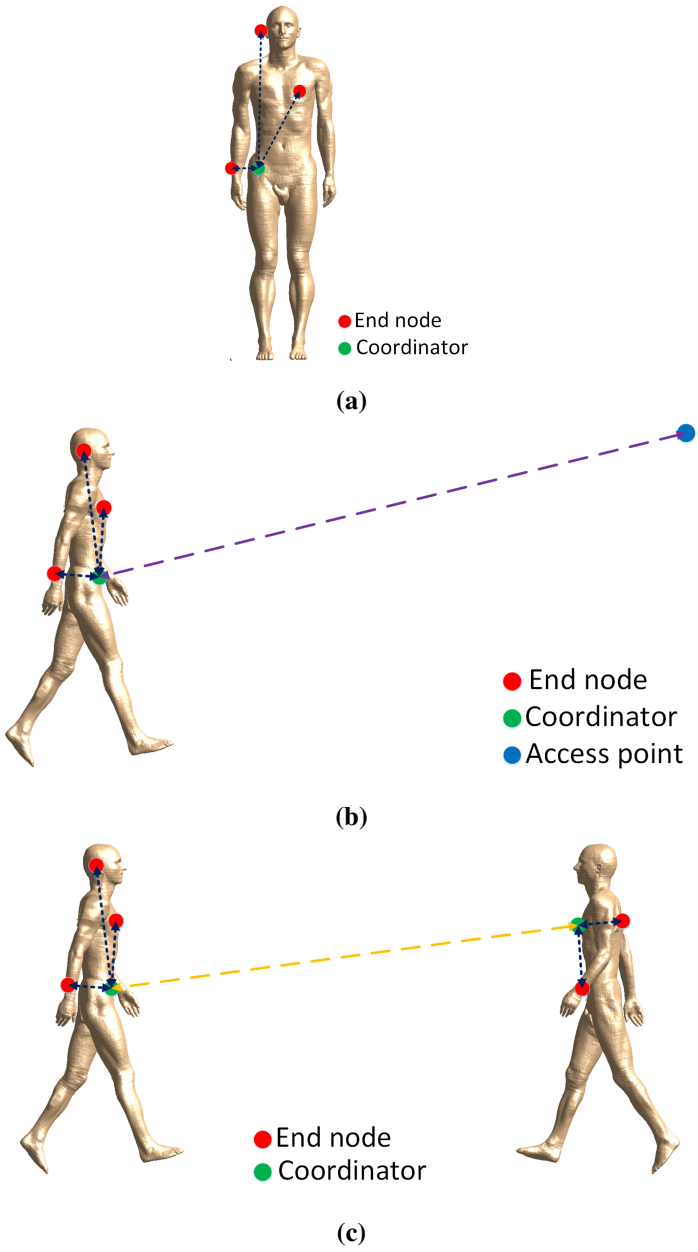

Figure 2.2: The communication architecture of WBANs. (a) On-body communication. (b) Off-body communication. (c) Body-to-body communication.

Table 2.1: Frequency Bands and Bandwidths for WBANs.

Frequency Range	Bandwidth	Standard	Communications
16 MHz	4 MHz	-	Human-Body
27 MHz	4 MHz	-	Human-Body
402–405 MHz	300 KHz	MICS	Narrowband
420–450 MHz	300 KHz	WMTS	Narrowband
863–870 MHz	400 KHz	-	Narrowband
902–928 MHz	500 KHz	-	Narrowband
950–956 MHz	400 KHz	-	Narrowband
2360–2400 MHz	1 MHz	-	Narrowband
2400–2483.5 MHz	1 MHz	ISM	Narrowband
3.2–4.7 GHz	499 MHz	-	Ultra-wideband
6.2–10.2 GHz	499 MHz	-	Ultra-wideband

thesis, WBAN refers to on-body, off-body, and body-to-body communications.

Three propagation methods were proposed in WBAN standard [4].

- **Narrowband communications:** This is the propagation method which is better suited to a greater number of applications. Its lower carrier frequencies suffer less attenuation from the human body, and its smaller bandwidth (1 MHz or less) reduces inter-symbol-interference caused by multipath [10].
- **Ultra-wideband communications:** This propagation method offers higher throughput due to its larger bandwidth (499 MHz) and it could be used when extremely high data are required in the application [14].
- **Human-body communications:** This propagation method is through galvanic coupling of signals over the surface of the human body, and transmission is over the medium of human skin by an electrode, rather than by an antenna [19].

This Ph.D. thesis focuses on narrowband communications due to its greater number of suitable applications. The available frequency bands for WBANs are given in Table 2.1. Medical Implant Communication Service (MICS) and Wireless Medical Telemetry Services (WMTS) bands are licensed bands used for implants communication and medical telemetry system respectively. MICS frequency band (402–405 MHz) lead to better penetration through the human tissue compared to higher frequency bands, and high-level integration which is difficult at lower frequencies [2]. Another popular band is the Industrial, Scientific and Medical

(ISM) band which can support high data rate applications, however, there are high chances of interference since it is an unlicensed band, and hence many wireless devices operate in this band. To tackle interference a band close to the ISM band (2360–2400 MHz) was assigned to medical device use [10]. In this Ph.D. project, all measurement were conducted in these two band (ISM and 2360–2400 MHz) due to popularity and the size of devices operating at these frequencies. The choice was also influenced by the availability of radio technologies which meet the WBAN requirements such as Bluetooth Low Energy (BLE), ZigBee, and ANT, already available at these frequencies [20].

2.3 Communication Challenges

Radio wave propagation in WBANs is significantly affected by human body tissue and frequency of transmission. Even in the line-of-sight (LOS), the on-body communication channels were found to have the path-loss exponent between 3 and 4, depending on the position of the device [16]. This is quite large compared to the path-loss exponent value of 2 normally observed in free space propagation. In non-line-of-sight (NLOS), the penetration through the body is negligible and instead the signal is diffracted around the body. This brings the diffraction losses, raising the path-loss exponent in the range of 5 to 6. In addition to that, fading due to multipath is more noticeable [21]. Additional losses occur due to the proximity of the antennas to the body. A difference of more than 20 dB was found between an antenna placed at 5 and 50 mm from the body [22], with the former expected in most of the aforementioned applications.

In addition to power losses, the WBANs channel is regularly changing due to movement of the body parts. Take for example an on-body channel between a coordinator placed on the chest and an end node placed at the arm wrist, the periodic movement of the arm back and forth while walking changes the channel periodically from LOS to NLOS. Similar effects can be found in off-body and body-to-body channels in which a body limb between the transmitter and receiver was found to cause shadowing of up to 20 dB [23]. When the body parts do not bring periodic shadowing to the channel, they act as moving reflectors which could contribute to fast fading effects, in which the multipath components reflected from different body parts sum-up in phase or out of phase at the receiver. The movements of body parts may also have an impact on the antenna as they may lead to a periodic change of the direction of maximum radiation [8]. The dynamic nature of WBANs communication channels is also contributed by the movement of the whole body from one location to the other, resulting in a change in environmental factors. A WBAN of a regular subject, on a regular day easily move from indoor environment (home, office, etc.), to outdoor environment (walking, jogging, etc.)

as the subject goes through his daily activities. These environments bring different challenges, to the performance of WBANs.

In addition to all those challenges, WBANs have power constraints due to their need for long battery life, and proximity of body surface nodes to human tissue. This makes the study and modeling of WBAN channel characteristics even more important [24]. There is a need to find simple and reliable models for prediction of WBAN channel properties in order to facilitate the design of robust and reliable WBANs. Channel models can then be used for simulating different capacity enhancing techniques such as adaptive coding and modulation, and for exploring new methods for the air interference, multiple access, and architectural approaches that include cooperation and interference mitigation techniques.

Chapter 3

Propagation Channel Modeling

For the design, simulation, and planning of WBAN systems, propagation channel models are needed. Propagation channel properties influence the development of communication systems including the WBANs. For system design, channel properties are required for the selection of suitable air interface such as center frequency, bandwidth, modulation method, and the multiple access scheme. The comparison and assessment of different solutions are possible by the use of propagation channel models. The models reflect the important properties of the propagation channels, that have an impact on system performance. Further, channel models provide valuable inputs for optimization of network parameters [25].

Different channels encounter different propagation mechanism, and the overall effect is what differentiates one channel from the other. When propagation takes place close to obstacles like the human body in an indoor environment, different propagation mechanisms occur. There is reflection, diffraction, and scattering from the human body as well as objects in the surrounding environment. This is in addition to the free space propagation between the two communicating terminals. This means that in this scenario the transmitted signal can reach the receiver via different paths, known simply as multipath propagation [26]. In addition to that, these multiple paths do not remain constant as the human body parts move. As the receiver adds up different multipath components, they form constructive and destructive interference, resulting in rapid changes in signal strength over a small movement of body parts called small-scale fading. Furthermore, body parts can block one or several multipath components, and any wave going around the body part is greatly attenuated, this effect is known as shadowing, and it gives rise to gradual fading known as large-scale fading. On top of all that there is path-loss which is the losses related to the separation distance between the transmitter and

the receiver [27].

The main purpose of propagation channel modeling is to have a model which can produce the aforementioned propagation properties involved in a channel so that they can be used in the simulation of the system in hand. The model could be a mathematical formulation such as path-loss models, or statistical characterization such as probability density function (PDF). For the dynamic channels in hand (WBAN), it is the second order statistics which are of more considerable importance as they provide information on the dynamic propagation characteristics of the channel. As mentioned in Section 1.2, propagation channel modeling may be classified into three main categories; physical, physical-statistical, and empirical. Physical modeling requires a detailed description of the propagation environment to achieve a precise modeling of the power attenuation at a specific location and time [26]. For dynamic channels, the power attenuation has to be recalculated at every sampling instance to obtain the channels' multipath effects. This limits the approach to simple scenarios, despite the fact that it is more accurate and gives a deeper understanding of the channel in hand. For more complex scenarios some of the burdens of physical calculations can be put on statistical approximation instead. This method is known as the physical-statistical modeling, which is more effective for simulating large scenarios while retaining some of the positive traits of the physical modeling. Empirical modeling, on the other hand, is achieved by foreseeing the propagation characteristics based on a given set of measurements. Thus, making them more suitable for complex environments and applications, but are applicable only to propagation scenarios with similar characteristics [14]. In this Ph.D. project, all three methods were used to achieve propagation channel models for various WBAN propagation scenarios.

3.1 Physical Channel Modeling

Physical channel modeling is a process of characterizing a channel, using electromagnetic wave propagation concepts. It takes into account the propagation in the considered media, together with reflections, transmissions, refraction, diffraction, and scattering produced by the objects present in the considered channel. This approach makes it easier to understand the role of each factor in the channel behavior, and hence a deeper understanding of the channel [25]. For the case of WBANs, the physical channel modeling process depends on two important factors.

- **The moving bodies:** Since the WBAN channels are in the vicinity of the moving bodies, modeling of the channels depends on the modeling of the bodies. A good approximation of the shape, movement, and electromagnetic properties of the bodies are needed for a more accurate channel model.

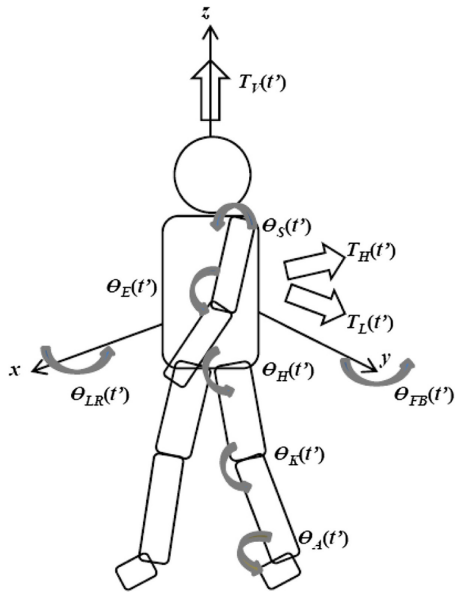

Figure 3.1: The Thalmann human model with translations and rotations [28].

- **The appropriate electromagnetic theory:** Considering the objects present in the channel, the appropriate electromagnetic theory has to be selected for calculating the dynamic total received signal. The choice will also depend on the accuracy needed and the complexity involved when such a theory is used in such a channel.

The discussion on the choice of the human model, as well as the electromagnetic theory used in relation to physical modeling of the WBAN channels in this thesis is considered in the following.

3.1.1 The Human Walking Model

There have been various physical channel models which include the effect of movement of a human body [29, 30]. The human in these studies was modeled as a metallic circular cylinder as proposed in [31]. However, the model proposed in [31] could be an oversimplification of shape and movement. This is precisely the case for WBANs, in which the human body is the centerpiece of the channel. The importance of more sophisticated human model could also apply to millimeter waves in which attenuation due to shadowing is so large that reflection from various body parts become significant. There is a need for a detailed information on the movement of the human body parts in characterizing the time-varying WBAN channels. Such description of the human gait has been studied extensively in the

Table 3.1: Human Body Parts Translations and Rotations Description.

Parameter	Symbol
Lateral translation	$T_L(t')$
Horizontal translation	$T_H(t')$
Vertical translation	$T_V(t')$
Forward/backward angle	$\theta_{FB}(t')$
Left/right angle	$\theta_{LR}(t')$
Shoulder angle	$\theta_S(t')$
Elbow angle	$\theta_S(t')$
Hip angle	$\theta_S(t')$
Knee angle	$\theta_S(t')$
Ankle angle	$\theta_S(t')$

biomechanics and robotics [32, 33], and has lead to one of the commonly used model known as the Thalmann walking model [28, 34, 35].

In the Thalmann walking model, the human body is comprised of 12 body parts in which 11 of them (legs, arms, trunk, etc.) are represented by cylinders of various size, and the head by a sphere as shown in Figure 3.1. These body parts are connected to each other by translation and rotation (see Table 3.1 for description) which are time-dependent. In the model, the movement of the body parts are expressed in terms of relative velocity v_r of walking, and relative time t' given by

$$v_r = \frac{v}{H_{th}} \tag{3.1}$$

and

$$t' = \left| \frac{t}{T} \right|_{\text{mod 1}} \tag{3.2}$$

where v is the velocity of walking, H_{th} is the height of the thigh, t is the time and T is the period of walking cycle.

For modeling the trajectories of flexing of the knee, hip, and elbow, cubic spline passing through control points located at the extremities of the trajectories are used. These control points define the angle of rotations and relative time and are a function of relative velocity. The cubic spline used is a basic Hermit spline given by

$$h = -2s^3 + 3s^2 \tag{3.3}$$

where s is the increased portion of the relative time. The trajectories of flexing of the shoulder are found by using

$$\theta_s(t') = -3 - 9.88v_r(0.5 + \cos(2\pi t')) \tag{3.4}$$

Figure 3.2(a) shows angular variations of the knee, hip, and elbow for the left side of the body during one walking cycle with a relative velocity of unity obtained using the cubic spline passing through control points. Similarly, angular variation of the left shoulder obtained using (3.4) are shown in Figure 3.2(b). The trajectories of the right part of the body are obtained by performing phase displacement of half a cycle given by

$$t'_r = \left| \frac{t}{T} + 0.5 \right|_{mod1} \tag{3.5}$$

These angular variations together with human dimensions can be used to estimate the exact location of each body part during walking.

3.1.2 The Finite-Difference Time-Domain

Finite-difference time-domain (FDTD) is a numerical analysis technique used in finding approximate solutions of electromagnetic wave interactions with material structures. The FDTD method employs finite difference as approximations to both the spatial and temporal derivatives that appear in Maxwell's equations [36]. Consider a simple one-dimensional propagation in free space, with a plane wave traveling in the z-direction represented by

$$\frac{\partial E_x}{\partial t} = -\frac{1}{\varepsilon_0}\frac{\partial H_y}{\partial z} \tag{3.6}$$

$$\frac{\partial H_y}{\partial t} = -\frac{1}{\mu_0}\frac{\partial E_x}{\partial z} \tag{3.7}$$

The finite difference approximation of 3.6 and 3.7 are

$$\frac{E_x^{n+1/2}(k)E_x^{n-1/2}(k)}{\Delta t} = -\frac{1}{\varepsilon_0}\frac{H_y^n(k+1/2) - H_y^n(k-1/2)}{\Delta z} \tag{3.8}$$

$$\frac{H_y^{n+1}(k+1/2) - H_y^n(k+1/2)}{\Delta t} = -\frac{1}{\mu_0}\frac{E_x^{n+1/2}(k+1) - E_x^{n+1/2}(k)}{\Delta z} \tag{3.9}$$

where n is the sample number in discrete time, and k is a sample number in discrete space. The accuracy of the method depends on the time and spatial resolution Δt and Δz respectively. The rule of thumb is to have

$$\Delta z \leq \frac{\lambda}{10} \tag{3.10}$$

and

$$\Delta t \leq \frac{\Delta z}{c_0} \tag{3.11}$$

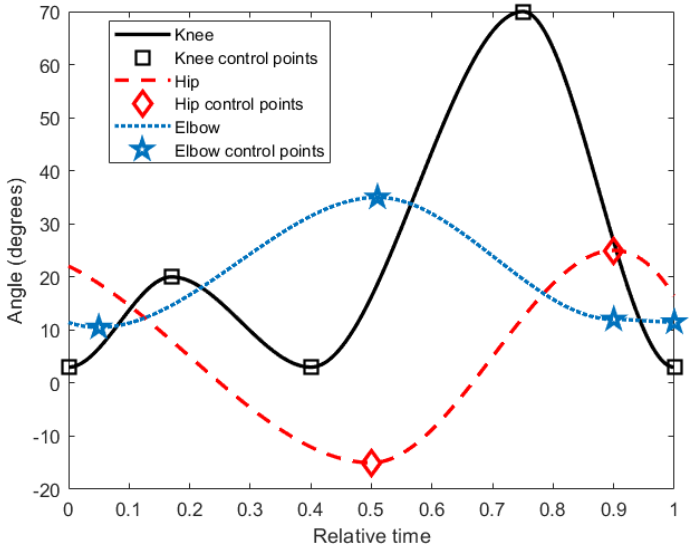

(a)

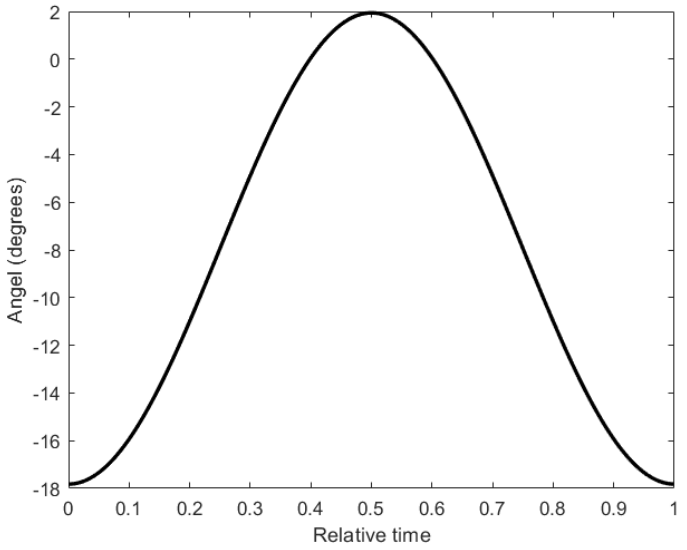

(b)

Figure 3.2: Angular rotations of body joints with $v_r = 1$. (a) knee, hip, and elbow obtained using cubic spline passing through control points. (b) Shoulder obtained using (3.4).

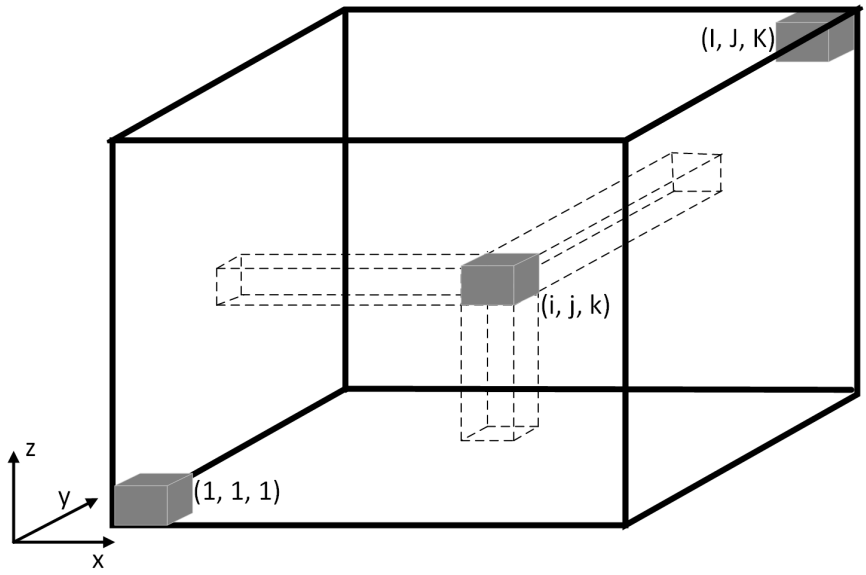

Figure 3.3: A three-dimensional FDTD computational space composed of $(I \times J \times K)$ cells.

where λ is the wavelength and c_0 is the speed of light in free space [37]. The approach can be extended to three-dimensional propagation through various kinds of medium, in which the number of equations to be approximated by finite difference is tripled, and the propagation environment is divided into cubic cells of Δz^3 dimension. Figure 3.3 illustrates an FDTD grid composed of $(I \times J \times K)$ cells. As the dimensions of the propagation environment increase so does the number of cells needed and hence the computation time and the amount of memory used becomes very large [36]. This confines the realistic application of FDTD to the environments with volumes of a few cubic meters. However, its alluring factor towards WBANs is the fact that heterogeneous phantom with different tissues having different dielectric properties, can be naturally and easily modeled. FDTD was used together with Thalmann walking model in Paper VI in which the channel gains were separated into propagation and antenna gain, for on-body, off-body, and body-to-body channels during walking. This could not be achieved through measurements since the body is within the near field of the antenna. Further, the study investigated the correlation between the channels and the application of multivariate normal distributions in the modeling of WBANs channels.

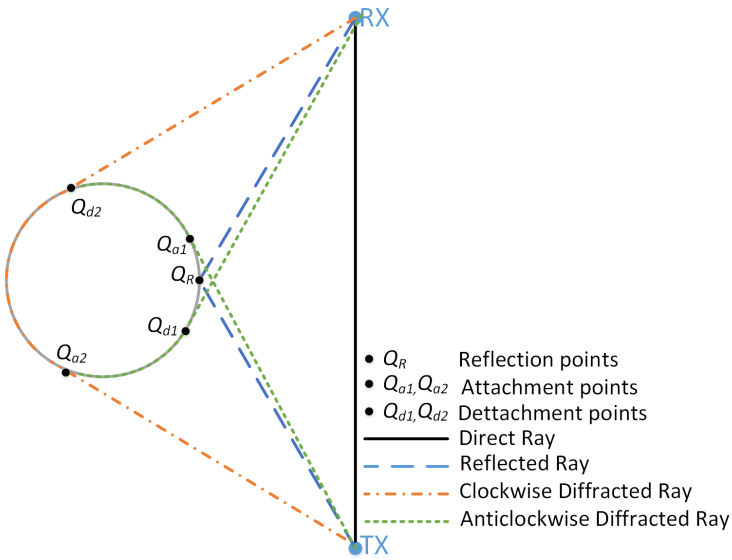

Figure 3.4: Ray tracing on a cylinder with both the transmitter and receiver away from the cylinder.

3.1.3 The Uniform Theory of Diffraction

The Thalmann model describes the human body parts in terms of cylinders and spheres. The propagation mechanisms on these kinds of shapes (canonical shapes) are different from those of plain surface. To be able to account for the reflected and diffracted waves in canonical shapes, we need to use the uniform theory of diffraction (UTD). UTD can account for the phenomenon of creeping waves which can not be predicted with geometrical optics, and Kirchhoff diffraction equation [38, 39]. In addition to that, it can also solve the radiation problem when a source is mounted on the body, or coupling problem when both the transmitter and receiver are on the same body part.

Figure 3.4 shows a typical application of UTD with both the transmitter and the receiver away from the cylinder. It shows three types of rays namely the direct ray, a reflected ray, and two diffracted rays, one going in clockwise and the other in anticlockwise direction. In this setup, the receiver is considered to be in the lit region since there is LOS between the transmitter and receiver. When the cylinder is blocking the LOS, only the diffracted rays remain and the receiver is considered to be in the shadow region. The direct field can be expressed as

$$E_i(Rx) = C_0 \frac{e^{-jks_0}}{s_0} \tag{3.12}$$

where s_0 is the distance between the point of transmission and the point of observation, and C_0 is a constant associated with incident field power [38]. The reflected field can be expressed as

$$E_r(Rx) = \sqrt{\frac{\rho_1^r.\rho_2^r}{(\rho_1^r + s_r)(\rho_2^r + s_r)}} R_{\parallel\perp}.E_i(Q_r).e^{-jks_r} \tag{3.13}$$

where s_r is the distance between the reflection point and the receiver, ρ_1^r and ρ_2^r are the radius of curvature of the reflected field, which can be expressed as [38]

$$\rho_1^r = \left[\frac{1}{s_i^r} + \frac{2(\sin\theta_0)^2}{a\cos\theta_i}\right]^{-1} \tag{3.14}$$

$$\rho_2^r = s_i^r \tag{3.15}$$

Here s_i^r is the distance between the transmitter and the point of reflection, θ_0 is the angle between the axis of the cylinder and the reflected field, a is the radius of the cylinder and θ_i is the angle of incident. The polarization dependent reflection coefficient $R_{\parallel\perp}$ in 3.13 is given by [40]

$$R_{\parallel\perp} = -\sqrt{\frac{-4}{\xi_l}}.e^{-j(\xi_l)^3/12}.\left[\frac{e^{-j\pi/4}}{2\xi_l\sqrt{\pi}}\left[1 - F(X_L)\right] + \widehat{P}_{\parallel\perp}(\xi_l)\right] \tag{3.16}$$

where ξ_l is the Fock parameter associated with the reflected field in the lit region, $F(X_L)$ is a UTD special function, and $\widehat{P}_{\parallel\perp}(\xi_L)$ is the Pekeris function used to describe the phenomenon of creeping waves. Typical values calculated with a cylinder of radius $a = 20$ cm and relative permittivity of human muscle at 2.45 GHz frequency are shown in Figure 3.5. The diffracted field can be expressed as

$$E_d(Rx) = \sqrt{\frac{\rho_2^d}{s_d(\rho_2^d + s_d)}}.D_{\parallel\perp}.\sqrt{\frac{d\eta(Q_{an})}{d\eta(Q_{dn})}}.E_i(Q_{an}).e^{-jks_d} \tag{3.17}$$

where ρ_2^d is the second radius of curvature of the diffracted field, which is expressed as

$$\rho_2^d = s_i + d \tag{3.18}$$

Here s_i is the distance between the transmitter and the attachment point, d is the distance along the curved surface between attachment and detachment points, s_d is the distance between the detachment point and the receiver, Q_{an} and Q_{dn} are the attachment and the detachment points. The polarization dependent diffraction coefficient $D_{\parallel\perp}$ of 3.17 is expressed as [40]

$$D_{\parallel\perp} = -m\sqrt{\frac{2}{k}}.e^{-jkd}.\left[\frac{e^{-j\pi/4}}{2\xi_d\sqrt{\pi}}\left[1 - F(X_d)\right] + \widehat{P}_{\parallel\perp}(\xi_d)\right] \tag{3.19}$$

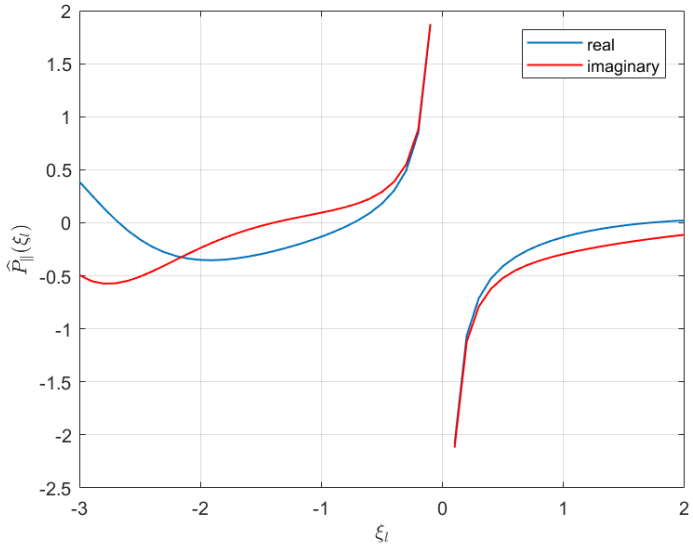

(a)

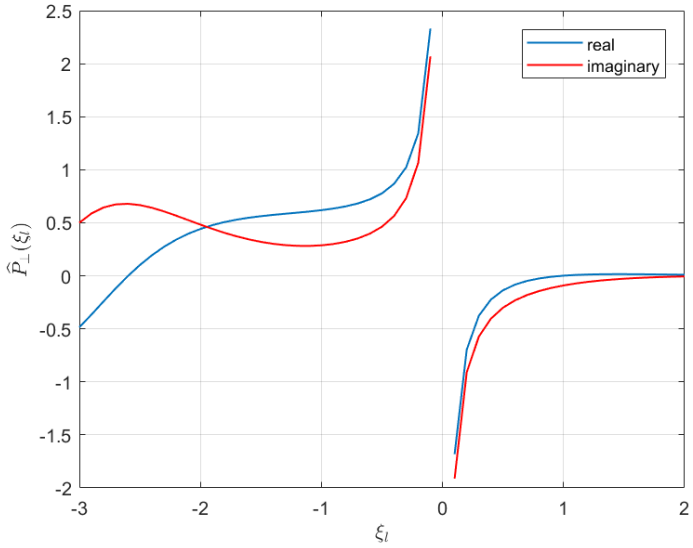

(b)

Figure 3.5: Plot of the Pekeris function with a cylinder of radius 20 cm, and permittivity of human tissue at 2.45 GHz. (a) Parallel polarization. (b) Perpendicular polarization

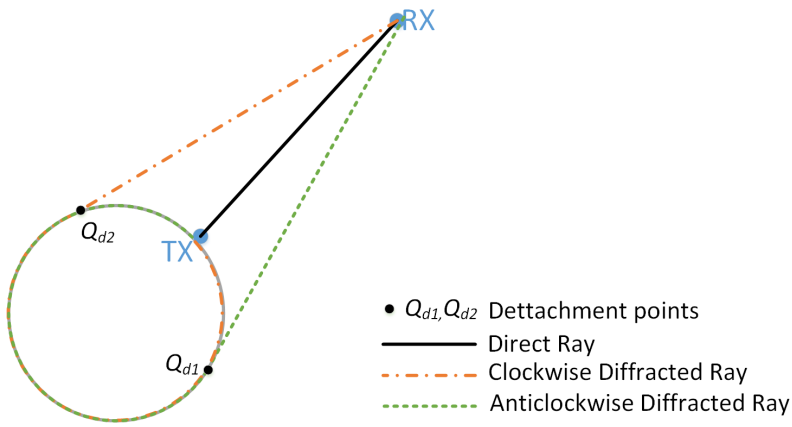

Figure 3.6: Ray tracing on a cylinder with the transmitter on the cylinder while the receiver is away from the cylinder.

where ξ_d is the Fock parameter associated with diffracted rays, m is the curvature parameter depending on the radius of the cylinder, and k is the wave number. The conservation of energy flux in the surface ray strip from attachment to detachment point $\sqrt{d\eta(Q_{an})/d\eta(Q_{dn})}$ of 3.17 can be expressed as [38]

$$\sqrt{\frac{d\eta(Q_{an})}{d\eta(Q_{dn})}} = \sqrt{\frac{s_i}{s_i + d}} \tag{3.20}$$

When the transmitter is mounted on the cylindrical surface itself, with observation point off the surface (e.g., off-body communication) as shown in Figure 3.6, the radiation principles of UTD can be used instead. Here the direct field can be expressed as

$$E_i(Rx) = C_0.H_{\parallel\perp}\frac{e^{-jks_0}}{s_0} \tag{3.21}$$

and the diffracted field can be expressed as

$$E_d(Rx) = C_0.H_{\parallel\perp}.e^{-jkd}\frac{e^{-jks_d}}{s_d} \tag{3.22}$$

where $H_{\parallel\perp}$ is the polarization dependent radiation function expresses as

$$H_{\parallel} = \begin{cases} G_{\parallel}(\xi).e^{-j(\xi)^3/3}, & \xi \leq 0 \\ G_{\parallel}(\xi), & \xi \geq 0 \end{cases} \tag{3.23}$$

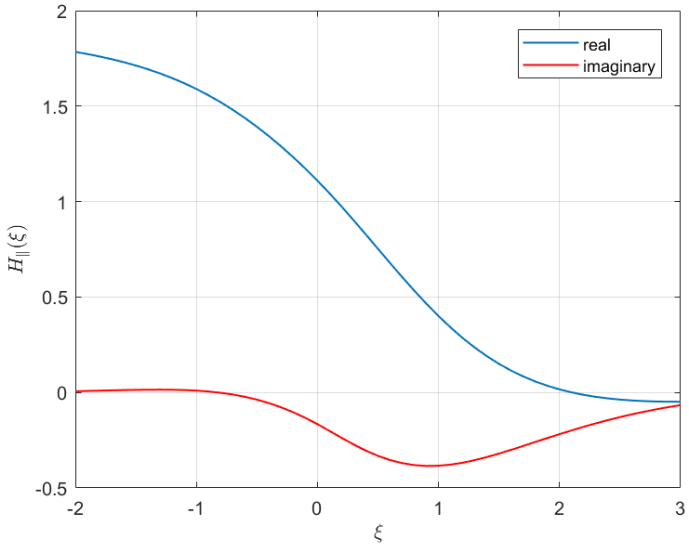

(a)

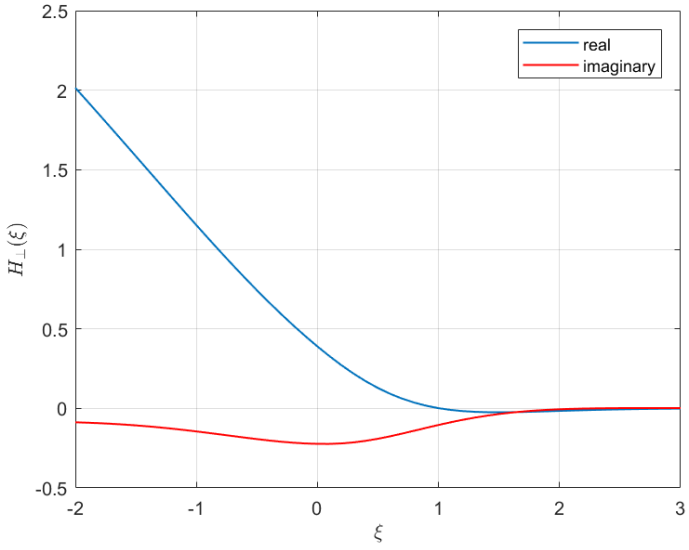

(b)

Figure 3.7: Plot of the radiation function with a cylinder of radius 20 cm, and permittivity of human tissue at 2.45 GHz. (a) Parallel polarization. (b) Perpendicular polarization

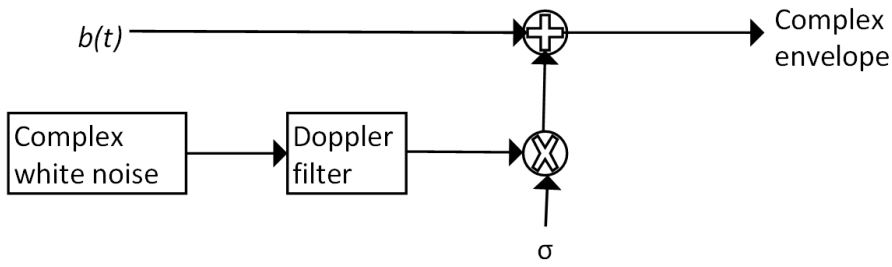

Figure 3.8: Example of a physical-statistical channel model. The variable $b(t)$ is calculated physically while the rest are statistical approximations.

$$H_{\perp} = \begin{cases} \frac{-j}{m} G_{\perp}(\xi).e^{-j(\xi)^3/3}, & \xi \leq 0 \\ \frac{-j}{m} G_{\perp}(\xi), & \xi \geq 0 \end{cases} \tag{3.24}$$

Here ξ is the Fock parameter, and $G_{\parallel\perp}(\xi)$ is the Fock radiation function. Typical values for $H_{\parallel\perp}$ calculated with a cylinder of radius $a = 20$ cm and relative permittivity of human muscle at 2.45 GHz frequency are shown in Figure 3.7

The UTD scattering and radiation principles were used in this research together with the Thalmann walking model in the modeling of the indoor wireless channels, and off-body communication channels (details are given in Paper I and Paper II).

3.2 Physical-Statistical Channel modeling

The physical channel models give a deeper understanding of the channels, however, they are difficult to use in simulation of large scenarios. Take for example tracing every ray in a highly reflective environment takes a lot of time and calculation power, and when the channel is dynamic these calculations have to be repeated again and again. One of the solutions to this problem is the use of physical-statistical channel modeling approach. Physical-statistical modeling take some of the burdens of physical calculations away by using statistical approximations, making them more effective for simulating large scenarios, while retaining some of the positive traits of physical modeling.

Figure 3.8 shows an example of a physical-statistical model for off-body channel conducted in the Ph.D. research (see Paper II for details). In this model, the position dependent contributions from the human body $b(t)$ are calculated using UTD, in which the movement and position of the body parts are determined using the Thalmann walking model. This contributes to the physical part of the channel modeling. The contributions from the environment are described statistically using a Rayleigh distribution. The Rayleigh distribution is obtained by passing a com-

plex white Gaussian process with zero mean and unity standard deviation through a Doppler filter for spectrum shaping. The resulting complex series is multiplied by the standard deviation, σ to represent the multipath contributions from the environmental scatterers. The overall model is a physical-statistical model, with contributions from the human body modeled physically, while the contributions from the environment modeled statistically.

3.3 Empirical Channel Modeling

Empirical propagation channel modeling is a process of characterizing a channel, by observing a given set of measurement data. This makes them more suitable for complex environments and applications in which physical models tend to be too complicated. The process of obtaining them requires a measurement campaign conducted specifically for that purpose. In other words, empirical channel modeling starts with the properly designed measurement campaign, followed by the analysis of the measurement results [2]. The resulting empirical models tend to be simple and provide practical channel statistics, however, they do not always provide meaningful insights to the physical phenomena associated with the channels, and the resulting models are applicable only to propagation scenarios with similar characteristics.

3.3.1 Measurement Campaign

There have been measurement campaigns for WBANs involving on-body, off-body, and body-to-body channels [24, 41, 42]. For on-body channels, studies were conducted in [41] in the frequency range of 3-5 GHz and in [43] for ultrawideband 3.1-10.6 GHz to develop models for fading in various on-body links. For off-body channels, path-loss was modeled in [44] from the measurements conducted in an indoor environment. The lognormal distribution proved to be a good fit in describing normalized signal amplitude. For body-to-body channels, a study to assess the impact of rotation, tilt, walking in LOS and NLOS conditions on the indoor environment was conducted in [42, 45] and at the ultra-wide frequency band of 2-8 GHz in [46]. The studies highlighted how movement affected the channel dynamic properties. This was confirmed by the study in [47] which was conducted in both indoor and outdoor environments to obtain the mean path-loss and the standard deviation for different body motion scenarios and antenna placements.

The aforementioned studies [41–47] were performed using antenna on the human body connected to the vector network analyzers (VNAs) through long cables. This restricted the movement of the subjects involved and suffered from cable parasitic effects. To increase mobility and achieve realistic scenarios, other researchers [48–52] used small wearable devices, which do not hinder any movement and

have capabilities of collecting data for long periods. Nevertheless, the studies were restricted to everyday activities and did not focus on specific applications such as sports activities. In this Ph.D. work, for the first time, a measurement campaign designed for body-to-body channel characterization during running and cycling in an outdoor environment was conducted. Naturally, these kinds of activities provide their own unique set of channel dynamics due to the movements and posture changes at both ends of the link.

The measurement campaign was conducted in 500 meters' outdoor stretch, which is part of a common running and cycling route in Gjøvik, Norway. The stretch was bounded by a road on one side and well-spaced industrial buildings on the other. The campaign was intended to represent communication channels between subjects performing sports activities. The body-to-body communication channel was implemented using one transmitting and one receiving node attached to the side of the upper arm of two male adults of height 1.80 m and mass 80 kg (subject A) and 1.85 m and mass 75 kg (subject B) respectively, using a small strip of Velcro. The location of the nodes on the body was chosen as it is commonly used for monitoring devices such as mobile phones during sports activities. The sports activities performed were running at a jogging pace (12 km/h), and cycling at a normal speed (18 km/h). The activity selected were meant to represent not only a small group of professional athletes, but also semi-professionals, and hobbyist. Two different scenarios, which could give an overall representation of the channel dynamics existing in these kinds of activities, as shown in Figure 3.9, were considered:

- Scenario 1, subject behind the other, Figure 3.9(a).
- Scenario 2, subject beside the other, Figure 3.9(b).

The test-bed was a programmable radio transceiver with non-volatile data storage, small enough to be attached to the test subjects, see Figure 3.10. It was made by integrating microSD memory card to a target board (eZ430-RF2500T) from Texas Instrument comprises a radio transceiver, antenna, microcontroller, and battery [53]. The radio transceiver in the board was CC2500, connected to omnidirectional chip antenna with a low profile which is a typical example of antennas to be used in body-mounted transceivers. The node was attached in such a way that the antenna was horizontally polarized. The device was set to transmit a packet every 4 ms with a constant transmission power of 1 dBm and carrier frequency of 2.425 GHz. This sampling period is way below the estimated coherence time of such channels [54]. At the receiving end, the packet number together with its received signal strength indicator (RSSI) was stored on the MicroSD memory

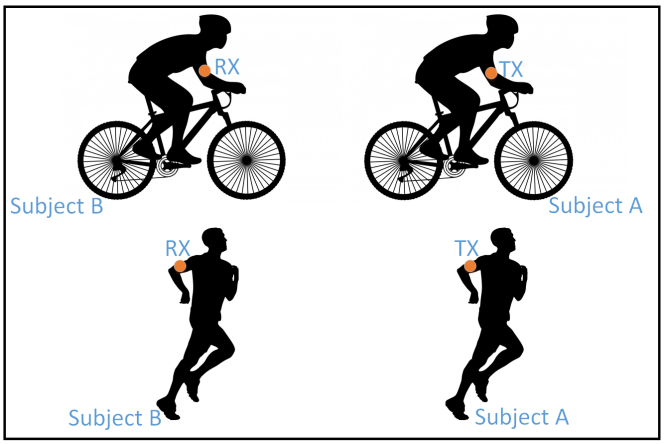

(a)

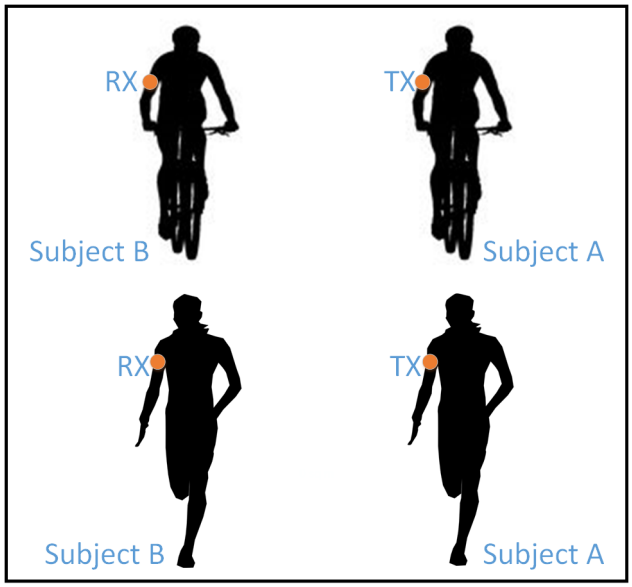

(b)

Figure 3.9: Investigated scenarios of the body-to-body measurement campaign. Activities involved were running and cycling. (a) Scenario 1, subject behind the other. (b) Scenario 2, subject beside the other. The nodes are attached to the side of the upper arms with radiation pattern away from the body

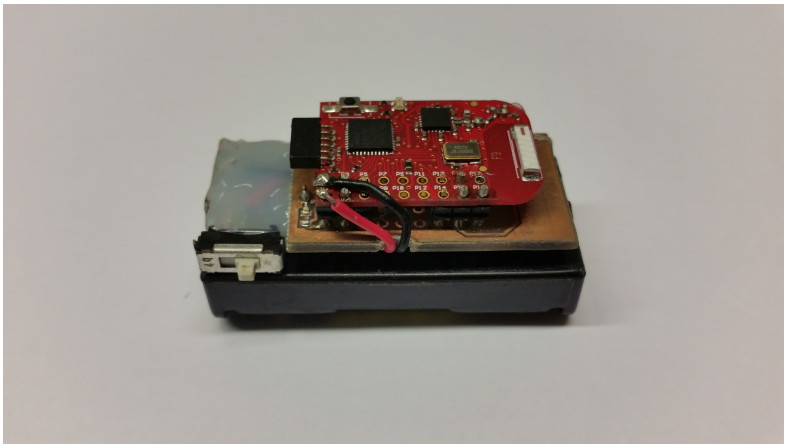

Figure 3.10: Wearable radio transceiver. The device is approximately 50 mm x 20 mm x 20 mm.

card. After completion of the measurement campaign, the data were exported from the memory card of the receiver node to a computer running MATLAB software for analysis. A total of four datasets (two scenarios for each, running and cycling) were collected, in which each had at least 25 kilo-samples, which is enough samples for statistical analysis.

3.3.2 First-order Statistical modeling

There are two most common types of empirical channel models. Those which described the relationship between the power loss and distance between the transmitter and receiver, simply known as path-loss models, and those which characterize the multipath propagation in term of first-order statics [14]. While the path-loss models have significant importance in the determination of coverage area and link budget, characterization of multipath propagation is essential in the performance analysis of a given network.

The characterization of the multipath propagation of a channel in terms of first-order statics is achieved by fitting statistical distributions that are commonly used to describe fading to the measured data. For WBAN, lognormal, Weibull, and Gamma distributions are often found to be the best fit, while the Rayleigh distribution is a poor fit for almost every scenario and environment for which it was attempted [19]. To obtain even better fits some attempts have been taken to deviate away from the standard distributions and the use of composite fading models instead [55, 56]. The approach was motivated by the presence of multiple peaks and skewed distribution curves in various empirical data [57, 58]. This may suggest

the existence of distinct scattering clusters, contributed by the movements of the different body components of the involved subjects at both ends of the communication channel. This kind of clustering behavior cannot be accurately modeled using a single distribution.

3.3.3 Lognormal Mixture Model

WBAN channels, particularly body-to-body channels, contain a large number of factors that contribute to the attenuation of the transmitted signal. These include reflection, diffraction, shadowing etc., which are additive in the logarithm domain and hence log-normally distributed. When the factors are caused by distinct scattering clusters, it results in distinct lognormal distributions, in which together they form a mixture. The resulting mixture can be modeled using the lognormal mixture model [59].

The probability density function (PDF) of lognormal mixture distributions can be described as

$$f(x) = \sum_{k=1}^{\infty} w_k \mathcal{LN}(\mu_k, \sigma_k) \tag{3.25}$$

where μ_k and σ_k are the distribution parameters of the kth mixture component (for $k = 1, 2, ...$). Parameter w_k is weighting proportion of the kth component such that $\sum_{k=1}^{\infty} w_k = 1$. The PDF of each component of (3.25) is lognormal and is given by

$$\mathcal{LN}(\mu_k, \sigma_k) = \frac{1}{x\sigma_k\sqrt{2\pi}} \exp\left[\frac{-(\ln x - \mu_k)^2}{2\sigma_k^2}\right] \tag{3.26}$$

The expectation maximization algorithm (EM) was utilized to estimate all the mixture model parameters. The algorithm is a technique that is used to simplify difficult maximum likelihood estimates (MLE) problems, which are encountered in mixture models and cannot be analytically solved. Although it was originally developed for normal mixture models, it can be expanded to lognormal mixtures by considering the fact that if X is distributed log-normally with parameters μ and σ, then $\ln(X)$ is distributed normally with mean μ and standard deviation σ [60]. The algorithm begins with some initial estimates of μ_k, σ_k, and w_k. This is followed by performing the probabilistic assignment of each data sample to some mixture component based on the current parameters. This step is known as expectation step (E-step). The mixture model parameters (μ_k, σ_k, and w_k) are then updated based on the new data assignments, done in the E-step. This step is known as the maximization step (M-step). The EM algorithm repeats E-step followed by M-step until the desired convergence level is reached [61].

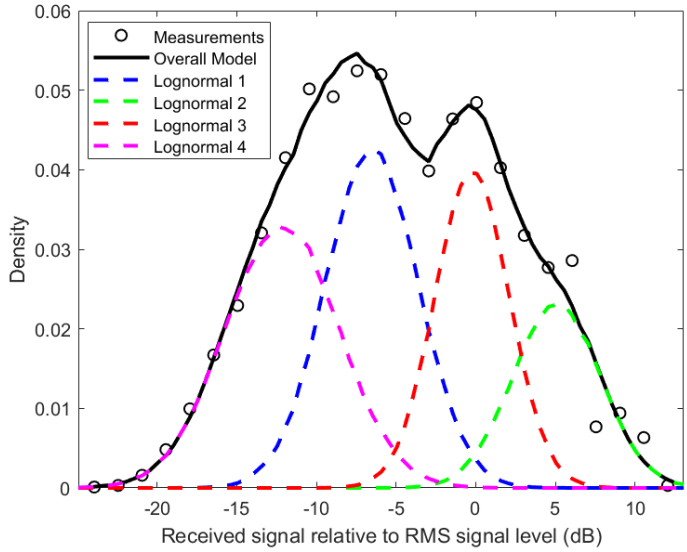

(a)

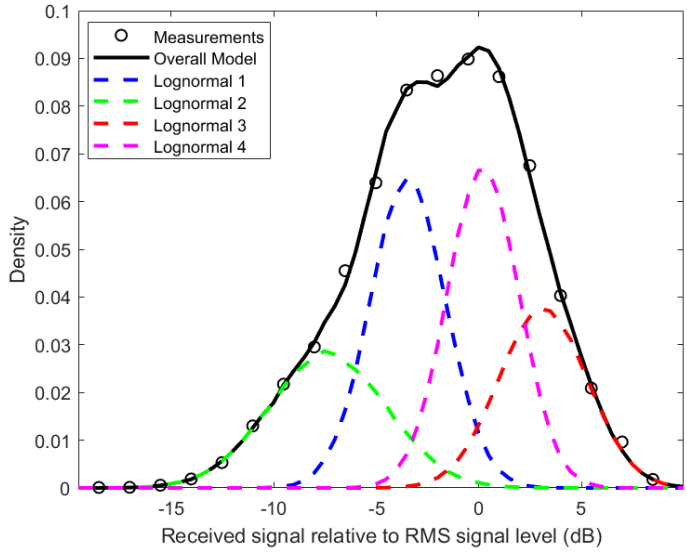

(b)

Figure 3.11: PDF of received signal amplitude of Scenario 2 normalized to its RMS value. (a) Running. (b) Cycling.

Figure 3.11 shows the overall model obtained from a mixture of four lognormal distribution together with the PDF of the measurement results. The approach takes care of the multiple peaks and the skew present in the measured data. The effect is less pronounced in the cycling activity due to the relatively stable arms and hence transceivers. For comparison with single standard distributions (lognormal, Gamma, and Nakagami) See Paper IV for more details.

3.3.4 Second-order Statistical modeling

The first-order statistical modeling of Section 3.3.3, gives a good approximation of the fading distribution in the channel and hence can be used in performance analysis of the wireless communication system. However, the model does not always provide the sequence of occurrence of the fade. Quantification of how often the signal crosses a certain threshold and how long it stays below it cannot be obtained from PDF alone. These statistics, known as level crossing rate (LCR) and average fade duration (AFD), are important time-varying property of the channel, and so is the simulation model which can produce them.

The channel model which can produce both first and second-order statistics can be obtained by analyzing the time series of the empirical data collected through the measurement campaign more closely. Our collected data has shown that the received signal power of body-to-body channels oscillate between interval where it is above certain threshold namely the 'good' state, and interval where it is below it namely the 'bad' state, as shown in Figure 3.12(a). Even when the arms where the transceivers were attached appear to be stationary as in cycling activity, the periodic movement of the body as the subjects pedal gives a similar effect as shown in Figure 3.12(b). The period of oscillation depends on the activity involved and can be approximated to be constant. These kinds of channels can be represented using the two-state semi-Markov model as done in land mobile satellite links [62, 63]. In addition to periodicity, we can also observe the change in the local mean, calculated from approximately 3 cycles of body motion as shown in Figure 3.13. This change is a result of the shadowing and fading effects caused by the change in the surrounding environment as well as the changes in the relative position between the subjects. Since these changes are relatively slow, they are normally considered as large-scale fading effects and are modeled using lognormal distribution [26, 64]. Finally, the simulation model can be completed by observing the power spectral density (PSD) of the channel. The PSD provides useful information on the frequency components of the signal, and hence the appropriate Doppler filter to be used in the simulations. For the case of running activity, shown in Figure 3.14(a), we can observe lowpass characteristic consistent with a radio channel having moving scatterers [65], in which the PSD decreases exponentially in logarithmic scale with the increase in frequency. As for the case of cycling activity shown in Figure

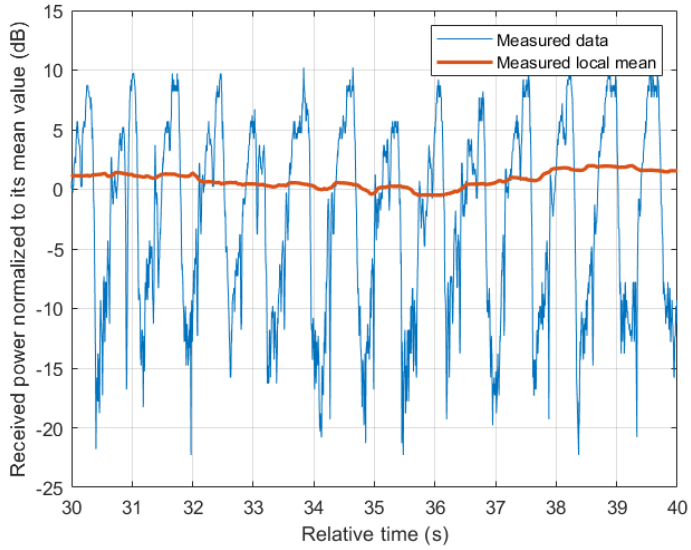

(a)

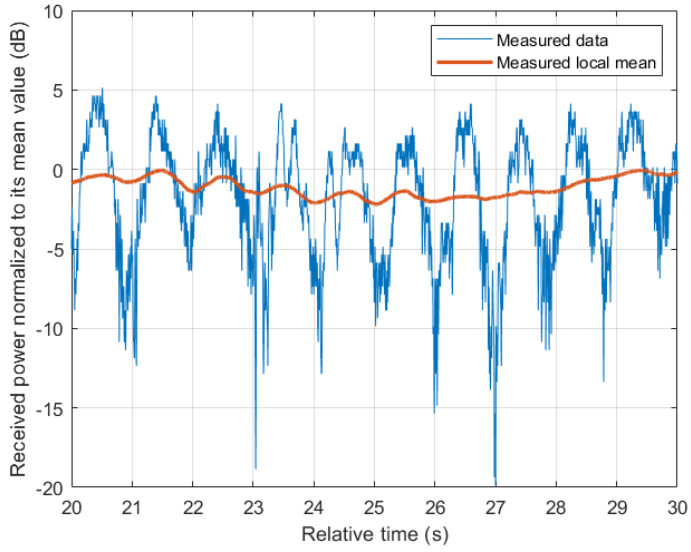

(b)

Figure 3.12: Example of measured time series collected in Scenario 1, (subject behind the other). (a) Running. (b) Cycling.

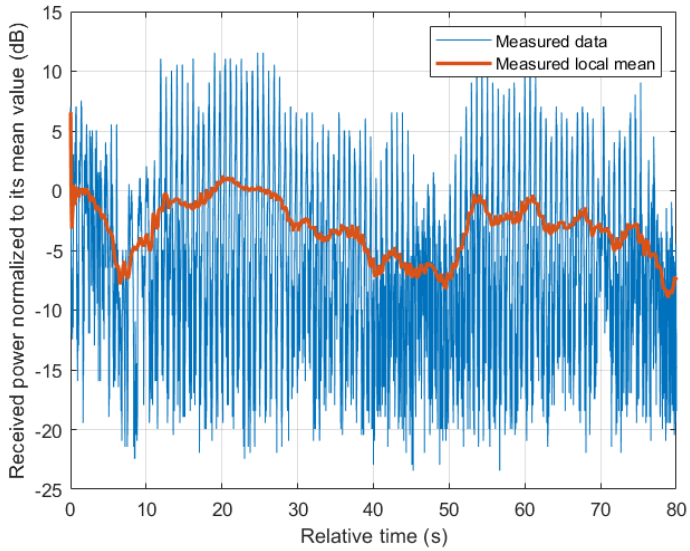

Figure 3.13: Example of measured time series collected in Scenario 2, (subject beside the other), running.

3.14(b), the PSD tends to settle between 20 and 50 Hz before it starts to decrease again, resulting in a local turning point at around 50 Hz. This phenomenon can be explained by the presence of the off-body scatterer (bicycle) in the cycling activity, which was absent in the running activity. Similar effects of off-body scatterers have been observed for on-body radio channels in [66]. A first-order Butterworth filter gives a good spectrum shape approximation for running, while for cycling a third-order Butterworth filter, with a cutoff frequency around the turning point could be used instead.

Figure 3.15 summarizes the simulation model for the body-to-body channels during running and cycling. In the simulation model, samples of good and bad states are generated from the corresponding D_g and D_b distributions for the specified T_g and T_b periods of time respectively. The outputs are then multiplied by $L(t)$, which is the large-scale fading component. The time series is then passed through the lowpass filter with appropriate cutoff frequency for spectrum shaping. The output from the simulator is a signal envelope which incorporates the overall fading characteristics of body-to-body channels under sporting activities. The resulting simulation model is capable of not only producing first-order statistics of the channel but also the second-order as shown in Figure 3.16, in which a good agreement is observed between the measurement results and the developed simulation model.

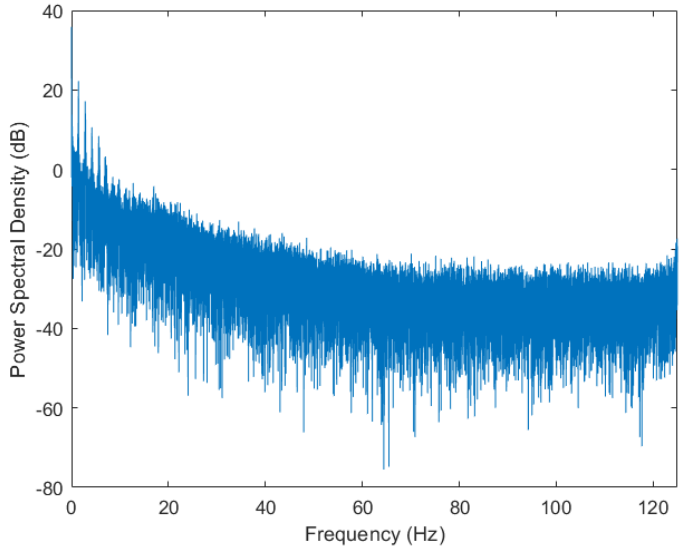

(a)

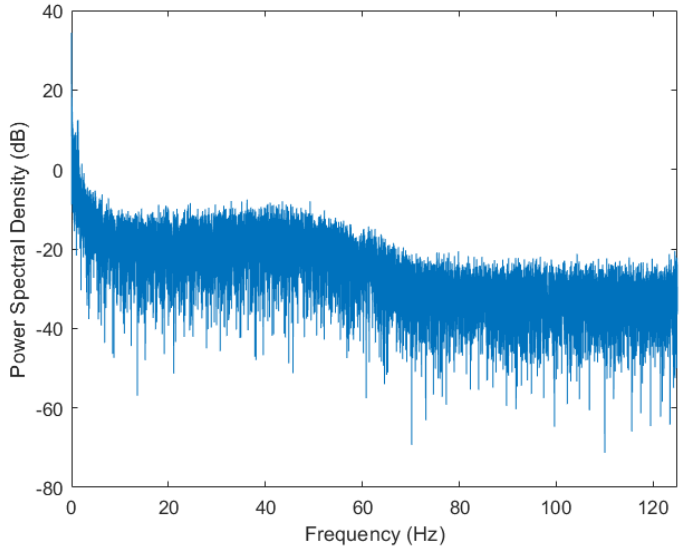

(b)

Figure 3.14: Example of measured PSD collected in Scenario 2, (subject beside the other). (a) Running. (b) Cycling.

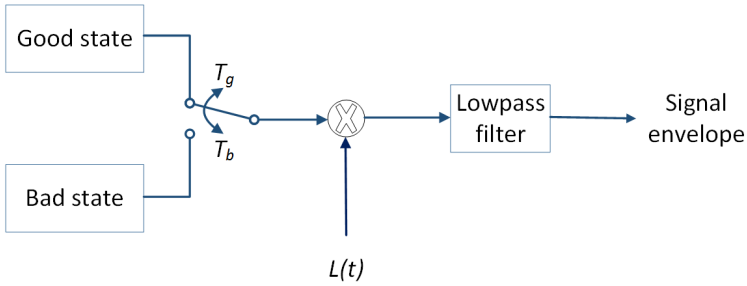

Figure 3.15: A simulation model for the body-to-body channels during running and cycling. $L(t)$ is the component of the large-scale fading, T_g and T_b are the periods of good and bad states respectively.

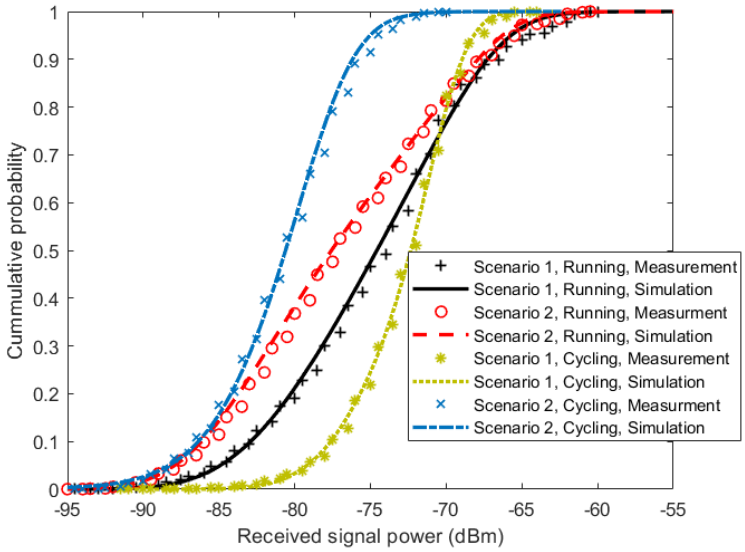

(a)

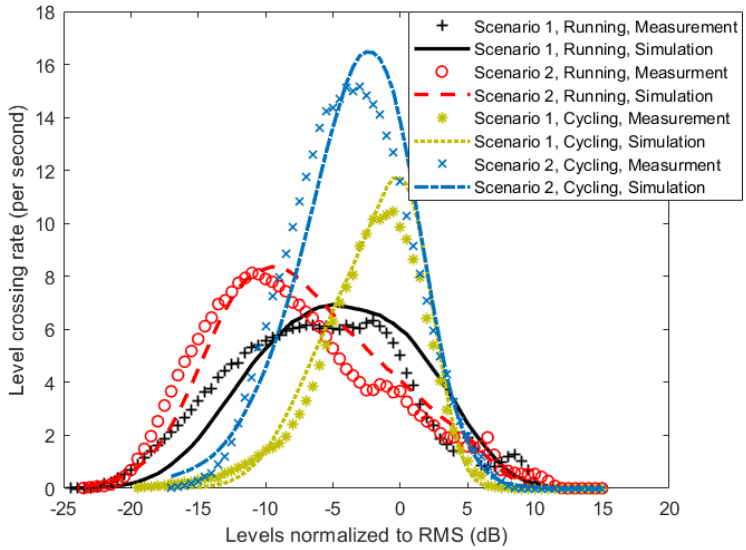

(b)

Figure 3.16: Comparison of first- and second-order statistics of the measurement results, and the developed simulation model results.(a) Cumulative distribution function. (b) Level crossing rate.

Chapter 4

Propagation Channel Fingerprinting

4.1 Introduction

The propagation channel models whether being physical, physical-statistical or empirically derived, are the fundamental requirement for designing robust and reliable WBANs. Channel models allow the designer to ensure that the channel behavior is well known prior to the system development and hence ensure that the device used provides robust performance against the full range of fading conditions likely to be encountered. Furthermore, for the already developed network, channel models allow engineers to validate crucial design parameters, and when possible, find ways to optimize them [26]. Take for example, the knowledge on the PDF of channel fading is essential in performance analysis of a network in terms of capacity, outage probability, bit error rates etc. This enables the engineers to choose the appropriate transmission power, as well as modulation techniques to meet the required performance threshold. Another good example is the impact of the LCR and AFD in the designing of error control codes and diversity schemes. The AFD helps determine the most likely number of bits that may be lost during a fading event and hence has a direct impact on the determination of the inter-leaver depth [67].

The aforementioned applications of propagation channel modeling are well established in the engineering world, however, the study of channel characteristics has lead to new areas of applications. It was demonstrated in [68] that the radio of wireless sensor nodes can be identified through its radio characteristics known as radio fingerprinting. In [69] the heterogeneous channel characteristics was ex-

ploited in secret key extraction scheme for intra-WBAN communication. Further, the authors in [70–72] attempt to exploit propagation characteristics or wireless channel to obtain behavioral fingerprint and use it for authentication. It uses the channel state information (CSI) of Wi-Fi signal to extract features that identify individuals by their intrinsic body movement during walking without attachments to the body. In this Ph.D. study, similar attempts were made to exploit radio propagation characteristics, in the improvement of security of WBANs. Specifically, RSSI based gait authentication method was proposed.

4.2 RSSI Based Gait Authentication

Various WBAN applications are known to involve sensitive and personal data, hence security and privacy measures are vital to their success [73]. Due to the difficulty for biometrics counterfeit, biometrics authentication has been proposed as a solution to improve security in the communication of such personal data [74]. One of the biometric traits which are attractive in WBAN applications security is gait. Unlike other biometrics traits such as voice, fingerprints, and facial recognition, gait is non-invasive and can be measured without subject intervention. This makes it more user-friendly especially in continuous identity re-verification [75]. Although the first gait recognition systems used video, the current trend is to use accelerometers included in wearables or portable smart devices [76]. Accelerometer based gait recognition systems have a lot of positive traits, however, they suffer from high energy consumption due to continuous accelerometer data sampling. Researcher in [77] tried to solve this problem by proposing a kinetic energy harvesting device and used its output voltage signal as the source of gait recognition.

In this Ph.D. work, an RSSI based gait authentication method was proposed. This method does not require hardware upgrades as it only relies on regular communication between body mounted sensors (e.g. smartwatch) and body mounted coordinator (e.g. smartphone). The gait information available in these kinds of channels can be extracted, processed and used for authentication by the coordinator. If processing power is a concern at the coordinator, the raw gait information could simply be forwarded to the server together with the rest of the data, and the authentication process could be performed there. This kind of authentication will ensure that the data uploaded to the server are indeed from the intended subject and will prevent impersonation attacks. Since it can be measured without subject intervention, it could be used as a continuous authentication method and set to trigger other security measures whenever it fails. This could add another security layer for applications in which one-time validation of the users' identity is insufficient. Unlike accelerometer based gait recognition systems, it does not require sampling of sensor data, making it more energy efficient. Moreover, it does not require any

additional packet transmission but instead makes use of the RSSI values already available in regular wireless communications.

4.3 Gait Radio Features

The gait information available in the radio channels can be extracted from the measurement of the power present in the received signal. This measurement is already being conducted by wireless radio transceivers and is indicated by their RSSI values [78]. The RSSI values are used to obtain radio features such as the variation of power received with time (the time series), the measure of the degree of time dependency (the auto-correlation function), and how often the signal crosses a certain threshold (the level crossing rate). It is through these radio features that one subject can be differentiated from the other.

4.3.1 The Time Series

It has been shown that the power received in WBANs is related to the dynamics involved with the specific activity of the subject. For the case of walking, the power received is periodic to the relative movement of the body parts where the nodes are attached to. The period of the signal tends to correspond to the period of the limb swinging, and the amplitude variation depends on the size of the limbs, distance from its rest position, and the amount of shadowing the body provide during walking [79]. Figure 4.1. shows the time series of the received signal power of 3 subjects during walking for the duration of 3 seconds. The transceivers were placed on the right wrist and the waist, and the fast fading effects in the received signal power were removed using a sliding window of length of 0.15 seconds. Although the time series of all 3 subjects are periodic with a period of around 1 second which is consistent with the oscillatory movement of the corresponding arms, the overall patterns have enough features to distinguish them from one another.

4.3.2 The Auto-Correlation Function

The Auto-correlation function (ACF) is a measure of the degree of time dependency among the observations of signals. It is used to characterize the periodicity in a fading signal envelope. For real discrete sampled data $x(t)$, it can be calculated using [67, 80]:

$$r_{xx}(\tau) = \sum_{t=1}^{N-\tau} (x(t) - \mu)(x(t-\tau) - \mu) \tag{4.1}$$

where τ is the time delay, N is the length and μ is the mean of the sampled data. The normalized ACF can then be obtained by using (4.2) to give an output with a

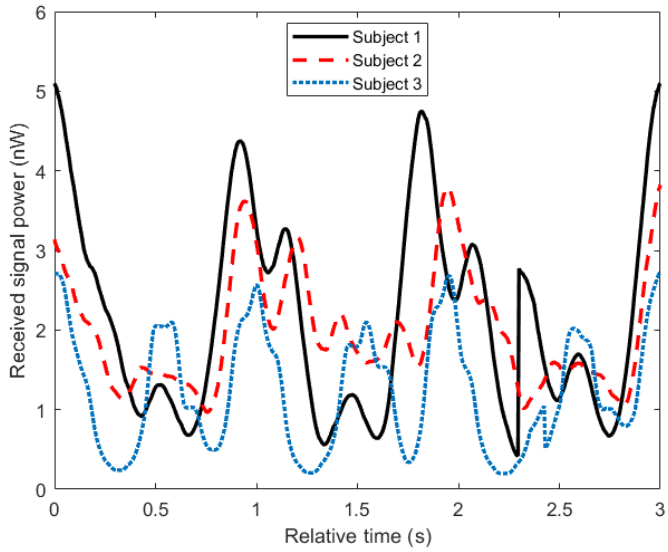

Figure 4.1: Example of time series of the received signal power of WBANs of 3 different subjects during walking. The transmitter was attached to the waist, and the receiver was attached to the right wrist.

maximum value of 1 at $\tau = 0$

$$\rho_{xx}(\tau) = \frac{r_{xx}(\tau)}{r_{xx}(0)} \tag{4.2}$$

since the received signal power is different from one subject to the other during walking, the normalized ACF has the potential of being different. Figure 4.2 shows the normalized ACF of the signals shown in Figure 4.1. The ACF of the 3 subjects show properties of a signal composed from a number of periodic signals, with the main envelope having a period of around 1s (0.92 s for Subject 1, 1.02 s for Subject 2, and 0.96 s for Subject 3), consistent with the oscillatory movement of the corresponding arms. However, the compositions of these periodic signals are different from one subject to the other, making the overall pattern of the ACF significantly different and hence could be used in gait recognition. In addition to that, ACF can be used as an indicator of change in activity. This is from the fact that, for a perfect periodic signal, the normalized ACF oscillates with its period corresponding to the period of the signal, and tends to decay exponentially If the signal is limited to a specific number of periods (it does not go to infinity). Such as, the normalized ACF of periodic signal limited to 3 periods will have a peak of 1 at $\tau = 0$, a peak of $\frac{2}{3}$ at $\tau = 1$ period, and a peak of $\frac{1}{3}$ at $\tau = 2$ periods as shown in Figure 4.3 for sinusoid, square, and triangle signals. These peaks values

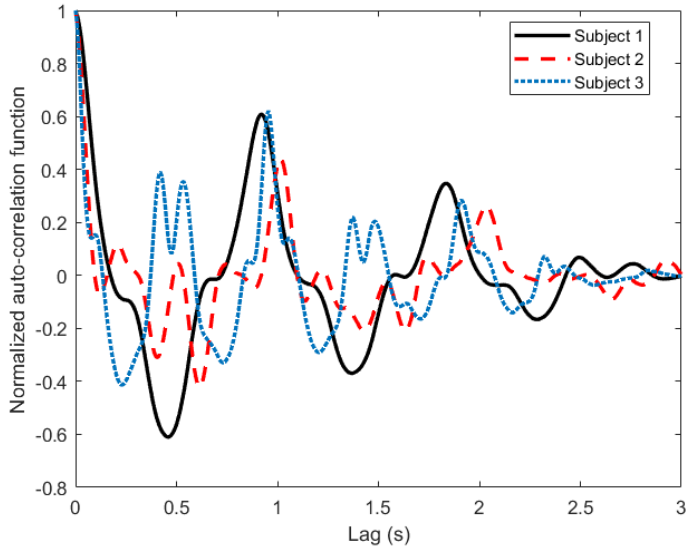

Figure 4.2: The normalized ACF of the signals shown in Figure 4.1. The ACFs show properties of periodic signals with significantly different patterns.

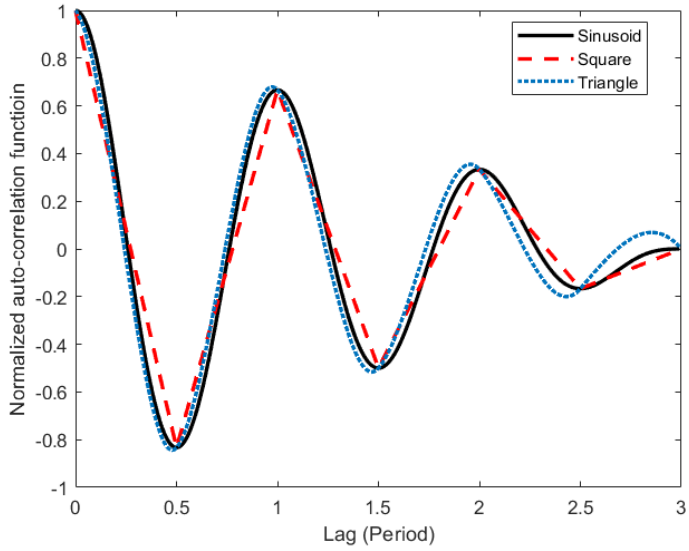

Figure 4.3: Example of normalized ACF of periodic signals of length of 3 periods. The ACF of all the signals have peaks at $\tau = 1$ of $\frac{2}{3}$, and at $\tau = 2$ of $\frac{1}{3}$

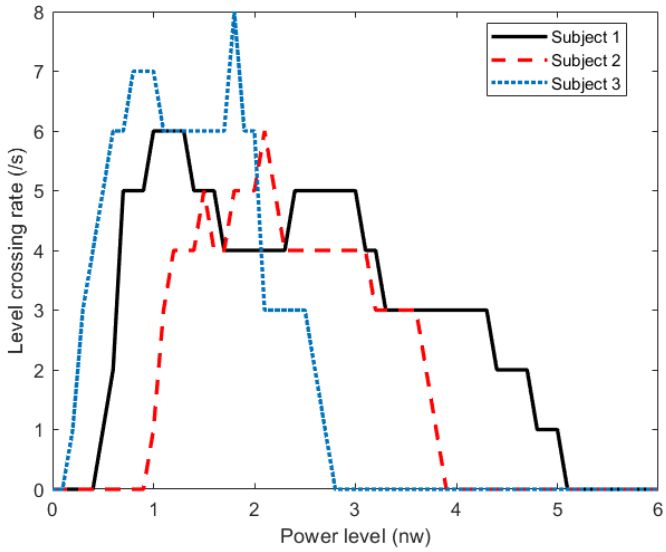

Figure 4.4: LCR representation of signals shown in Figure 4.1.

tend to decrease as the noise in the periodic signal increase. Take for example if a walking subject stops in the middle of sampling, the peak value at $\tau = 1$ period will be significantly smaller than the expected value and hence the change in activity could be detected.

4.3.3 The Level Crossing Rate

Another manner of quantifying periodic signals is using the LCR, which is the measure of how often a signal crosses a certain threshold going in a positive direction [67]. LCR represent signals in such a way that the primary focus is on power levels and frequency of crossing them. It emphasizes the location of the high-frequency component of the signal and clearly shows the signal range. Figure 4.4 shows the LCR representation of the signals shown in Figure 4.1. As expected the LCR of the 3 subjects are different due to the difference in the subjects' gait, and the size of their bodies. The LCR shows clearly the minimum and the maximum power level received by each subject. LCR could be too simple as a differentiating factor on its own, however, it could have a good contribution as an additional feature.

4.4 Method Evaluation

The dataset used to evaluate the RSSI based gait recognition consist of 20 healthy subjects (14 males and 6 females), with different age, height, and weight. During the data collection phase, 3 transceivers were attached on the participants, a transmitter on the right side of the waist representing devices such as smartphones, and a receiver on the wrist of the right and left arms representing devices such as smartwatches. The participants were asked to walk at their normal speed in both indoor and outdoor environments in order to capture the influence of different environment. The indoor environment was a cafeteria with a tiled surface, while the outdoor environment was a parking lot with an asphalt surface. Each participant walked for approximately 4 minutes outdoors followed by 4 minutes indoors to include natural gait changes over time and environments.

The collected data was split into segments of 3 seconds giving us a total of 150 segments from each subject. In each segment, 3 radio channel features namely the time series, ACF, and LCR were extracted. The radio features were later used in classification learners for testing the performance of the RSSI based gait authentication system. For the case of time series, the signal was shifted on time axis so that all the segments have their peaks at $t = 0$ as in Figure 4.1. Whenever ACF was used as a radio feature, an additional process of eliminating segments with periodicity noise was used. The process was set to eliminate any segment in which its ACF does not have a peak greater than 0.3 at $\tau = 1$ period.

The following 3 success criteria were used to measure the performance of the method [77].

- **True positive rate (TPR)**: Also know as sensitivity, is the probability that the authentication system correctly accepts the access request from the genuine users.
- **True negative rate (TNR)**: Also known as specificity, is the probability that the authentication system correctly rejects the access request from an imposter.
- **Recognition accuracy**: It represents the percentage of correct classifications which is simply the number of true classifications (acceptance from genuine users and rejection from imposter) over the total number of tests.

For each radio channel feature obtained from the channel between the right wrist and the waist (one channel), the performance of each classification learner in terms of TPR, TNR, and accuracy was evaluated independently, and in combination with

Table 4.1: Performance Results Using Artificial Neural Networks

Radio features	Performance metric	One channel	Two channels
Time series	TPR	67.8%	80.8%
	TNR	70.9%	82.5%
	Accuracy	73.9%	83.6%
ACF	TPR	85.1%	89.6%
	TNR	86.1%	90.6%
	Accuracy	85.8%	90.5%
LCR	TPR	72.9%	80.8%
	TNR	74.1%	80.9%
	Accuracy	75.8%	83.1%
Time series+ACF	TPR	89.9%	95.1%
	TNR	90.8%	95.6%
	Accuracy	91.3%	95.9%
Time series+LCR	TPR	84.5%	92.7%
	TNR	85.2%	93.3%
	Accuracy	87.2%	94.3%
ACF+LCR	TPR	92.6%	96.1%
	TNR	93.6%	96.2%
	Accuracy	93.9%	96.6%
Time series+ACF+LCR	TPR	94.4%	97.5%
	TNR	95.2%	97.6%
	Accuracy	95.3%	97.9%

each other. The same analyses were repeated when additional radio features were extracted from the channel between the left wrist and the waist and used together with those from the channel between the right wrist and the waist (two channels).

Table 4.1 shows the performance of the artificial neural networks classifier using time series, ACF, LCR, and different combination of those features, obtained from one and two radio channels. When only a single radio feature is used, LCR has shown to give the worst results, while ACF gave the best performance. When the radio features are used in pairs, ACF+LCR pair gives the best results, while the combination of all 3 features archives an accuracy of 95.3%. When additional radio features are extracted from the channel between the left wrist and the waist and are used together with those from the channel between the right wrist and the waist, we notice improvements in all performance metric, with the most improvement in accuracy of 9.7% achieved when time series is used as a single radio feature, and the least of 2.6% achieved when all the radio features (Time series+ACF+LCR)

are used together. This suggests that if all 3 radio features are used in the RSSI based gait authentication, the features extracted from a single radio channel could be enough to provide good performance and that the addition of similar features from the second channel does not provide significant improvement.

Chapter 5

Summary

This chapter summarizes the research contributions of the thesis work and discusses the future works.

5.1 Short Presentation of the Included Papers

A brief summary of the included papers is as follows:

Physical Channel Modeling Using UTD

Paper I: M. Mohamed, M. Cheffena, F. P. Fontan, and A. Moldsvor, "A dynamic channel model for indoor wireless signals: Working around interference caused by moving human bodies," *IEEE Antennas and Propagation Magazine*, vol. 60, no. 2, pp. 82-91, 2018.

Paper II M. Mohamed, M. Cheffena, A. Moldsvor, and F. P. Fontan, "Physical-statistical channel model for off-body area network," *IEEE Antennas and Wireless Propagation Letters*, vol. 16, pp. 1516-1519, 2017.

These papers utilized a dynamic human walking model, which provides a detailed description of the movement of the different body parts, and UTD to accurately calculate the time varying shadowing and scattering effects due to the movements of the body parts. A dynamic channel model for the signal affected by moving human bodies in an indoor environment was developed. The developed model was validated using RF measurements at 2.45 GHz at two different heights to study the effects on the channel from the movement of both lower and upper body parts. The results were also compared with those obtained with a simpler model being used to tackle similar problems, and showed significant difference for the lower body parts at measured frequency, and for both lower and upper body parts at millimeter-wave

region.

Further the method was used to develop a physical-statistical channel model for off-body communication. Here, a Rayleigh distribution was used to represent the multipath fading effects by the scatters around the human body. The model was validated in terms of first- and second-order statistics using 2.36 GHz measurement data, showing good agreement.

Empirical Channel Modeling

Paper III: M. Mohamed, M. Cheffena, and A. Moldsvor, "Characterization of the body-to-body propagation channel for subjects during sport activities," *Sensors*, vol. 18, no. 2, p. 620, 2018.

Paper IV: M. Cheffena and M. Mohamed, "The application of lognormal mixture shadowing model for B2B channels," *IEEE Sensors Letters*, vol. 2, no. 3, pp. 1-4, 2018.

These papers present the results of the measurement campaign of the body-to-body channels during sports activities. The sports activities considered were running at a jogging pace, and cycling at a normal speed to represent not only a small group of professional athletes but also semi-professionals and hobbyist. The PDF of the measured data showed mixture and skewed distribution curves, which suggested the existence of distinct scattering clusters, due to the movements of the different body components of the involved subjects at both ends of the communication channel. This motivated the use of a mixture of lognormal distributions in the first-order statistical modeling of the body-to-body channel. The resulting model outperformed single lognormal, Gamma, and Nakagami distributions by having much smaller error parameters.

To be able to simulate the second-order statistics, further analysis of the measured data was conducted. The time series showed periodic transitions between a good state, where the received signal power is above a certain threshold, and a bad state in which the signal is below it. This motivated the use of a two-state semi-Markov model approach in the design of the simulation model of the body-to-body channels. The resulting simulation model showed good agreement with the measured data in terms of first- and second-order statistics.

Further, the first-order statistics obtained were used to conduct performance analysis of the channels in terms of channel capacity and outage probability. Cycling activities sowed better performance than running activities for having higher channel capacity and lower outage probability regardless of the speed of cycling being significantly higher. This is mainly because, during cycling, the arms were the

transceivers were attached are more stable.

Propagation Channel Fingerprinting

Paper V: M. Mohamed and M. Cheffena, "Received signal strength based gait authentication," *IEEE Sensors Journal*, vol. 18, no. 16, pp. 6727-6734, 2018.

An RSSI based gait authentication method was proposed in this paper. The method could be used together with other authentication approaches, to add another security layer for applications in which one-time validation of the users' identity is insufficient. The method has advantages over other gait authentication systems, as it does not require additional hardware or sampling of sensor data making it more economical and energy efficient. The method extracts gait features from the radio signal namely, the time series, ACF, and LCR through the RSSI values available in regular communications and use them as input in classification learners. The evaluation of the method showed some promising results, with an accuracy of up to 98%.

Physical Channel Modeling Using FDTD

Paper VI M. Mohamed, W. Joseph, G. Vermeeren, E. Tanghe, and M. Cheffena, "Characterization of dynamic wireless body area network channels during walking," *Submitted to EURASIP Journal on Wireless Communications and Networking,* 2018.

In this paper, FDTD was used in the investigation of WBAN channel characteristics during walking for on-body, off-body, and body-to-body communication, in the same conditions so that a more complete picture of the overall network can be observed and compared. FDTD was used as it could separate the channel gain into propagation loss and antenna gain, which cannot be achieved through measurement since the body is within the near field of the antenna. Correlation between the channels and the application of multivariate normal distributions in the modeling of WBAN channels was also investigated in the paper.

5.2 Future Work

A lot of work can be done to further extend the research results obtained in this Ph.D. research, e.g,

- Technological advancements in agriculture and livestock farming are expected to play a significant role in ensuring adequate food supply for a rapidly increasing world population which is estimated to reach 9.7 billion by 2050 [81]. Typical examples include precision feeding systems, milking robots, and stable farm management systems. In addition to that, monitoring

the health of the individual animals is important in order to prevent animal epidemics and for early treatment of sick animals. In this regard, animal WBANs can provide the cost-effective solutions for monitoring the well-being of livestock. The current WBAN standard is primarily tailored for human use. The air interface technologies are designed taking into account the characteristics of the propagation channel utilizing excessive RF measurement results from human bodies. Thus, it may not provide the desired quality of service requirement when used for animals as the propagation characteristics of RF signals on animals might be completely different to that of humans.

- The large bandwidth available at millimeter wave spectrum can open the way for various new indoor and outdoor WBAN applications. For example, in search and rescue, the bandwidth could facilitate a three-dimensional video streaming necessary for augmented reality and hence could provide more details in the running of the operation. The same could be applied to the entertainment area, such as live music performance, sports etc. so that the distant spectators could get a full experience. The impact of human bodies and their movement can cause additional challenges in communication at such frequencies. Thus, further studies and measurements are required to fully characterize the propagation channel of WBANs over the millimeter wave spectrum.

- The role of WBANs in detecting human activities such as gait, exercises, and emergencies such as fall for elderly, through the sensing devices attached to the body is unquestionable. However, the sensing device with a limited battery, has to allocate power for the process of sampling of sensor data (e.g., accelerometer for gait). Radio fingerprinting has a potential of removing the need of using sensors for activity detection. This could result in compact, cheaper and energy efficient devices. The study of propagation channel characteristics should be expanded beyond the purpose of increasing performance of the investigated network. The role of the radio channels in complementing or even replacing sensors for activity monitoring and radio fingerprinting needs further investigation.

Bibliography

[1] I. S. Association *et al.*, "IEEE standard for local and metropolitan area networks part 15.6: Wireless body area networks," *IEEE Standard for Information Technology, IEEE*, vol. 802, no. 6, pp. 1–271, 2012.

[2] Y. Hao and P. S. Hall, *Antennas and Propagation for Body-centric Wireless Communications.* Norwood, MA: Artech House, 2012, vol. 2nd ed.

[3] M. Cheffena, "Performance evaluation of wireless body sensors in the presence of slow and fast fading effects," *IEEE Sensors Journal*, vol. 15, no. 10, pp. 5518–5526, 2015.

[4] K. S. Kwak, S. Ullah, and N. Ullah, "An overview of IEEE 802.15.6 standard," in *Proceedings of 3rd International Symposium on Applied Sciences in Biomedical and Communication Technologies (ISABEL)*, 2010, pp. 1–6.

[5] L. A. Al Dulaimi, R. Ahmad, L. Hassnawi, P. Ehkan, and I. Shihab, "Performance comparison of different MAC protocols over wireless body area networks (WBAN)," *Australian Journal of Basic and Applied Sciences*, vol. 11, pp. 34–40, 02 2017.

[6] Q. H. Abbasi, M. U. Rehman, K. Qaraqe, and A. Alomainy, *Advances in Body-centric Wireless Communication: Applications and State-of-the-art*. Stevenage, UK: Institution of Engineering and Technology, 2016.

[7] T. Aoyagi, M. Kim, J.-i. Takada, K. Hamaguchi, R. Kohno *et al.*, "Body motion and channel response of dynamic body area channel," in *Proceedings of 5th European Conference on Antennas and Propagation (EUCAP)*, 2011, pp. 3138–3142.

[8] M. Mackowiak and L. M. Correia, "A statistical model for the influence of body dynamics on the gain pattern of wearable antennas in off-body radio channels," *Wireless Personal Communications*, vol. 73, no. 3, pp. 381–399, 2013.

[9] C. Roblin, J.-M. Laheurte, R. D'Errico, A. Gati, D. Lautru, T. Alvés, H. Terchoune, and F. Bouttout, "Antenna design and channel modeling in the BAN context—Part II: Channel," *Annals of Telecommunications*, vol. 66, no. 3-4, pp. 157–175, 2011.

[10] S. Movassaghi, M. Abolhasan, J. Lipman, D. Smith, and A. Jamalipour, "Wireless body area networks: A survey," *IEEE Communications Surveys & Tutorials*, vol. 16, no. 3, pp. 1658–1686, 2014.

[11] S. Ullah, H. Higgins, B. Braem, B. Latre, C. Blondia, I. Moerman, S. Saleem, Z. Rahman, and K. S. Kwak, "A comprehensive survey of wireless body area networks," *Journal of Medical Systems*, vol. 36, no. 3, pp. 1065–1094, 2012.

[12] D. He and S. Zeadally, "Authentication protocol for an ambient assisted living system," *IEEE Communications Magazine*, vol. 53, no. 1, pp. 71–77, 2015.

[13] R. Al-Shaqi, M. Mourshed, and Y. Rezgui, "Progress in ambient assisted systems for independent living by the elderly," *SpringerPlus*, vol. 5, no. 1, p. 624, 2016.

[14] E. Sazonov and M. R. Neuman, *Wearable Sensors: Fundamentals, Implementation and Applications*. Amsterdam, Netherlands: Elsevier, 2014.

[15] M. Chen, S. Gonzalez, A. Vasilakos, H. Cao, and V. C. Leung, "Body area networks: A survey," *Mobile Networks and Applications*, vol. 16, no. 2, pp. 171–193, 2011.

[16] B. Latré, B. Braem, I. Moerman, C. Blondia, and P. Demeester, "A survey on wireless body area networks," *Wireless Networks*, vol. 17, no. 1, pp. 1–18, 2011.

[17] C. Tachtatzis, F. Di Franco, D. C. Tracey, N. F. Timmons, and J. Morrison, "An energy analysis of IEEE 802.15.6 scheduled access modes," in *Proceedings of IEEE GLOBECOM Workshops (GC Wkshps)*, 2010, pp. 1270–1275.

[18] M. Sukor, S. Ariffin, N. Fisal, S. S. Yusof, and A. Abdallah, "Performance study of wireless body area network in medical environment," in *Proceedings of Second Asia International Conference on Modeling & Simulation (AICMS)*, 2008, pp. 202–206.

[19] D. B. Smith, D. Miniutti, T. A. Lamahewa, and L. W. Hanlen, "Propagation models for body-area networks: A survey and new outlook," *IEEE Antennas and Propagation Magazine*, vol. 55, no. 5, pp. 97–117, 2013.

[20] H. Cao, V. Leung, C. Chow, and H. Chan, "Enabling technologies for wireless body area networks: A survey and outlook," *IEEE Communications Magazine*, vol. 47, no. 12, 2009.

[21] B. Latré, G. Vermeeren, L. Martens, and P. Demeester, "Networking and propagation issues in body area networks," in *Proceedings of 11th Symposium on Communications and Vehicular Technology in the Benelux (SCVT)*, 2004.

[22] L. Roelens, S. Van den Bulcke, W. Joseph, G. Vermeeren, and L. Martens, "Path loss model for wireless narrowband communication above flat phantom," *Electronics Letters*, vol. 42, no. 1, pp. 10–11, 2006.

[23] M. Di Renzo, R. M. Buehrer, and J. Torres, "Pulse shape distortion and ranging accuracy in UWB-based body area networks for full-body motion capture and gait analysis," in *Proceedings of IEEE Global Telecommunications Conference (GLOBECOM)*, 2007, pp. 3775–3780.

[24] D. B. Smith, L. W. Hanlen, J. A. Zhang, D. Miniutti, D. Rodda, and B. Gilbert, "First- and second-order statistical characterizations of the dynamic body area propagation channel of various bandwidths," *Annals of Telecommunications*, vol. 66, no. 3-4, pp. 187–203, 2011.

[25] A. F. Molisch, *Wireless Communications*, 2nd ed. Hoboken, NJ, USA: John Wiley & Sons, 2012.

[26] A. Aragon-Zavala, *Antennas and Propagation for Wireless Communication Systems*, 2nd ed. Hoboken, NJ, USA: John Wiley & Sons, 2008.

[27] L. Ahlin, J. Zander, and S. Ben Slimane, *Principles of Wireless Communications*. Lund, Sweden: Studentlitteratur, 2006.

[28] M. Cheffena, "Time-varying on-body wireless channel model during walking," *EURASIP Journal on Wireless Communications and Networking*, vol. 2014, no. 1, p. 29, 2014.

[29] F. Villanese, N. E. Evans, and W. G. Scanlon, "Pedestrian-induced fading for indoor channels at 2.45, 5.7 and 62 GHz," in *Proceedings of IEEE 52nd Vehicular Technology Conference (VTC)*, vol. 1, 2000, pp. 43–48.

[30] Y. Huang, A. Charbonneau, L. Talbi, and T. A. Denidni, "Effect of human body upon line-of-sight indoor radio propagation," in *Proceedings of Canadian Conference on Electrical and Computer Engineering (CCECE)*, 2006, pp. 1775–1778.

[31] M. Ghaddar, L. Talbi, T. A. Denidni, and A. Sebak, "A conducting cylinder for modeling human body presence in indoor propagation channel," *IEEE Transactions on Antennas and Propagation*, vol. 55, no. 11, pp. 3099–3103, 2007.

[32] M. Girard, "Interactive design of 3D computer-animated legged animal motion," *IEEE Computer Graphics and Applications*, vol. 7, no. 6, pp. 39–51, June 1987.

[33] M. Girard and A. A. Maciejewski, "Computational modeling for the computer animation of legged figures," *ACM SIGGRAPH Computer Graphics*, vol. 19, no. 3, pp. 263–270, July 1985.

[34] R. Boulic, N. M. Thalmann, and D. Thalmann, "A global human walking model with real-time kinematic personification," *The Visual Computer*, vol. 6, no. 6, pp. 344–358, 1990.

[35] P. van Dorp and F. Groen, "Human walking estimation with radar," *IEE Proceedings-Radar, Sonar and Navigation*, vol. 150, no. 5, pp. 356–365, 2003.

[36] A. Z. Elsherbeni and V. Demir, *The Finite-Difference Time-Domain Method: Electromagnetics with MATLAB Simulations*. Stevenage, UK: The Institution of Engineering and Technology, 2016.

[37] J. B. Schneider, "Understanding the finite-difference time-domain method," *School of Electrical Engineering and Computer Science Washington State University*, 2010.

[38] E. Plouhinec, "D2.1b—On-body antennas characterization and exploitable radiation properties—Updated document: 3-D deterministic modeling of electromagnetic wave interactions with a dielectric cylinder," Agence Nationale de la Recherche, Paris, France, Tech. Rep. CORMORAN ANR 11-INFR-010, 2012.

[39] M. Cheffena, "Physical-statistical channel model for signal effect by moving human bodies," *EURASIP Journal on Wireless Communications and Networking*, vol. 2012, no. 1, p. 77, 2012.

[40] D. McNamara, C. Pistorius, and J. Malherbe, *Introduction to the Uniform Geometrical Theory of Diffraction*. Norwood, MA: Artech House, 1990.

[41] R. D'Errico and L. Ouvry, "A statistical model for on-body dynamic channels," *International Journal of Wireless Information Networks*, vol. 17, no. 3-4, pp. 92–104, 2010.

[42] R. Rosini, R. Verdone, and R. D'Errico, "Body-to-body indoor channel modeling at 2.45 GHz," *IEEE Transactions on Antennas and Propagation*, vol. 62, no. 11, pp. 5807–5819, 2014.

[43] D. Goswami, K. Sarma, and A. Mahanta, "Experimental determination of path loss and delay dispersion parameters for on-body UWB WBAN channel," in *Proceedings of IEEE International Conference on Signal Processing, Informatics, Communication and Energy Systems (SPICES)*, 2015, pp. 1–4.

[44] D. B. Smith, D. Miniutti, and L. W. Hanlen, "Characterization of the body-area propagation channel for monitoring a subject sleeping," *IEEE Transactions on Antennas and Propagation*, vol. 59, no. 11, pp. 4388–4392, 2011.

[45] F. Mani and R. D'Errico, "A spatially aware channel model for body-to-body communications," *IEEE Transactions on Antennas and Propagation*, vol. 64, no. 8, pp. 3611–3618, 2016.

[46] T. Kumpuniemi, M. Hämäläinen, K. Y. Yazdandoost, and J. Iinatti, "Measurements for body-to-body UWB WBAN radio channels," in *Proceedings of 9th European Conference on Antennas and Propagation (EuCAP)*, 2015, pp. 1–5.

[47] S. J. Ambroziak, L. M. Correia, and K. Turbic, "Radio channel measurements in body-to-body communications in different scenarios," in *Proceedings of URSI Asia-Pacific Radio Science Conference (URSI AP-RASC)*, 2016, pp. 1376–1379.

[48] S. L. Cotton, W. G. Scanlon, and J. Guy, "The $\kappa - \mu$ distribution applied to the analysis of fading in body to body communication channels for fire and rescue personnel," *IEEE Antennas and Wireless Propagation Letters*, vol. 7, pp. 66–69, 2008.

[49] S. L. Cotton and W. G. Scanlon, "An experimental investigation into the influence of user state and environment on fading characteristics in wireless body area networks at 2.45 GHz," *IEEE Transactions on Wireless Communications*, vol. 8, no. 1, pp. 6–12, 2009.

[50] H. Chebbo, S. Abedi, T. A. Lamahewa, D. B. Smith, D. Miniutti, and L. Hanlen, "Reliable body area networks using relays: Restricted tree topology," in *Proceedings of International Conference on Computing, Networking and Communications (ICNC)*, 2012, pp. 82–88.

[51] S. L. Cotton, W. G. Scanlon, and A. McKernan, "Improving signal reliability in outdoor body-to-body communications using front and back positioned antenna diversity," in *Proceedings of 6th European Conference on Antennas and Propagation (EUCAP)*, 2012, pp. 3393–3396.

[52] M. G. Doone and S. L. Cotton, "Fading characteristics of body-to-body channels subject to vehicular traffic conditions at 2.45 GHz," in *Proceedings of IEEE Antennas and Propagation Society International Symposium (APSURSI)*, 2014, pp. 723–724.

[53] T. Instruments, *eZ430-RF2500 Development Tool User's Guide*, Texas Instruments, Dallas, TX, USA, 2015.

[54] D. Smith, J. Zhang, L. Hanlen, D. Miniutti, D. Rodda, and B. Gilbert, "Temporal correlation of dynamic on-body area radio channel," *Electronics Letters*, vol. 45, no. 24, pp. 1212–1213, 2009.

[55] S. K. Yoo, S. L. Cotton, P. C. Sofotasios, and S. Freear, "Shadowed fading in indoor off-body communication channels: A statistical characterization using the $\kappa - \mu$/gamma composite fading model," *IEEE Transactions on Wireless Communications*, vol. 15, no. 8, pp. 5231–5244, 2016.

[56] S. L. Cotton, "A statistical model for shadowed body-centric communications channels: Theory and validation," *IEEE Transactions on Antennas and Propagation*, vol. 62, no. 3, pp. 1416–1424, 2014.

[57] R. Rosini, R. Verdone, and R. D'Errico, "Body-to-body indoor channel modeling at 2.45 GHz," *IEEE Transactions on Antennas and Propagation*, vol. 62, no. 11, pp. 5807–5819, 2014.

[58] T. Kumpuniemi, M. Hämäläinen, K. Y. Yazdandoost, and J. Iinatti, "Human body shadowing effect on dynamic UWB on-body radio channels," *IEEE Antennas and Wireless Propagation Letters*, vol. 16, pp. 1871–1874, 2017.

[59] A. Fort, C. Desset, P. De Doncker, P. Wambacq, and L. Van Biesen, "An ultra-wideband body area propagation channel model-from statistics to implementation," *IEEE Transactions on Microwave Theory and Techniques*, vol. 54, no. 4, pp. 1820–1826, 2006.

[60] S. Büyükçorak, M. Vural, and G. K. Kurt, "Lognormal mixture shadowing," *IEEE Transactions on Vehicular Technology*, vol. 64, no. 10, pp. 4386–4398, 2015.

[61] T. K. Moon, "The expectation-maximization algorithm," *IEEE Signal processing magazine*, vol. 13, no. 6, pp. 47–60, 1996.

[62] E. Lutz, D. Cygan, M. Dippold, F. Dolainsky, and W. Papke, "The land mobile satellite communication channel-recording, statistics, and channel model," *IEEE Transactions on Vehicular Technology*, vol. 40, no. 2, pp. 375–386, 1991.

[63] L. E. Braten and T. Tjelta, "Semi-Markov multistate modeling of the land mobile propagation channel for geostationary satellites," *IEEE Transactions on Antennas and Propagation*, vol. 50, no. 12, pp. 1795–1802, 2002.

[64] F. P. Fontán and P. M. Espiñeira, *Modelling the Wireless Propagation Channel: A Simulation Approach with MATLAB*. Hoboken, NJ, USA: John Wiley & Sons, 2008.

[65] J. B. Andersen, J. O. Nielsen, G. F. Pedersen, G. Bauch, and G. Dietl, "Doppler spectrum from moving scatterers in a random environment," *IEEE Transactions on Wireless Communications*, vol. 8, no. 6, 2009.

[66] R. D'Errico and L. Ouvry, "Doppler characteristics and correlation proprieties of on-body channels," in *Proceedings of 5th European Conference on Antennas and Propagation (EUCAP)*, 2011, pp. 2977–2981.

[67] T. S. Rappaport *et al.*, *Wireless Communications: Principles and Practice*. Upper Saddle River, NJ, USA: Prentice Hall, 1996.

[68] K. B. Rasmussen and S. Capkun, "Implications of radio fingerprinting on the security of sensor networks," in *Proceedings of Third International Conference on Security and Privacy in Communications Networks and the Workshops (SecureComm)*, 2007, pp. 331–340.

[69] L. Shi, J. Yuan, S. Yu, and M. Li, "Mask-ban: Movement-aided authenticated secret key extraction utilizing channel characteristics in body area networks," *IEEE Internet of Things Journal*, vol. 2, no. 1, pp. 52–62, 2015.

[70] Y. Li and T. Zhu, "Using Wi-Fi signals to characterize human gait for identification and activity monitoring," in *Proceedings of First IEEE International Conference on Connected Health: Applications, Systems and Engineering Technologies (CHASE),*, 2016, pp. 238–247.

[71] Q. Xu, Y. Chen, B. Wang, and K. R. Liu, "Radio biometrics: Human recognition through a wall," *IEEE Transactions on Information Forensics and Security*, vol. 12, no. 5, pp. 1141–1155, 2017.

[72] C. Shi, J. Liu, H. Liu, and Y. Chen, "Smart user authentication through actuation of daily activities leveraging WiFi-enabled IoT," in *Proceedings of 18th ACM International Symposium on Mobile Ad Hoc Networking and Computing*, 2017, p. 5.

[73] N. Zhao, A. Ren, M. U. Rehman, Z. Zhang, X. Yang, and F. Hu, "Biometric behavior authentication exploiting propagation characteristics of wireless channel," *IEEE Access*, vol. 4, pp. 4789–4796, 2016.

[74] J. Andreu-Perez, D. R. Leff, H. M. Ip, and G.-Z. Yang, "From wearable sensors to smart implants—Toward pervasive and personalized healthcare," *IEEE Transactions on Biomedical Engineering*, vol. 62, no. 12, pp. 2750–2762, 2015.

[75] Y. Zhang, G. Pan, K. Jia, M. Lu, Y. Wang, and Z. Wu, "Accelerometer-based gait recognition by sparse representation of signature points with clusters," *IEEE transactions on cybernetics*, vol. 45, no. 9, pp. 1864–1875, 2015.

[76] R. Ferrero, F. Gandino, B. Montrucchio, M. Rebaudengo, A. Velasco, and I. Benkhelifa, "On gait recognition with smartphone accelerometer," in *Proceedings of 4th Mediterranean Conference on Embedded Computing (MECO)*, 2015, pp. 368–373.

[77] W. Xu, G. Lan, Q. Lin, S. Khalifa, N. Bergmann, M. Hassan, and W. Hu, "KEH-Gait: Towards a mobile healthcare user authentication system by kinetic energy harvesting," in *Proceedings of Network and Distributed System Security Symposium (NDSS)*, 2017.

[78] S. A. Salehi, M. Razzaque, I. Tomeo-Reyes, and N. Hussain, "IEEE 802.15.6 standard in wireless body area networks from a healthcare point of view," in *Proceedings of 22nd Asia-Pacific Conference on Communications (APCC)*, 2016, pp. 523–528.

[79] S. Van Roy, F. Quitin, L. Liu, C. Oestges, F. Horlin, J.-M. Dricot, and P. De Doncker, "Dynamic channel modeling for multi-sensor body area networks," *IEEE Transactions on Antennas and Propagation*, vol. 61, no. 4, pp. 2200–2208, 2013.

[80] L. Hanlen, V. Chaganti, B. Gilbert, D. Rodda, T. Lamahewa, and D. Smith, "Open-source testbed for body area networks: 200 sample/sec, 12 hrs continuous measurement," in *Proceedings of IEEE 21st International Symposium on Personal, Indoor and Mobile Radio Communications Workshops (PIMRC Workshops)*, 2010, pp. 66–71.

[81] N. Alexandratos, J. Bruinsma *et al.*, "World agriculture towards 2030/2050: The 2012 revision," Food and Agriculture Organization of the United Nations, Tech. Rep. 12-03, 2012.

Part II

Included Papers

Paper I

M. Mohamed, M. Cheffena, F. Perez-Fontan, and A. Moldsvor, "A dynamic channel model for indoor wireless signals: Working around interference caused by moving human bodies," *IEEE Antennas and Propagation Magazine,* vol. 60, no. 2, pp. 82-91, 2018.

Paper I

A Dynamic Channel Model for Indoor Wireless Signals: Working Around Interference Caused by Moving Human Bodies

Marshed Mohamed, Michael Cheffena, Fernando P. Fontán, and Arild Moldsvor

1 Introduction

The use of indoor wireless devices has substantially increased in recent years. This escalation is due to the expansion of traditional communication devices such as mobile phones and laptop computers, to less traditional ones such as wirelessly communicating sensor nodes present in smart homes, office buildings, and industrial environments. The placement of these nodes varies considerably from one application to the next, but when the nodes are placed indoors and within the vicinity of human height, a body's movement can cause significant time-varying channel conditions. The movement is even more compelling in such networks because of the power constraints involved [1]. Thus, an accurate study on the impact of a moving body and the characteristics of indoor propagation channels is important.

Many of the studies on the effects of human bodies on radio propagation in an indoor environment are purely statistically based as in [2–5]. These types of studies provide empirical insights about the channel based on the conducted measure-

ments. To gain a deeper understanding, however, a deterministic approach must be taken. To do this, a good approximation of the shapes of obstacles and their positions in the propagation environment is needed. M. Ghaddar et al. [6] demonstrated that a conducting cylinder at microwave frequencies can approximate the presence of a human body. With the canonical shape of a conducting cylinder, the uniform theory of diffraction (UTD) can be used to compute the total received field. The UTD can account for the reflected waves and, more importantly, the phenomenon of creeping waves, which cannot be predicted with geometrical optics and the Kirchhoff diffraction equation [7, 8].

A single-cylinder human model presented in [6] together with ray tracing and UTD was used in [9] and [10] to study the fading effects caused by the movement of a human body in an indoor environment. However, the cylindrical human model proposed in [6] could be an oversimplification of shape and movement, especially when it comes to the lower part of the human body. This is because neither the human shape nor the movement is as uniform as assumed in the model. A more accurate model of representing a human body and its movement is presented in [11] and [12]. We used this model in conjunction with ray tracing and UTD calculations to determine a more accurate characterization of the propagation mechanisms of indoor radio channels as they are affected by moving human bodies, which is important for the design of robust indoor wireless systems in crowded environments.

We investigated the effect of a moving human body crossing the line-of-sight (LOS) link of the transmitter and receiver at different heights, and we developed a dynamic channel model to account for this interference (Figure 1). Unlike the scenarios reported in [8–10], we used a human body model with 12 body parts represented by dielectric cylindrical volumes of different radii, except for the head, which was represented as a sphere. We also utilized a human walking model to describe the movement of the different body parts [11, 12]. We used ray tracing and UTD to accurately calculate the received direct, reflected, and diffracted rays during time-varying channel conditions caused by the movement of the human body parts. We compared our developed model to one reported in [6] with radio-frequency (RF) measurements at different heights of the transmitting and receiving antennas.

2 The Human Walking Model

The human gait has been studied extensively in bio-mechanics and robotics, leading to the development of computer-animated walking models as reported in [13] and [14]. Such models provide detailed information on the movement of human body parts, which is necessary to characterize the impact of such movement on time-varying wireless channels. One commonly used computer-animated walking

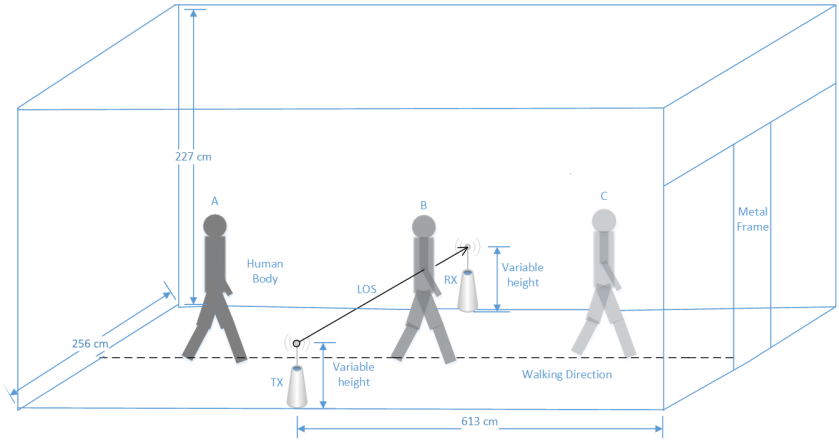

Figure 1: An indoor propagation scenario for a signal affected by a moving human body. The height of Tx and Rx was varied so that the effect of the upper body (the trunk and arms) and the lower body (the legs) on the radio propagation channel could be studied in similar conditions.

sequence is the Thalmann model [11, 12, 15].

In the Thalmann model, the human body is composed of 12 body parts (legs, arms, trunk, head, and so on), 11 of which can be represented by cylinders of various sizes. The head is represented by a sphere, as shown in Figure 3 [11, 15]. These body parts are connected to each other by translations and rotations (see Table 1 for descriptions) that are time dependent.

In the Thalmann model a walking cycle is defined as the portion of motion between two successive contacts of the left heel with the floor, as shown in Figure 2 [11, 15]. While the temporal structure is normalized by performing modular arithmetic between the time and period, the spatial values are normalized by the height of the thigh (H_{th}). We will be using relative velocity, v_r, and relative time, t_r, which can be expressed as shown in (1) and (2) where v is velocity, t is time, and T is the period of one cycle.

$$v_r = \frac{v}{H_{th}} \tag{1}$$

and

$$t_r = \left| \frac{t}{T} \right|_{\text{mod } 1} \tag{2}$$

There is an important relationship between the relative velocity of a normal walk-

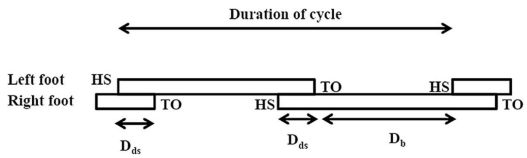

Figure 2: The temporal structure of the walking cycle. HS: heel strike; TO: toe off; D_{ds}: duration of double support; D_b: duration of balance [15].

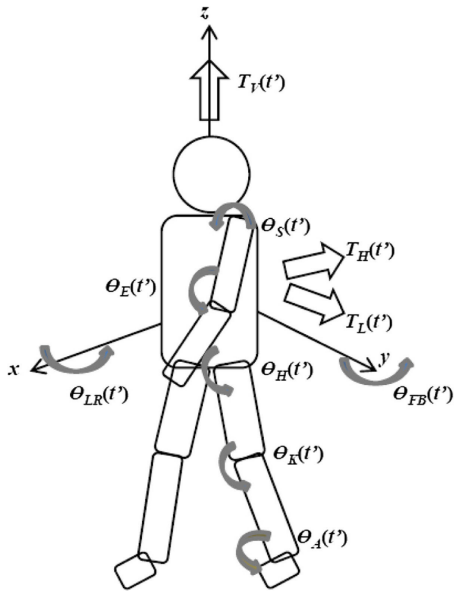

Figure 3: The human body model with translations and rotations [15].

Table 1: Human Body Parts Translations and Rotations Description.

Parameter	Symbol
Lateral translation	$T_L(t')$
Horizontal translation	$T_H(t')$
Vertical translation	$T_V(t')$
Forward/backward angle	$\theta_{FB}(t')$
Left/right angle	$\theta_{LR}(t')$
Shoulder angle	$\theta_S(t')$
Elbow angle	$\theta_S(t')$
Hip angle	$\theta_S(t')$
Knee angle	$\theta_S(t')$
Ankle angle	$\theta_S(t')$

ing person and its cycle period, T, given by (3) [11, 12, 15] as

$$T = \frac{1.346}{\sqrt{v_r}} \tag{3}$$

All of the trajectories in [12] are expressed as a function of relative time, which ranges between zero and one. They are synchronized with the left leg motion, and the left heel strike is the origin [12, 15]. The trajectories of the right part of the body are obtained by performing phase displacement of half a cycle given by

$$t_{rr} = \left| \frac{t}{T} + 0.5 \right|_{mod1} \tag{4}$$

For modeling the trajectories of flexing at the knee, hip, and elbow, a cubic spline that passes through control points located at the extremities of the trajectories is used. These control points define the angle of rotations and relative time and are a function of the relative velocity. The cubic spline used is a basic Hermit spline given by [12] as

$$h = -2s^3 + 3s^2 \tag{5}$$

where s is the increasing portion of relative time.

On the other hand, the trajectories of flexing the shoulder are found by using

$$\theta_s(t_r) = -3 - 9.88v_r[0.5 + \cos(2\pi t_r)] \tag{6}$$

Figure 4 shows the variation of the elbow and the knee (for the left side of the body) for one walking cycle with relative velocity of unity obtained using the described method. Details of the human walking model can be found in [12]. The time dependent body part translations and rotations are used with ray tracing and UTD calculations to characterize the time varying channel conditions of indoor wireless systems caused by moving human bodies.

3 Ray Tracing and UTD

A method where diffraction can be incorporated into a geometrical strategy and phrased in geometric terms forms the basis for what has become known as the geometrical theory of diffraction. The original form of this theory, however, suffers from the shadow boundaries problems. The UTD was developed to solve this problem [16, 17]. The first step before applying the UTD is to use ray tracing techniques to find different paths for the electromagnetic waves [7]. We first considered circular cylinders to represent two human legs crossing the LOS path between the

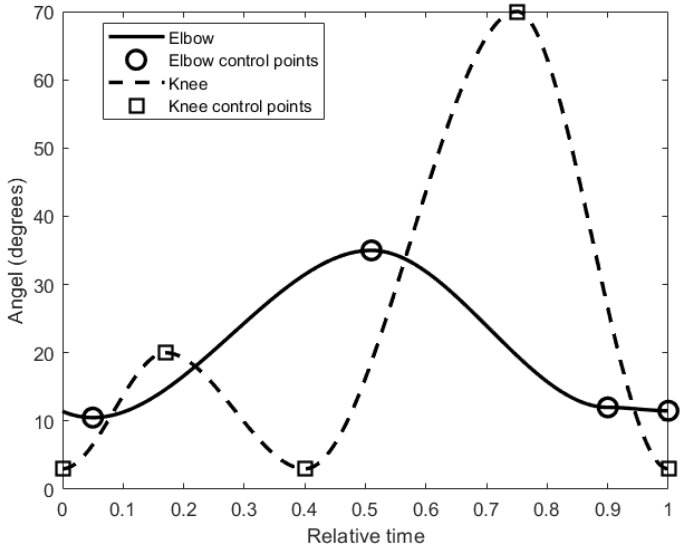

Figure 4: The angular rotation of the elbow and knee with $v_r = 1$ obtained using a cubic spline passing through control points.

transmitter and the receiver as shown in Figure 5(a). A maximum of four types of rays could exist depending on the relative position between the cylinders and the transmission link: a direct ray that exists when none of the cylinders are blocking the LOS, in which case the receiver is considered to be in a lit region; a reflected ray from each cylinder that can only exist when laws of reflection can be satisfied and neither the incident nor the reflected ray is blocked from its path; and two diffracted rays from each cylinder that can only exist if neither the incident ray nor the diffracted ray from one cylinder is blocked from its direct path by the other cylinder. Higher orders of reflected and diffracted rays are neglected. A similar ray-tracing method is used for the upper body, using three cylinders representing the two arms and the trunk [Figure 5(b)].

If we consider transmission in an indoor environment, reflections from the floor, ceiling, and walls will contribute to the total received signal. The total received electric field, ET, can then be found by summing the contributions given by each ray as in [7, 16]:

$$E_T(Rx) = E_i(Rx) + \sum_{n=1}^{K} E_{rn}(Rx) + \sum_{n=1}^{M} E_{dn}(Rx) + \sum_{n=1}^{N} E_{rfn}(Rx) \qquad (7)$$

where E_i is the incident field, K is the total number of cylinder reflected fields

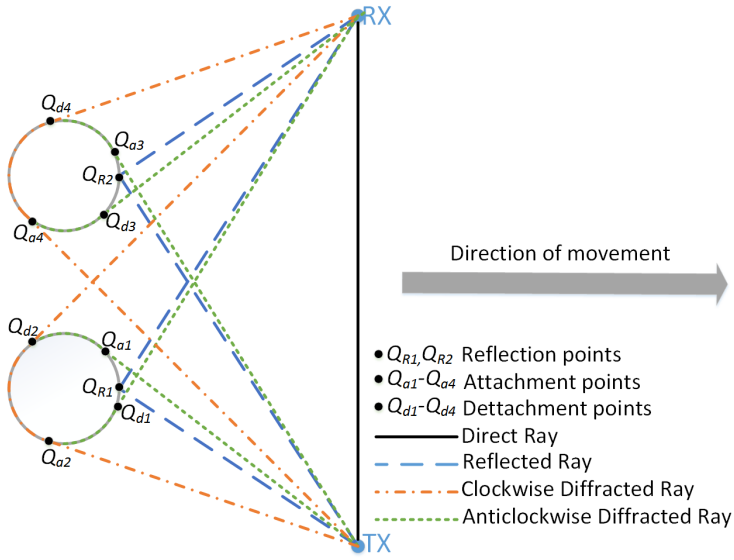

(a)

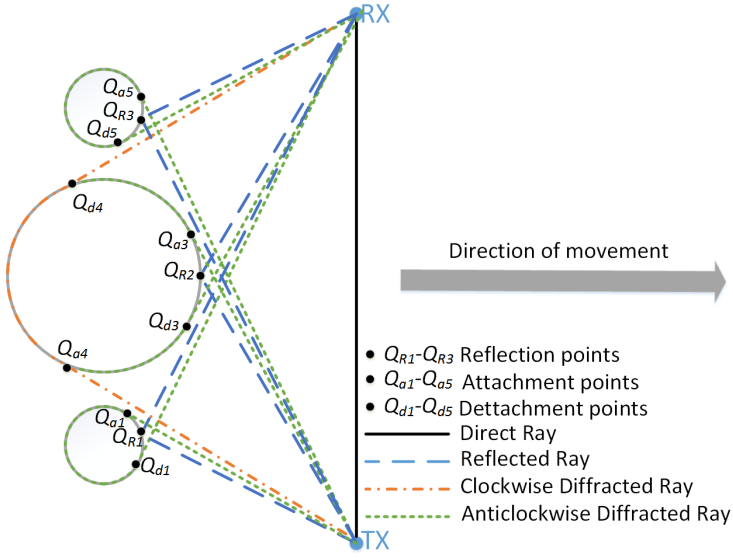

(b)

Figure 5: Ray tracing. (a) Two cylinders representing two legs. (b) Three cylinders representing two arms and the trunk. In the current position, the arm's clockwise diffracted rays are blocked by the trunk.

E_{rn}, M is the total number of diffracted fields E_{dn}, and N is the total number of the flat surface-reflected fields E_{rfn}.

The incident field can be expressed as

$$E_i(Rx) = C_0 \frac{e^{-jks_0}}{s_0} \tag{8}$$

where s_0 is the distance between the point of transmission and the point of observation, and C_0 is a constant associated with incident field power [7, 16].

The cylinder-reflected field can be expressed as

$$E_{rn}(Rx) = \sqrt{\frac{\rho^r_{1n}.\rho^r_{2n}}{(\rho^r_{1n}+s_{rn})(\rho^r_{2n}+s_{rn})}} R^n_{\parallel\perp}.E_i(Q_{Rn}).e^{-jks_{rn}} \tag{9}$$

where s_{rn} is the distance between the reflection point and the receiver, ρ^r_{1n} and ρ^r_{2n} are the radii of curvature of the reflected field, and $R^n_{\parallel\perp}$ is the polarization-dependent reflection coefficient as given in [7, 16], where the diffracted field can be expressed as

$$E_{dn}(Rx) = \sqrt{\frac{\rho^d_{2n}}{s_{dn}(\rho^d_{2n}+s_{dn})}}.D^n_{\parallel\perp}.\sqrt{\frac{d\eta(Q_{an})}{d\eta(Q_{dn})}}.E_i(Q_{an}).e^{-jks_{dn}} \tag{10}$$

Here, ρ^d_{2n} is the second radius of curvature of the diffracted field, s_{dn} is the distance between the detachment point and the receiver, Q_{an} and Q_{dn} are the attachment and the detachment points, respectively, $D^n_{\parallel\perp}$ is the polarization dependent diffraction coefficient, and $\sqrt{d\eta(Q_{an})/d\eta(Q_{dn})}$ is the conservation of energy flux in the surface ray strip from attachment to detachment point [7, 16].

The flat surface-reflected field is given by

$$E_{rfn}(RX) = E_i(Q_{RFn}) R^n_{f\parallel\perp}.\frac{e^{-jks_{rn}}}{s_r n} \tag{11}$$

where Q_{RFn} is a reflection point on a flat surface and $R^n_{f\parallel\perp}$ is the reflection coefficient of the flat surface [8, 18].

During the walking sequence, the overall signal fading is caused by the position-dependent reflection, diffraction, and shadowing of direct fields related to the movement of specific body parts. These body parts are represented by cylinders, and their movement and position are determined using the human walking model discussed in the section, "The Human Walking Model." The total field is obtained by summing the contributions from these dynamic body parts calculated using the UTD along with first-order contributions from the environment.

Table 2: The Human Model Parameters.

Human Element	Length Symbol	Length Value	Radius Value
Head	R_H	-	0.11
Torso	H_T	0.72	0.13
Upper leg	H_{UL}	0.45	0.09
Lower leg	H_{LL}	0.45	0.06
Upper arm	H_{UA}	0.30	0.05
Lower arm	H_{UA}	0.40	0.04
Feet	H_F	0.18	0.06

4 Measurement Setup

Indoor RF measurements were taken to validate the developed channel model and to compare it with existing models. The principal measurement setup is shown in Figure 6. The vector network analyzer was used to transmit and receive an RF signal at 2.45 GHz with a power of 10 dBm at the transmitting port. Vertically polarized omnidirectional antennas were used at both the transmitting and the receiving ports. The received signal was measured for a period of 8 s, with a sampling time of 1 ms between two adjacent points. The transmitting and receiving antennas were separated by a distance of 206 cm, both adjusted to a height of 25.5 cm to represent crossing of the LOS path by the lower body (the legs), and then at a height of 128.5 cm to represent crossing of the LOS path by the upper body (the trunk and arms) as shown in Figure 6.

The selected low heights are common in wireless sensor networks found in smart homes and offices, and industrial environments where the position of the sensor depends on the phenomenon being monitored (e.g., machine health monitoring, greenhouse monitoring, geofencing of robots, and so on). A single person with parameters given in Table 2 walked past the antennas during the experiments at a continuous speed of approximately 1.1 m/s along a path that was perpendicular to the LOS direction, as shown in Figure 1. A complex permittivity of the materials involved is given in Table 3 [18, 19]. At frequencies where attenuation through the body is quite large, the dielectric properties of the human body can be assumed to be equal to that of the outer layer of the body; hence, the permittivity of human muscle tissues was used [20].

5 Model Validation

To validate the developed model explained in the section "Ray Tracing and UTD," measurements were taken at two different heights to represent crossing of the LOS

(a)

(b)

Figure 6: The measurement setup at different antenna heights: (a) 25.5 cm and (b) 128.5 cm.

Table 3: The Relative Permittivity of Different Materials.

Material	Relative Permittivity at 2.45 GHz	Relative Permittivity at 31.8 GHz
Plasterboard	$2.94 - 0.1607i$	$2.94 - 0.07591i$
Concrete	$5.31 - 0.4947i$	$5.31 - 033036i$
Ceiling board	$1.50 - 0.0104i$	$1.50 - 0.0158i$
Ceiling muscle	$52.73 - 13.0410i$	$19.01 - 23.7125i$

path by the lower body (the legs) and the upper body (the trunk and arms) and compared with the results obtained from the simulation of the scenario shown in Figure 1. The results were also compared with simulation results obtained when a human body is modeled as a single, vertically oriented, dielectric cylinder (i.e., a single cylinder model) as proposed in [6].

We started the comparison in the time domain where the overall shape of the signal and its fading was established. It is important to note that, in both models, the received signal could be categorized into two regions: 1) a lit region where no obstacle is blocking the LOS path and 2) a shadow region where an obstacle blocks the LOS path. Although the different models yield different magnitudes, shapes, and duration of fades, these two regions can easily be observed in both models and in the measurements. The distribution of the signal and its fading can be further observed using the cumulative distribution function (CDF), which provides the probability of a signal being below a certain value. The CDF is commonly used in the performance evaluation of a channel with regard to the channel capacity, outage probabilities, and so on.

Figure 7 shows the comparison between the developed model, a single-cylinder model, and measured data when the transmitter and the receiver are set at a height of 25.5 cm. The results reveal agreement between the developed model simulation's results and the measurements. We also observed that the single-cylinder model over predicted the magnitude of fading in the shadow region. The difference is caused by the physical interaction of the electromagnetic waves when the legs are represented using two swaying cylinders with small radii (6 cm) [see Figure 5(a)] instead of a single cylinder with a large radius (13 cm) moving at a constant speed.

Additional comparisons were performed by processing the data of both models and the measurements to obtain their second-order statistics. More specifically, we measured the rapidity of the fading by quantifying how often the signal crosses a certain threshold and how long it stays below it. These statistics, known as level crossing rate and average fade duration, respectively, are important in comparing the time-varying properties of the received signals. Figure 8 shows the comparison of level crossing rate and the average fade duration of the received signal normalized to their root mean square (rms) values when the transmitter and receiver are set at a height of 25.5 cm. As in Figure 7, we observed an agreement between the developed model simulation's results and the measurements and a significant difference with the results of the single-cylinder model.

When the height of the transmitter and the receiver is changed to 128.5 cm, representing the upper body crossing the LOS path, the difference between the single-

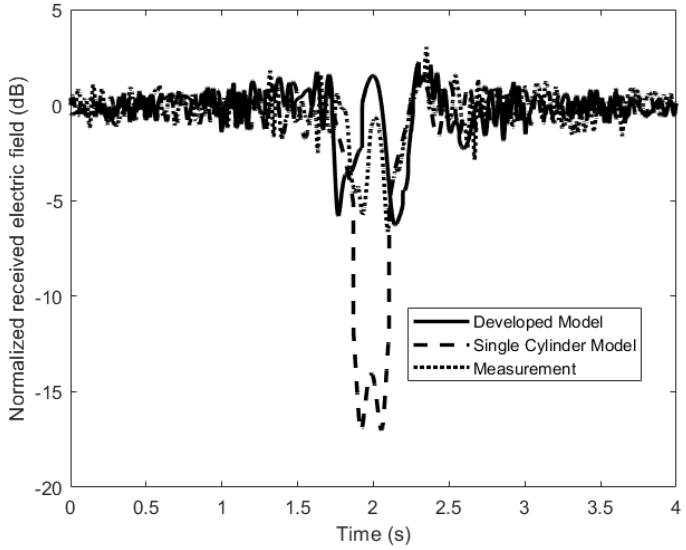

(a)

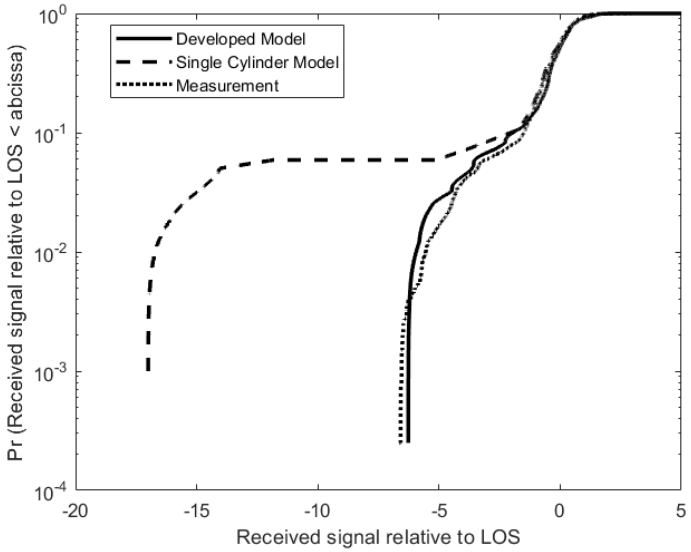

(b)

Figure 7: A comparison of a normalized received signal obtained from a developed model simulation, a single-cylinder simulation, and collected data when both the transmitter and receiver are at a height of 25.5 cm. (a) shows the time series, and (b) shows the CDF.

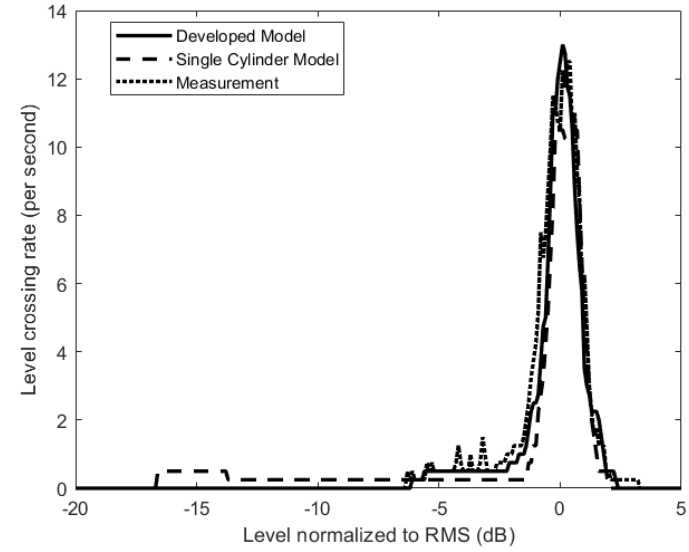

(a)

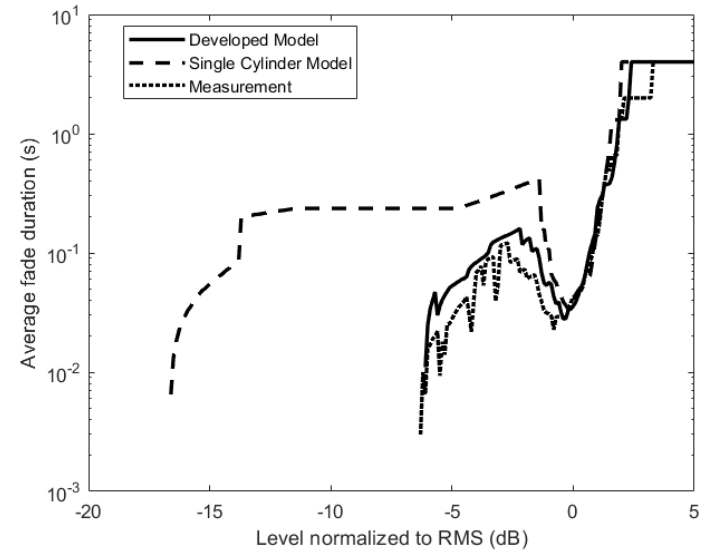

(b)

Figure 8: A comparison of second-order statistics obtained from a developed model simulation, a single-cylinder simulation, and collected data when both the transmitter and receiver are at a height of 25.5 cm. (a) shows the level crossing rate, and (b) shows the average fade duration.

cylinder model and the developed model is decreased. This is because, at this height, the only difference between the two models is the inclusion of the arms and their movement in the developed model. Comparison between the two models and measurement values when the transmitter and receiver are set at a height of 128.5 cm are shown in Figure 9 (time domain and CDF) and in Figure 10 (second-order statistics). Again, we observed excellent agreement between the developed model simulation and the measurements.

At the measured frequency of 2.45 GHz, the differences at the 128.5 cm height are relatively small between the two models. However, at higher frequencies, e.g., the millimeter-wave region, the differences are much more pronounced. At these frequency bands, the attenuation of the diffracted rays is quite large, causing very deep fades in the non-LOS (NLOS) region when a single-cylinder model is used. The addition of arms and their relative movement in the developed model significantly increased the overall power received in the NLOS region due to the overall contribution (through reflection and diffraction) from these body parts and thus became more important to include. Figure 11 shows the results of a simulation of the two models performed at a frequency of 31.8 GHz, which is relevant for future fifth-generation systems. There is a clear difference between the results of the single-cylinder model and those of the developed model for the effects of upper body parts.

The measured results validate the model and show the large difference in radio link characterization in the presence of human disturbances when the height of the transmission link is changed [Figure 12(a)]. When the transmission link is set at a height where an upper body crosses the LOS path, there are deeper fades in the shadow region. These fades are two-times lower in the decibel scale compared to fades that occur when the transmission link is set at a height where the lower body crosses the LOS path. This is because the size and movement of the body parts involved are significantly different for these two heights.

The difference in the fading characteristics is emphasized even more by looking at the average fade duration of the two transmission links. In addition to the presence of deeper fading, the links obstructed by the upper body also have longer average fade duration in the shadow region. In the lit region, however, the average fade duration are approximately the same regardless of the link height, and they are determined primarily by the walking velocity. This is shown in Figure 12(b) when the level normalized to the rms is greater than -3.5 dB. These results show how significant the height of the transmission link is in an indoor environment. Additionally, the validation obtained here encourages the use of the developed model to be applied to similar studies and not limited to the propagation scenario of Figure 1.

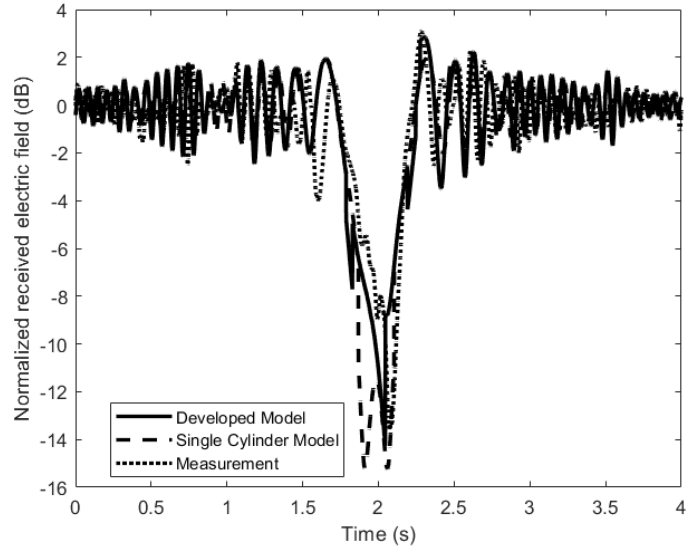

(a)

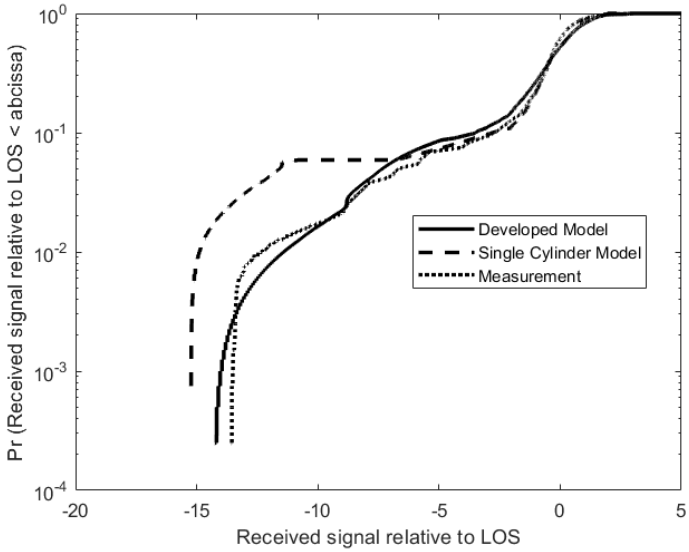

(b)

Figure 9: A comparison of a normalized received signal obtained from a developed model simulation, a single-cylinder simulation, and collected data when both the transmitter and receiver are at a height of 128.5 cm. (a) shows the time series, and (b) shows the CDF.

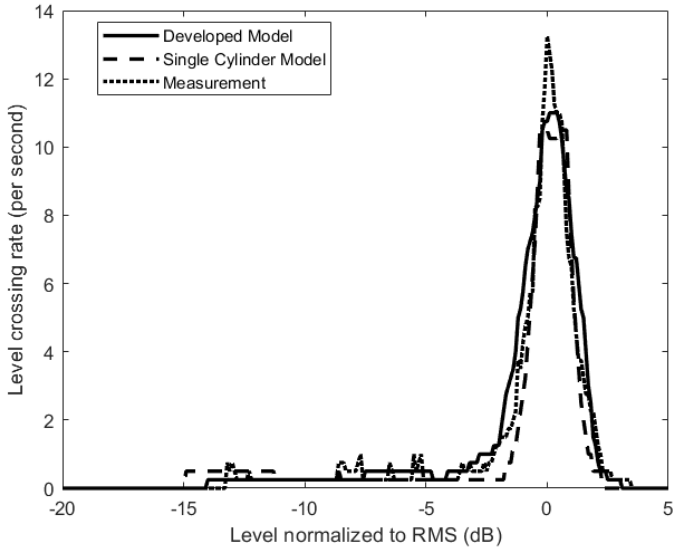

(a)

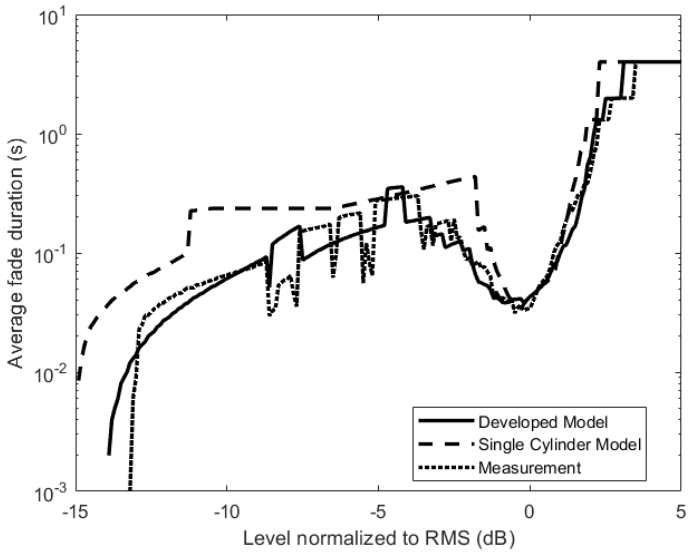

(b)

Figure 10: A comparison of second-order statistics obtained from a developed model simulation, a single-cylinder simulation, and collected data when both the transmitter and receiver are at a height of 128.5 cm. (a) shows the level crossing rate, and (b) shows the average fade duration.

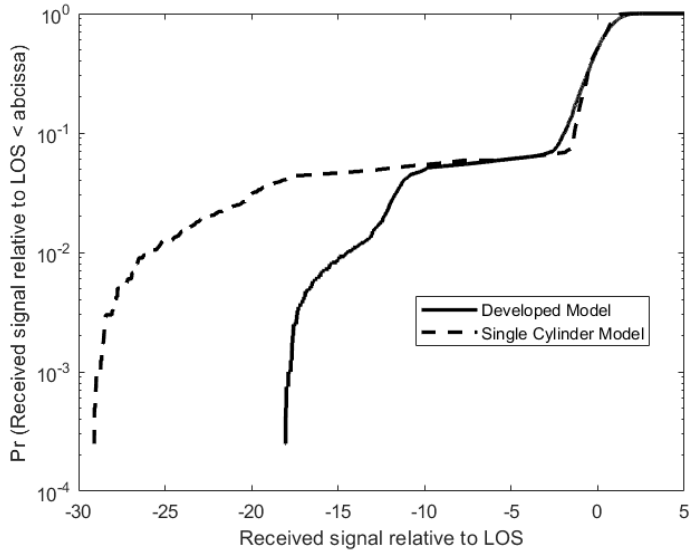

(a)

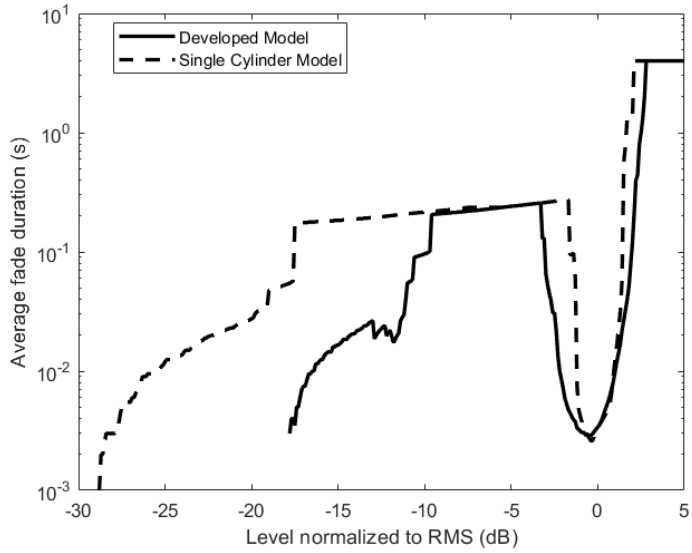

(b)

Figure 11: A comparison of fading characteristics of a normalized received signal obtained from a developed model simulation and a single-cylinder simulation when both the transmitter and receiver are at a height of 128.5 cm with a transmission frequency of 31.8 GHz. (a) shows the CDF, and (b) shows the average fade duration.

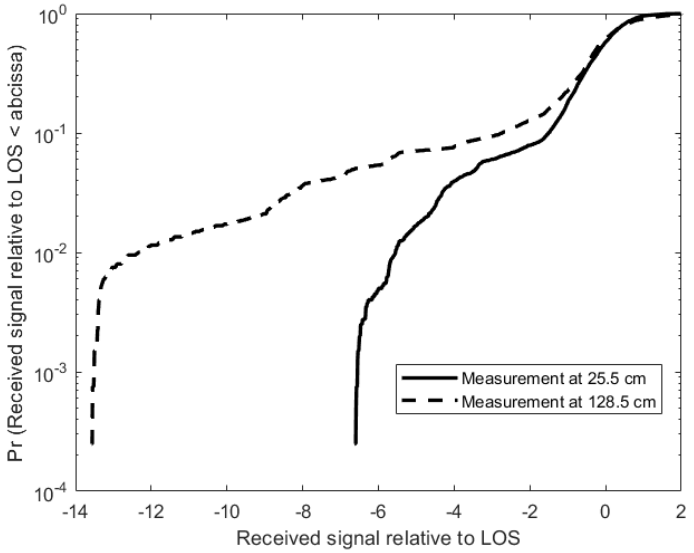

(a)

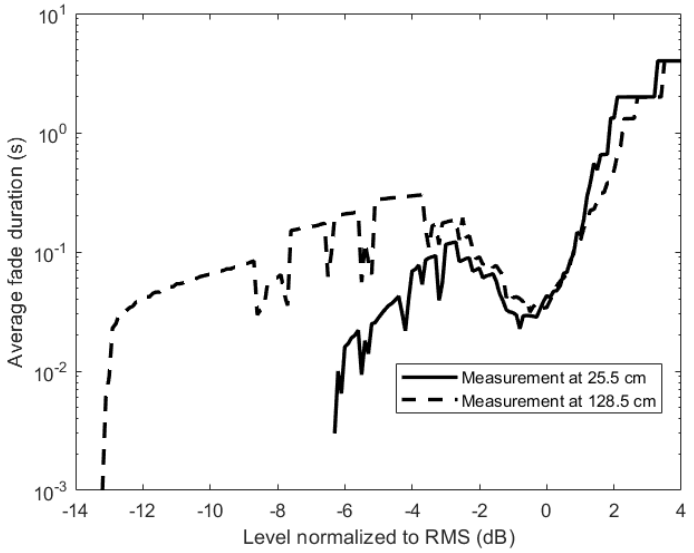

(b)

Figure 12: A comparison of fading characteristics of a normalized measured received signal obtained when both the transmitter and receiver are at a height of 25.5 cm and then at 128.5 cm. Transmission frequency was set at 2.45 GHz. (a) shows the CDF, and (b) shows the average fade duration.

6 Conclusions

We have presented a dynamic channel model for the signal affected by moving human bodies in an indoor environment. We modeled the human body as a combination of 11 vertically oriented, dielectric, cylindrical volumes and a spherical head. The received signal was composed of a direct component, together with first-order reflected and diffracted components from the human body, which were subjected to time-varying shadowing effects in relation to the dynamic movement of body parts. The diffracted field from the canonically shaped body parts was calculated using UTD. First-order reflected components from the environment were also taken into consideration.

The developed model was validated using RF measurements at 2.45 GHz. The measurement was conducted at two different heights to study the effects on the channel from the movement of both lower and upper body parts. The results showed a strong agreement between the developed model and the measurements at both heights. We also compared these results with those obtained with a simpler model consisting of only one vertical cylinder moving with a constant speed. As expected, the differences between the two models were quite large for the lower body parts, while the differences were smaller for the upper body parts at the measured frequency. When we increased the frequency into the millimeter-wave region (i.e., from 2.45 to 31.8 GHz), the simulations showed a substantial difference between the two models.

The measurements and the conducted simulations also showed that there is a significant difference on the propagation channel characteristics with different transmitter and receiver antenna heights and that a more accurate model is increasingly important for future applications where the frequency will increase into the millimeter-wave region.

Author Information

Marshed Mohamed (marshed.mohamed@ntnu.no) is a Ph.D. candidate at the Norwegian University of Science and Technology, Trondheim. His research interests include the modeling and prediction of radio channels for wireless body area networks.

Michael Cheffena (michael.cheffena@ntnu.no) is a full professor at the Norwegian University of Science and Technology, Trondheim. His research interests include modeling and prediction of radio channels for both terrestrial and satellite links.

Fernando Pérez Fontán (fpfontan@tsc.uvigo.es) is a full professor with the Tele-

communications Engineering School, University of Vigo, Spain. His research interests are in the field of terrestrial and satellite mobile and fixed radio communication propagation channel modeling.

Arild Moldsvor (arild.moldsvor@ntnu.no) is an associate professor at the Norwegian University of Science and Technology, Trondheim. His research interests include antenna design for both terrestrial and satellite links.

References

[1] I. F. Akyildiz, W. Su, Y. Sankarasubramaniam, and E. Cayirci, "Wireless sensor networks: A survey," *Computer Networks*, vol. 38, no. 4, pp. 393–422, 2002.

[2] M. Ayadi and A. B. Zineb, "Body shadowing and furniture effects for accuracy improvement of indoor wave propagation models," *IEEE Transactions on Wireless Communications*, vol. 13, no. 11, pp. 5999–6006, 2014.

[3] K. Saito, K. Kitao, T. Imai, Y. Okano, and S. Miura, "Data analysis and modeling method for indoor human body-shadowing MIMO channels," in *Proceedings of 6th European Conference on Antennas and Propagation*, 2012, pp. 1431–1435.

[4] H. Hongwei, S. Wei, X. Youzhi, and Z. Hongke, "The effect of human activites on 2.4 GHz radio propagation at home environment," in *Proceedings of 2nd IEEE International Conference on Broadband Network & Multimedia Technology*, 2009, pp. 95–99.

[5] A. Kara and H. L. Bertoni, "Effect of people moving near short-range indoor propagation links at 2.45 GHz," *Journal of Communications and Networks*, vol. 8, no. 3, pp. 286–289, 2006.

[6] M. Ghaddar, L. Talbi, T. A. Denidni, and A. Sebak, "A conducting cylinder for modeling human body presence in indoor propagation channel," *IEEE Transactions on Antennas and Propagation*, vol. 55, no. 11, pp. 3099–3103, 2007.

[7] E. Plouhinec, "D2.1b—On-body antennas characterization and exploitable radiation properties—Updated document: 3-D deterministic modeling of

electromagnetic wave interactions with a dielectric cylinder," Agence Nationale de la Recherche, Paris, France, Tech. Rep. CORMORAN ANR 11-INFR-010, 2012.

[8] M. Cheffena, "Physical-statistical channel model for signal effect by moving human bodies," *EURASIP Journal on Wireless Communications and Networking*, vol. 2012, no. 1, p. 77, 2012.

[9] Y. Huang, A. Charbonneau, L. Talbi, and T. A. Denidni, "Effect of human body upon line-of-sight indoor radio propagation," in *Proceedings of 2006 Canadian Conference on Electrical and Computer Engineering*, pp. 1775–1778.

[10] F. Villanese, N. E. Evans, and W. G. Scanlon, "Pedestrian-induced fading for indoor channels at 2.45, 5.7 and 62 GHz," in *Proceedings of IEEE 52nd Vehicular Technology Conference*, vol. 1, 2000, pp. 43–48.

[11] P. van Dorp and F. Groen, "Human walking estimation with radar," *IEE Proceedings-Radar, Sonar and Navigation*, vol. 150, no. 5, pp. 356–365, 2003.

[12] R. Boulic, N. M. Thalmann, and D. Thalmann, "A global human walking model with real-time kinematic personification," *The Visual Computer*, vol. 6, no. 6, pp. 344–358, 1990.

[13] M. Girard, "Interactive design of 3D computer-animated legged animal motion," *IEEE Computer Graphics and Applications*, vol. 7, no. 6, pp. 39–51, June 1987.

[14] M. Girard and A. A. Maciejewski, "Computational modeling for the computer animation of legged figures," *ACM SIGGRAPH Computer Graphics*, vol. 19, no. 3, pp. 263–270, July 1985.

[15] M. Cheffena, "Time-varying on-body wireless channel model during walking," *EURASIP Journal on Wireless Communications and Networking*, vol. 2014, no. 1, p. 29, 2014.

[16] D. McNamara, C. Pistorius, and J. Malherbe, *Introduction to the Uniform Geometrical theory of diffraction*. Norwood, MA: Artech House, 1990.

[17] P. Pathak, W. Burnside, and R. Marhefka, "A uniform GTD analysis of the diffraction of electromagnetic waves by a smooth convex surface," *IEEE Transactions on Antennas and Propagation*, vol. 28, no. 5, pp. 631–642, 1980.

[18] "Effects of building materials and structures on radiowave propagation above about 100 MHz," International Telecommunications Union Recommendation, Tech. Rep. ITU-R P.2040-1, July 2015.

[19] C. Gabriel, "Compilation of the dielectric properties of body tissues at RF and microwave frequencies," Armstrong Laboratory, Brooks Air Force Base, San Antonio, TX, Tech. Rep. AL/OE-TR-1996-0037, 1996.

[20] G. Koutitas and C. Tzaras, "A UTD solution for multiple rounded surfaces," *IEEE Transactions on Antennas and Propagation*, vol. 54, no. 4, pp. 1277–1283, 2006.

Paper II

M. Mohamed, M. Cheffena, A. Moldsvor, and F. P. Fontan, "Physical-statistical channel model for off-body area network," *IEEE Antennas and Wireless Propagation Letters,* vol. 16, pp. 1516-1519, 2017.

Paper II

Physical-Statistical Channel Model for Off-Body Area Network

Marshed Mohamed, Michael Cheffena, Arild Moldsvor, and Fernando P. Fontán

Abstract

In this letter, a physical-statistical-based channel model for off-body wireless communications is presented. The model utilizes a dynamic human walking model, which provides detailed description of the movement of the different body parts. The received signal is composed of a direct component, which might be subject to shadowing by the body parts, and a multipath component due to reflections from the environmental scatterers. The uniform theory of diffraction (UTD) is utilized to accurately calculate the time-varying shadowing and scattering effects of the direct signal due to the moving of body parts. A Rayleigh distribution is used to represent the multipath fading effects by the scatterers around the human body. The model is validated in terms of first- and second-order statistics using 2.36 GHz measurement data, showing good agreement.

Index Terms

Fading channels, indoor propagation, off-body communication, time varying channels, wireless body area network (WBAN).

1 Introduction

In recent years, there has been substantial research on wireless body area network (WBAN) due to its potential applications in health monitoring, sports activities, and any other application that requires monitoring and transmission of human physiological data. The communication could involve among others the transmission between nodes mounted on the human body (body surface node) and a node away from the human body (external node) acting as an access point [1]. This kind of communication is known as off-body communications, and is subjected to periodic signal shadowing caused by the human body movement, between the body surface node and the external node. Due to the close proximity of body surface nodes, and their need for a long battery life, WBAN requires a low-power communication approach. This demands a close understanding of the wireless channel characteristics [2].

There have been several studies on improvement of the performance of an off-body communication system. For example, in [3], diversity gain for various off-body channels was investigated, and its importance in off-body communication was noted. Measurement conducted in [4] showed that using multiple-input-multiple-output antennas drastically improves the reliability of the off-body link. A methodology for determining the optimal positions of these antennas, independent of frequency or communication standard used, was presented in [5].

The performance improvement methods presented in, e.g., [3–5] rely on good understanding of the propagation channel characteristics. An empirical characterization of off-body wireless channels is presented in [6]. The measurements were conducted in an anechoic chamber, and lognormal and Ricean distributions were used to model the path loss. In [7], similar studies were conducted in an indoor environment, where lognormal distribution proved to be a good fit in describing the normalized signal amplitude. Further studies were conducted in [8] in which also the impact of antenna polarization on channel characteristics was investigated. Nakagami distribution was used to describe the fading component.

Unlike the models in [6–8], which are purely empirically based and applicable only in the environments similar to the measurement site, we propose a more accurate physical-statistical-based channel model for off-body communications. Generally, physical-statistical models are more accurate than merely empirical models as they rely on electromagnetic-based methods for calculating the needed model parameters. They are also more effective for simulating large scenarios compared to purely physical models [9].

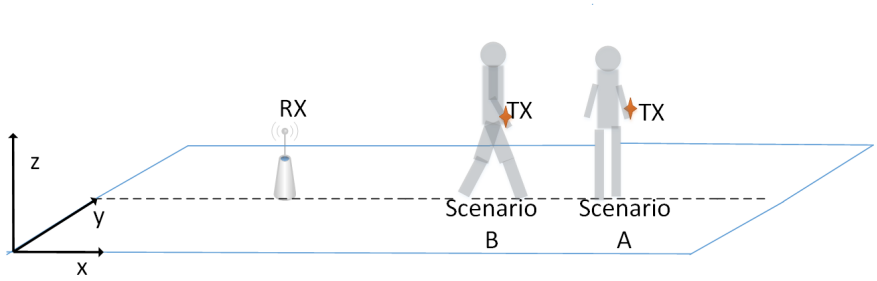

Fig. 1: Considered propagation scenarios where a person walks: A) with direction of motion perpendicular to the receiver; B) direction of motion parallel to the receiver.

2 Physical-Statistical Off-Body Channel Model

The considered propagation scenarios are shown in Fig. 1. In both scenarios, the transmitter is on the right wrist of the subject's body walking on the spot. The two scenarios are differentiated by orientation and motion of the transmitter (Tx) relative to the receiver (Rx). To obtain the locations of the body parts during movements, a human walking model, described in [10], is used. In the model, the human body is represented by 12 dielectric cylindrical volumes of different radii, except for the head that is represented by a sphere. Due to their canonical shapes, the uniform theory of diffraction (UTD) will be used to calculate, by electromagnetic computation (physically), the time-varying signal contributions from the human body. UTD can also account for the creeping waves that cannot be predicted with geometrical optics and Kirchhoff diffraction equation [9, 11]. The environmental contributions to the total received signal causes multipath fading, and will be described statistically using a Rayleigh distribution.

2.1 Contribution From the Human Body

Based on our propagation scenario shown in Fig. 1, the most significant signal contributions from the human body come from the two arms and the trunk. Considering the three cylinders representing the two arms and a trunk as shown in Fig. 2, three types of rays will exist depending on the relative position between the cylinders and the receiver. From the right arm where the transmitter is positioned, there will be diffracted rays. These rays can only exist if the trunk is not blocking their path to the receiver. From the trunk, there will be diffracted-reflected rays that only exist when the laws of reflection are satisfied, and diffracted-diffracted rays, see Fig. 2. Like the trunk, the left arm will have similar rays, but will only exist when the trunk is not blocking the left arm.

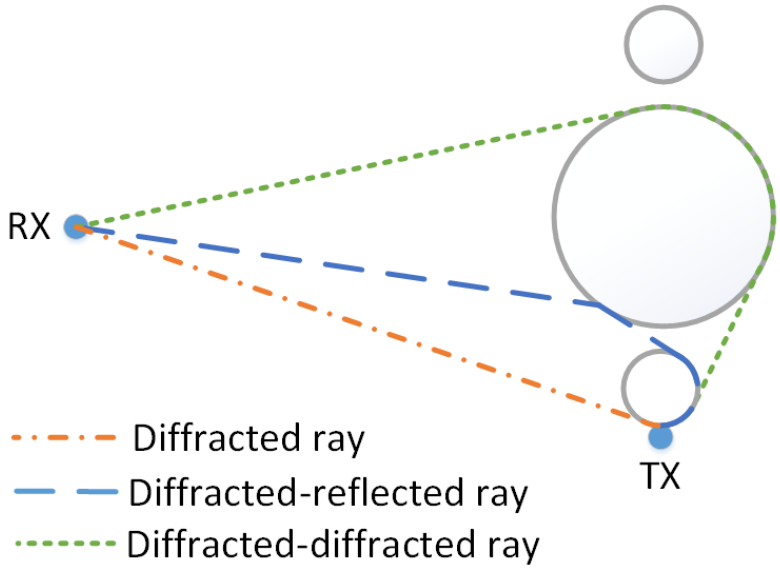

Fig. 2: Ray tracing of three cylinders. Small circles represent arms, and the large circle represents the trunk. For clarity, only one ray from each type is shown in the figure. Left arm is shadowed by the trunk from the transmitter at current position.

The diffracted field can be expressed as [12, 13]

$$E_d(Rx) = C.H_{\parallel\perp}.e^{-jkx}.\frac{e^{-jks_d}}{s_d} \tag{1}$$

where s_d is the distance between the detachment point and the receiver, and x is the distance along the surface of the cylinder between the transmitter location and the detachment point, C is a constant associated with the transmission field power, and $H_{\parallel\perp}$ is intermediate function depending on hard and soft Fock radiation functions. The diffracted-reflected field can be expressed as in [11]

$$E_{dr}(Rx) = \sqrt{\frac{\rho_1^r.\rho_2^r}{(\rho_1^r + s_r)(\rho_2^r + s_r)}} R_{\parallel\perp}.E_d(Q_R).e^{-jks_r} \tag{2}$$

where s_r is the distance between the reflection point and the receiver, ρ_1^r and ρ_2^r are the radii of curvature of the reflected field, Q_R is the reflection point, $E_d(Q_R)$ is the diffracted field given by (1), and $R_{\parallel\perp}$ is the polarization-dependent reflection coefficient as given in [11]. The total diffracted-diffracted field can be expressed as

$$E_{dd}(Rx) = \sqrt{\frac{\rho_2^d}{s_d(\rho_2^d + s_d)}}.T_{\parallel\perp}.\sqrt{\frac{d\eta(Q_1)}{d\eta(Q_2)}}.E_d(Q_1).e^{-jks_d} \tag{3}$$

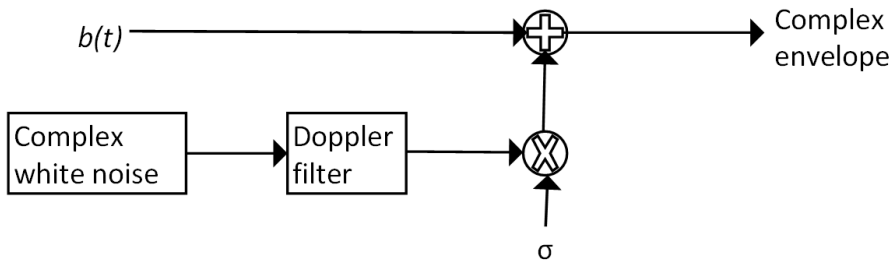

Fig. 3: Channel simulator for off-body communication. The parameter σ is the standard deviation of the multipath component, and $b(t)$ is the time-varying contribution from the human body.

Here, ρ_2^d is the second radius of curvature of the diffracted field, Q_1 and Q_2 are the attachment and detachment points, respectively, $T_{\parallel\perp}$ is the polarization-dependent diffraction coefficient, and $\sqrt{d\eta(Q_1)/d\eta(Q_2)}$ is the conservation of energy flux in the surface ray strip from the attachment to the detachment point [11]. The summation of all these fields makes up the human contribution $b(t)$ on the overall received signal, as illustrated by Fig. 3.

2.2 Contributions From the Environment

The reflection of the signal from objects around the human body results in multipath fading effects, which is described statistically using a Rayleigh distribution. The movement of the transmitter as well as the movements of people in the environment create time-varying channel conditions. Characterizing the Doppler spectra is thus important for the determination of the variance of the off-body wireless channel. The Doppler spectrum associated with this kind of movement is given by [14]

$$S(f) = \frac{1}{f^2 + e} \tag{4}$$

where e is a model constant of a value 0.094

2.3 Overall Simulation Model

The proposed physical-statistical channel model for simulating the off-body wireless channel is shown in Fig. 3. In the model, a complex white Gaussian process with zero mean and unity standard deviation is passed through a Doppler filter given in 4 for spectrum shaping. The resulting complex series is multiplied by the standard deviation σ to represent the multipath contributions from the environmental scatterers. Then, the position-dependent contributions from the human body $b(t)$, as described in Section 2.1, are added. The movement and position of

the body-worn transmitter is determined using the human walking model presented in [10].

3 Experimental Data

Publicly available experimental data collected by the National ICT Australia [2] is used for validating the developed channel model. For off-body measurements, a commercial wearable antenna was strapped to the right wrist of a 181.5-cm/78-kg male test subject and used as a transmitting antenna. Due to large movement of the arm during walking, the location is ideal for testing the performance of the proposed model under high signal dynamic conditions. The antenna was worn such that the E-plane of the antenna was perpendicular to the floor of the environment. The receive antenna was placed on an aluminum tripod 2 m away from the test subject. Both the transmitting and receiving antenna were omnidirectional and were considered as channel parts. A vector signal analyzer (VSA) was used to transmit a tone of 2.36 GHz and measure the received signal. The received signal amplitude was recorded for every 1 ms over a period of 20 s. The measurements were taken while the subject walked on a treadmill with the receiver on his left side in scenario A, and the receiver behind him in scenario B, as shown in Fig. 1. See [2] for more information on the measurement setup.

4 Model Validation and Discussion

Two different scenarios (shown in Fig. 1) are considered for validating the model developed in Section II. The resulting simulation data were then compared to the measurement data collected in [2]. The simulation parameters are shown in Table 1, where ε_r is obtained from [15], σ_A and σ_A were selected such that the simulations results fits the measured data, and the remaining parameters were obtained from the experimental setup [2]. Figs. 4(a) and 5(a), show good agreements between the measured and modeled cumulative distribution functions (CDFs) of the received signal for the two scenarios shown in Fig. 1. To validate the model further, the time-varying properties of the signal were compared by observing their level crossing rates and average fade duration for the two scenarios; see Figs. 4(b), 4(c), 5(b), and 5(c). These second-order statistics quantify how often the signal crosses a certain threshold and how long it stays below the threshold. Good agreement between the developed model simulation results and the measurement results is observed.

The agreement of both first- and second-order statistics with the measured data illustrates the accuracy of the proposed channel model. The model proposed is not limited to the location of transmitter on the arm, but can be adjusted to suit other node locations, considering their movement in relation to the human body

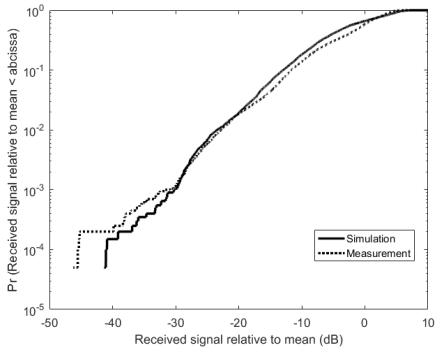

(a)

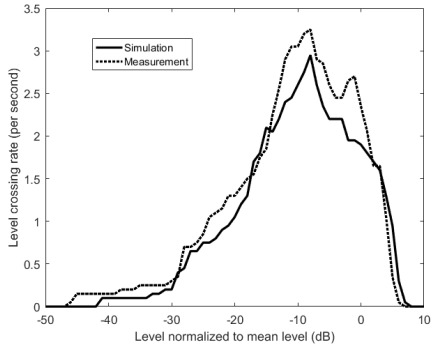

(b)

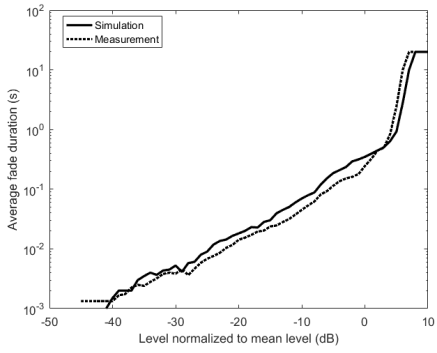

(c)

Fig. 4: Scenario A. Comparison between simulation and measurement data statistics. (a) CDF. (b) Level crossing rate. (c) Average fade duration.

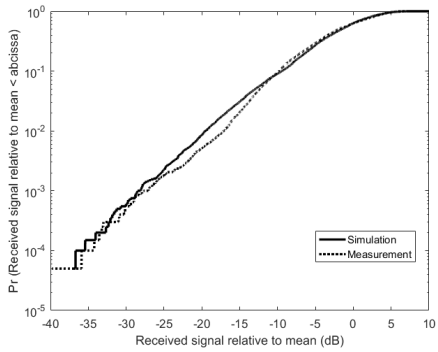

(a)

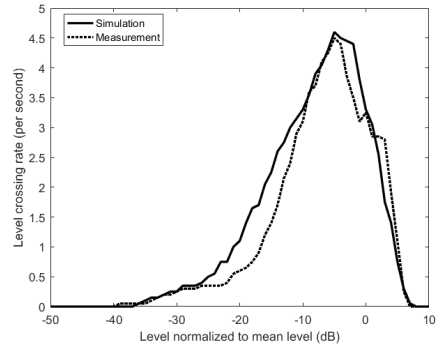

(b)

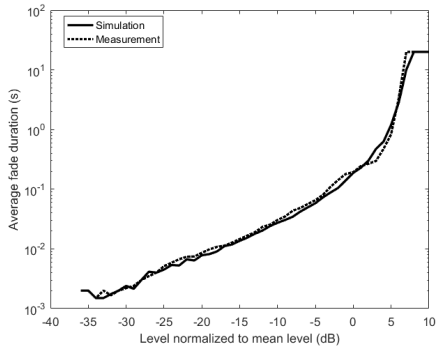

(c)

Fig. 5: Scenario B. Comparison between simulation and measurement data statistics. (a) CDF. (b) Level crossing rate. (c) Average fade duration.

Table 1: Simulation Parameters.

Parameter	Value
Frequency (f)	2.36 GHz
Relative permittivity of human skin (ε_r)	$38.0630 - 10.5847i$
Relative velocity (v_r)	1.6 m/s
Length of the upper and lower arms (l_a)	0.30 m
Radius of the arms (r_a)	0.04 m
Radius of the trunk (r_t)	0.20
σ of scenario A (σ_A)	0.0032
σ of scenario B (σ_b)	0.3700

is known. This gives an advantage over empirical models in which measurement results of one node in a given environment may not be similar or applicable to another node location or another environment.

5 Conclusion

A physical-statistical-based channel model for off-body wireless communications was developed. In this method, the detailed description of the movement of the different body parts were obtained from a dynamic human walking model. The received signal was composed of a direct component subjected to time-varying shadowing, reflection, and diffraction effects in accordance with the dynamic movement of the body parts, and a multipath component due to reflection from environmental scatterers. The human walking model together with UTD was used to calculate time-varying contributions from the body parts, and the multipath components from the environment were represented by a Rayleigh distribution. The developed model was validated in terms of first- and second-order statistics utilizing 2.36-GHz measurement data for two different propagation scenarios. The simulations showed good agreement with the measured data.

References

[1] Q. H. Abbasi, M. U. Rehman, K. Qaraqe, and A. Alomainy, *Advances in Body-Centric Wireless Wommunication*. London, UK: Institution of Engineering and Technology, 2016.

[2] D. B. Smith, L. W. Hanlen, J. A. Zhang, D. Miniutti, D. Rodda, and B. Gilbert, "First- and second-order statistical characterizations of the dynamic body area propagation channel of various bandwidths," *Annals of Telecommunications*, vol. 66, no. 3-4, pp. 187–203, 2011.

[3] Q. H. Abbasi, M. U. Rehman, H. T. Chattha, K. Qaraqe, A. Alomainy, Y. Hao, and C. Parini, "Ultra wideband antenna diversity characterisation for off-body communications in an indoor environment," *IET Microwaves, Antennas & Propagation*, vol. 8, no. 14, pp. 1161–1169, 2014.

[4] P. Van Torre, L. Vallozzi, C. Hertleer, H. Rogier, M. Moeneclaey, and J. Verhaevert, "Indoor off-body wireless MIMO communication with dual polarized textile antennas," *IEEE Transactions on Antennas and Propagation*, vol. 59, no. 2, pp. 631–642, 2011.

[5] M. Marinova, A. Thielens, E. Tanghe, L. Vallozzi, G. Vermeeren, W. Joseph, H. Rogier, and L. Martens, "Diversity performance of off-body MB-OFDM UWB-MIMO," *IEEE Transactions on Antennas and Propagation*, vol. 63, no. 7, pp. 3187–3197, 2015.

[6] S. Cotton, A. McKernan, A. Ali, and W. Scanlon, "An experimental study on the impact of human body shadowing in off-body communications channels at 2.45 GHz," in *Proceedings of the 5th European Conference on Antennas and Propagation*, 2011, pp. 3133–3137.

[7] D. Smith, L. Hanlen, J. Zhang, D. Miniutti, D. Rodda, and B. Gilbert, "Characterization of the dynamic narrowband on-body to off-body area channel," in *Proceedings of IEEE International Conference on Communications*, 2009, pp. 1–6.

[8] R. Rosini and R. D'Errico, "Off-body channel modelling at 2.45 GHz for two different antennas," in *Proceedings of 6th European Conference on Antennas and Propagation*, 2012, pp. 3378–3382.

[9] M. Cheffena, "Physical-statistical channel model for signal effect by moving human bodies," *EURASIP Journal on Wireless Communications and Networking*, vol. 2012, no. 1, p. 77, 2012.

[10] R. Boulic, N. M. Thalmann, and D. Thalmann, "A global human walking model with real-time kinematic personification," *The Visual Computer*, vol. 6, pp. 344–358, 1990.

[11] E. Plouhinec, "D2.1b—On-body antennas characterization and exploitable radiation properties—Updated document: 3-D deterministic modeling of electromagnetic wave interactions with a dielectric cylinder," Agence Nationale de la Recherche, Paris, France, Tech. Rep. CORMORAN ANR 11-INFR-010, 2012.

[12] D. McNamara, C. Pistorius, and J. Malherbe, *Introduction to the Uniform Geometrical theory of diffraction*. Norwood, MA: Artech House, 1990.

[13] P. Pathak, N. Wang, W. Burnside, and R. Kouyoumjian, "A uniform GTD solution for the radiation from sources on a convex surface," *IEEE Transactions on Antennas and Propagation*, vol. 29, no. 4, pp. 609–622, 1981.

[14] L. Liu, R. D'Errico, L. Ouvry, P. De Doncker, and C. Oestges, "Dynamic channel modeling at 2.4 GHz for on-body area networks," *Advances in Electronics and Telecommunications*, vol. 2, no. 4, pp. 18–27, 2011.

[15] C. Gabriel, "Compilation of the dielectric properties of body tissues at RF and microwave frequencies." Armstrong Laboratory, Brooks Air Force Base, TX, USA,, Tech. Rep. AL/OE-TR-1996-0037, 1996.

Paper III

M. Mohamed, M. Cheffena, and A. Moldsvor, "Characterization of the body-to-body propagation channel for subjects during Sports Activities," *Sensors,* vol. 18, no. 2, p. 620, 2018.

Paper III

Characterization of the Body-to-Body Propagation Channel for Subjects During Sport Activities

Marshed Mohamed, Michael Cheffena and Arild Moldsvor

Abstract

Body-to-body wireless networks (BBWNs) have great potential to find applications in team sports activities among others. However, successful design of such systems requires great understanding of the communication channel as the movement of the body components causes time-varying shadowing and fading effects. In this study, we present results of the measurement campaign of BBWN during running and cycling activities. Among others, the results indicated the presence of good and bad states with each state following a specific distribution for the considered propagation scenarios. This motivated the development of two-state semi-Markov model, for simulation of the communication channels. The simulation model was validated using the available measurement data in terms of first and second order statistics and have shown good agreement. The first order statistics obtained from the simulation model as well as the measured results were then used to analyze the performance of the BBWNs channels under running and cycling activities in terms of capacity and outage probability. Cycling channels showed better performance than running, having higher channel capacity and lower outage

probability, regardless of the speed of the subjects involved in the measurement campaign.

Keyword

body area networks; body-to-body communication; personal communication networks; radio propagation; time-varying channels; performance analysis

1 Introduction

The aspiration to share information in real-time between co-located body area networks has led to the creation of body-to-body wireless networks (BBWNs). In such a network, wireless devices worn by one person will transmit information wirelessly to a device worn by another person. This kind of communication will find applications in a range of areas such as team sports, emergency services, military as well as other social networking experiences [1]. As in on-body and off-body communications, BBWNs are subject to time-varying body movement and shadowing effects at both ends of the link as all transceivers will be attached to the user in one way or the other. To ensure reliable communication in such time-variant channel conditions, robust hardware and correct decision making tools throughout the protocol stack should be carefully engineered. Such engineering can only be achieved with a greater understanding of the communications channel [2].

An empirical study on the signal characteristics of outdoor body-to-body communication channels was conducted in [3] to assess the impact of typical human body movements. The movements taken into consideration are rotation, tilt, walking in line-of-sight (LOS) and non-line-of-sight (NLOS) conditions. A similar study in an indoor environment was conducted in [4] and it highlighted how a specific movement resulted in different effects on the channel dynamic properties. The study in [5] takes it further, by comparing deterministic and semi-deterministic approaches in the simulation of on-body and body-to-body networks, a semi-deterministic approach was found to be the best option. A more specific study was conducted in [6] to analyze body-to-body communications channels susceptible to shadowed fading. The statistical model proposed in [6] showed an improved fit to the signal fading compared to established models such as Lognormal, Nakagami and Rice. Unlike [6], the work in [2] focused on LOS cases in different indoor environments and showed that the communication channels have considerable variability depending on the local propagation conditions. To mitigate human body shadowing in outdoor body-to-body communication, diversity combining schemes were investigated in [7] and have shown some promising results.

While the studies performed in [2–7] cover everyday activities, there has not been

significant research into more specific applications such as sport activities. In this paper, for the first time, the body-to-body communication channel characteristics, particularly during running and cycling in an outdoor environment, are investigated. Naturally, these kinds of activities provide their own unique set of channel dynamics due to the movements and posture changes at both ends of the link. This paper presents statistical channel characteristics of two different running and cycling scenarios at the 2.4 GHz Industrial, Scientific, and Medical (ISM) band that is utilized in several standards, which are suitable for short range BBWNs. Due to the imperfection of utilizing single standard distributions in modeling BBWNs channels, [4, 8], we investigate the application of the two-state semi-Markov model (TSSMM) in the characterization of such channels. A simulation model based on TSSMM is developed and validated using the measurement data. The measurement results could also provide physical layer parameters for network simulators such as those developed in [5]. Furthermore, we analyze the performance of the investigated scenarios in terms of channel capacity and outage probability and present the results.

The rest of the paper is organized as follows: Section 2 describes the measurement campaign, presenting the body worn transceivers used and the investigated scenarios. Experimental data analysis are discussed in Section 3, followed by simulation model and its validation in Section 4. Performance analysis is presented in Section 5, Section 6 concludes the paper.

2 Measurement Campaign

The BBWN was implemented using one transmitting and one receiving node attached to the upper arm of two adult males of height 1.80 m and mass 80 kg (Subject A) and 1.85 m and mass 75 kg (Subject B), respectively, using a small strip of Velcro. The body location was chosen as it is commonly used for monitoring devices such as mobile phones during sport activities. The experiments conducted in this study were performed in a 500 m' outdoor stretch, which is part of a common running and cycling route in Gjøvik, Norway. The stretch was bounded by a road on one side and well-spaced industrial buildings on the other. The testbed was a programmable radio transceiver with non-volatile data storage, small enough to be attached on the test subjects (see Figure 1).

It is comprised of a radio transceiver, antenna, microcontroller, microSD memory card and battery. The radio transceiver is CC2500 from Texas Instruments [9]. The nodes use Wurth Electronik Group's omni-directional chip antenna with a low profile, which is a typical example of antennas to be used in body-mounted transceivers. The device was set to transmit a packet every 4 ms with a constant transmission power of 1 dBm and carrier frequency of 2.425 GHz. This sampling

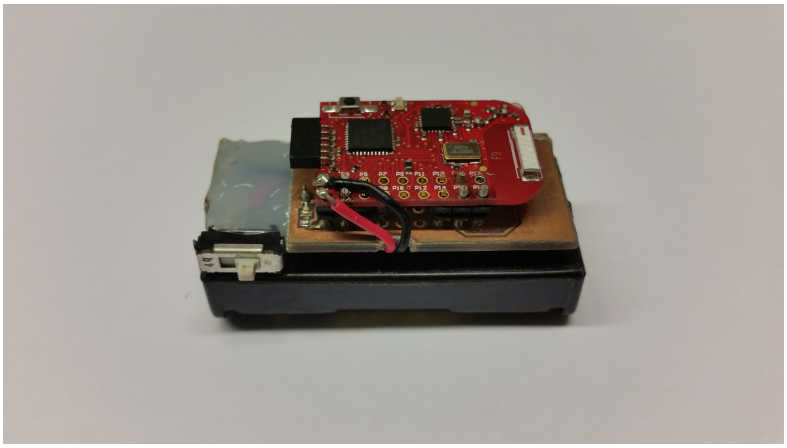

Figure 1: Wearable radio transceiver at 2.4 GHz ISM band. The device is approximately 50 mm $\times$ 20 mm $\times$ 20 mm.

period is way below the estimated coherence time (e.g., 31 ms was reported in [10]) of such channels [10]. At the receiving end, the packet number together with its received signal strength indicator (RSSI) was stored on the MicroSD memory card. The measurement was conducted during two different activities, running at an average speed of 3.33 m/s, and cycling at an average speed of 5 m/s for 500 m. With these conditions, at least 25 kilo-samples for each data set were obtained, which is enough samples for statistical analysis. In each activity, the subjects tried to maintain a separation distance of 1 m between each other. Two different scenarios, which could give an overall representation of the channel dynamics existing in these kind of activities, as shown in Figure 2, were considered:

- Scenario 1, subject behind the other, Figure 2(a).
- Scenario 2, subject beside the other, Figure 2(b).

3 Measurement Results and Analysis

A total of four data sets (two scenarios for each, running and cycling) were collected and analyzed separately. The data set were normalized to their corresponding mean values before they were processed. The data accuracy is limited by the sampling of the RSSI every 4 ms with step size of 0.5 dB. In this section, the time and frequency dynamic characteristics of the measurement results are presented using the time series, auto-correlation functions (ACF) and power spectral density (PSD).

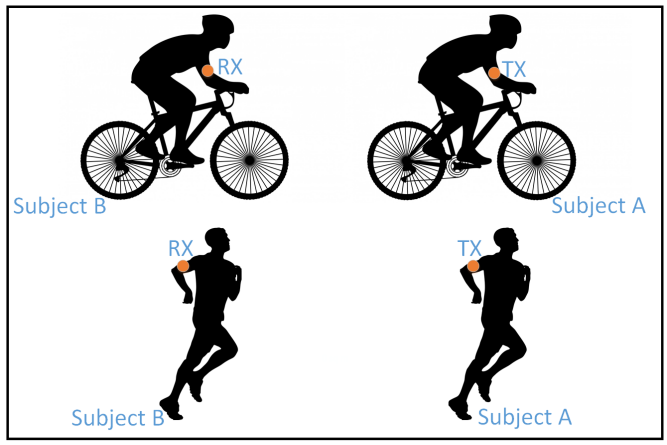

(a)

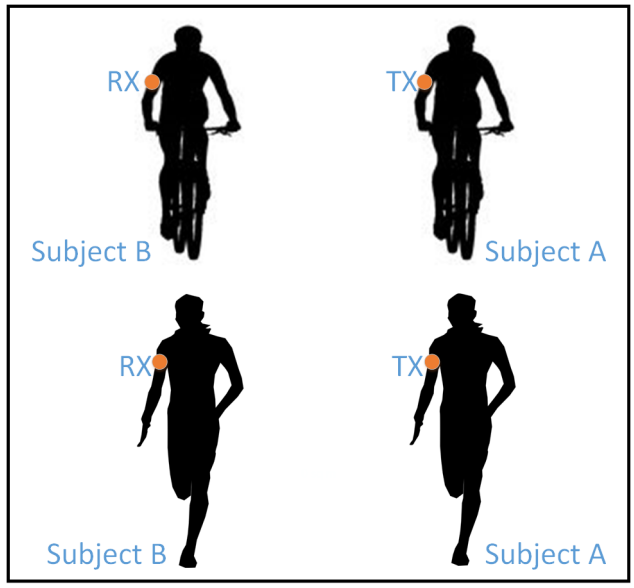

(b)

Figure 2: Investigated scenarios of the BBWN measurement campaign. Activities involved were running and cycling. (**a**) Scenario 1, subject behind the other; (**b**) Scenario 2, subject beside the other. The nodes are attached to the side of the upper arms with a radiation pattern away from the body.

3.1 The Time Series

In body-to-body communications, it is hard to categorize the communication link as LOS or NLOS, but more as a periodic transition between the two states. The periodicity depends on the dynamics involved with the specific activity, related to the movements of the body parts and posture changes [11] of the subjects involved. Our collected data has shown that there is a periodic fluctuation of received signal power regardless of the scenario or activity involved. Even when the arms where the transceivers are attached appear to be stationary as in cycling activity, the periodic movement of the body as the subject pedals gives a similar effect. This underlines the significance of the movement of the body in BBWN channels. Figure 3 shows the measured results for Scenario 1, where the periodicity is seen in both running and cycling activities, in which running shows sharper transitions due to movements of the arms. Similar observations are seen in Scenario 2 performed in this measurement campaign. Other contributing factors in the channel properties are the changes in the local environment, and the relative position of the subjects as they perform their activities. This leads to a large scale fading observed by the change in local mean as shown in Figure 4. The local mean was calculated using a sliding window with length of 750 samples, corresponding to 3 s (approximately three cycles of body motion).

3.2 The Auto-correlation Function

One method of characterizing the periodicity in a fading signal envelope is to calculate the auto-correlation function (ACF) of the signal. The ACF provides a useful measure of the degree of time dependency among the observations of stationary signals. For real discrete sampled data $x(n)$, the empirical ACF is given as [12, 13]:

$$r_{xx}(\tau) = \sum_{n=1}^{N-\tau} (x(n) - \mu)(x(n-\tau) - \mu), \tag{1}$$

where τ is the time delay, N is the length and μ is the mean of the sampled data. The correlation was performed over the entire data sample, and was normalized using $r_{xx}(0)$ to give $\rho_{xx}(\tau)$. Figure 5 shows plots of the normalized ACF $\rho_{xx}(\tau)$, for lags of up to 3 s ($\tau = 750$ samples). It can be observed that the ACFs resemble exponentially decreasing sinusoids with an approximately constant period. For running activity, the period is consistent with the oscillatory movement of the upper arms where the transceivers are attached, and was found to be approximately 0.7 s. For the case of cycling activity, where there is no backward and forward movement of the upper arm, there still exists a minor periodic movement from leaning and tilting of the body as the subjects pedal the bicycles. This movement is comparatively smaller, and hence can only dominate the ACF in the presence of

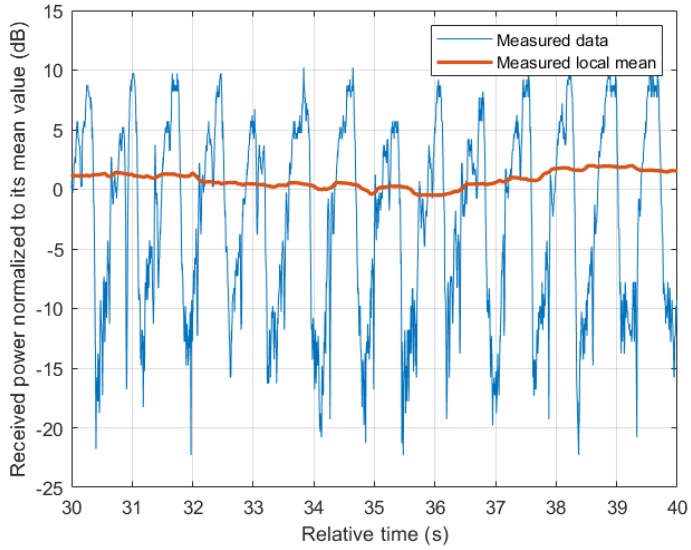

(a)

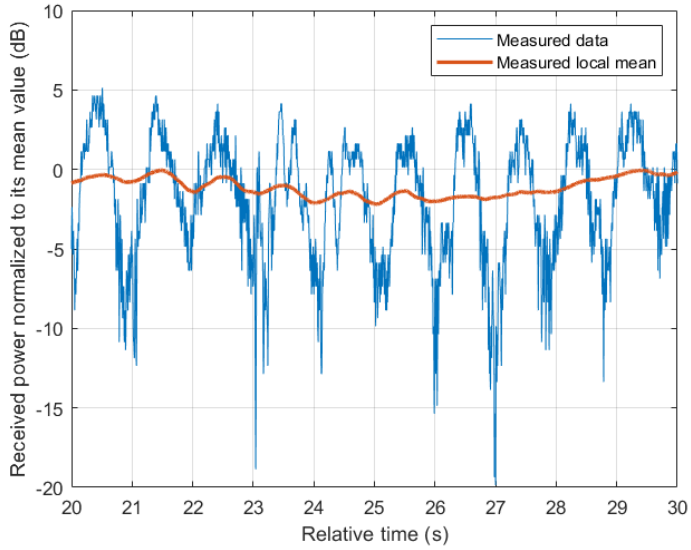

(b)

Figure 3: Example of measured time series collected in Scenario 1, (subject behind the other). (**a**) running; (**b**) cycling.

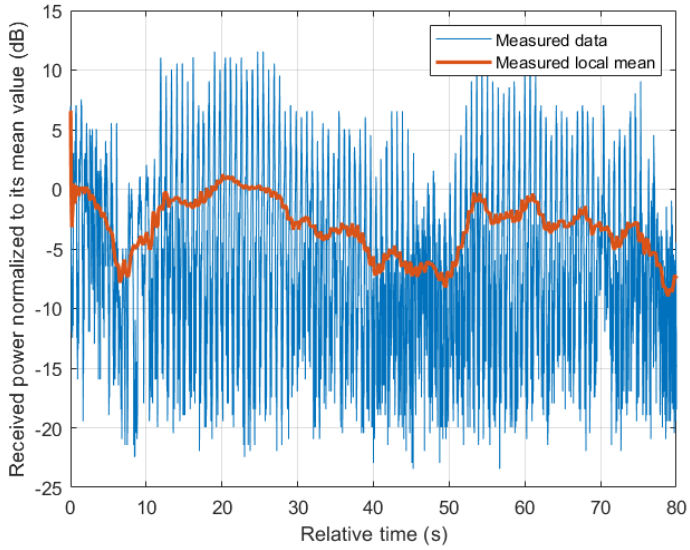

(a)

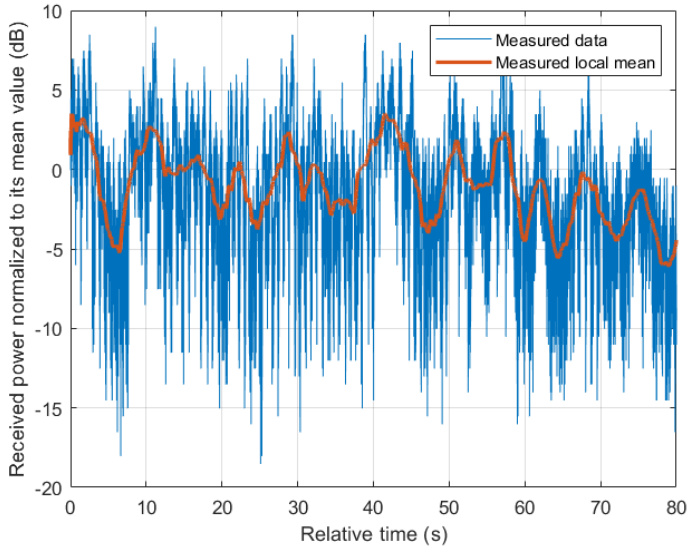

(b)

Figure 4: Example of measured time series collected in Scenario 2, (subject beside the other). (**a**) running; (**b**) cycling.

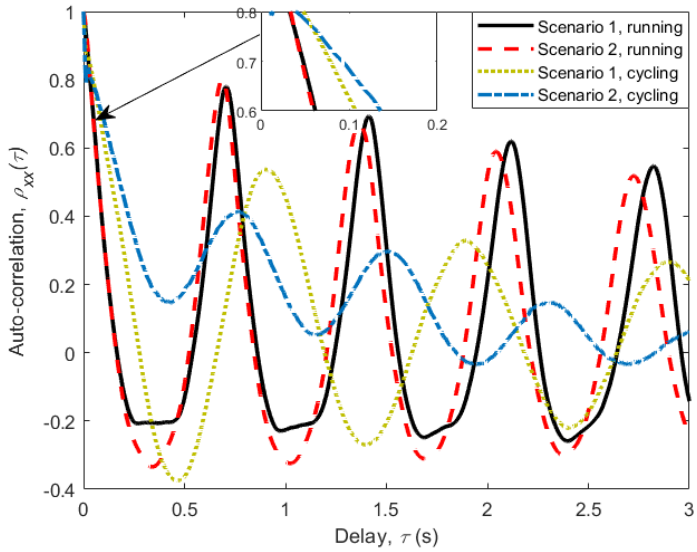

Figure 5: The auto-correlation function of all measured scenarios with a delay of up to three seconds.

Table 1: Coherence Time: Time Before Auto-correlation Crosses the Value of 0.7

	Coherence time (ms)	
Scenario	Running	Cycling
Scenario 1	48	80
Scenario 2	48	92

a permanent LOS condition. In the absence of permanent LOS, such as in Scenario 2 (subject beside the other), other factors such as change in the surrounding environment and subjects' relative positions start to dominate.

Another important piece of information that can be deduced from the figures depicting ACFs is the channel coherence time T_C. It is used to describe the time-varying nature of the channel caused by relative motion between the transceivers, and characterizes the frequency selectivity of the channel in time domain. It gives us the lower limit on the transmission rate for the channel not to cause distortion due to motion. It can be defined as the time lag for which the channel correlation coefficient remains above 0.7 [13]. The channel coherence time T_C for each scenario and activity are given in Table 1. When the subjects' motion dominates (e.g., running all scenarios), we observe smaller coherence times. The largest coherent time was 92 ms observed in Scenario 2 (subject beside the other) of cycling.

3.3 The Power Spectral Density

Another method of characterizing dynamic channels is by observing their power spectral density (PSD). The PSD provides useful information on the frequency composition of the signal. It describes how the power of the signal is distributed over the frequency range. Figures 3.14(a) and 3.14(b) show the PSD for running activity and cycling activities, respectively. We can observe that there is a strong spectral components with high power at 0 Hz followed by other components at higher frequencies in both activities. In addition to that, the PSD tends to decrease exponentially in the logarithmic scale. This lowpass characteristic of the spectrum is consistent with a radio channel having moving scatterers [14], and has been observed in on-body WBAN [15]. As for the case of cycling activity (see Figure 7), the PSD tends to settle between 20 and 50 Hz before it start to decrease again, resulting in a local turning point at around 50 Hz. This phenomenon can be explained by the presence of the off-body scatterer (bicycle) in the cycling activity, which was absent in the running activity. Similar effects of off-body scatterers have been observed for on-body radio channels in [16].

4 The Channel Model

It has been observed in Section 3 that the received signal power for BBWNs oscillates between intervals where it is above a certain threshold, and an interval where it is below it (see Figures 3). In addition, the oscillations can be approximated to have a constant period depending on the activity involved. These kinds of channels can be represented using the two-state semi-Markov model (TSSMM) as done in land mobile satellite links [17, 18]. In this section, a TSSMM for BBWN channels under various running and cycling scenarios is developed.

We start the modeling process by obtaining the appropriate type of amplitude distribution for the 'good' state D_g, representing an interval in which the received signal is above the local mean, and for the 'bad' states D_b, representing an interval in which the received signal is below the local mean. For simplicity, the choice was restricted to the use of same type of distribution for both states. The distribution was determined by obtaining the maximum likelihood (ML) estimates of the measured received signal amplitudes of the two states for Gamma, Lognormal, Nakagami-m, Rayleigh, Rician, and Weibull distributions, and comparing their total negative-log-likelihood. The distribution which gave the largest value of the total negative-log-likelihood was chosen as the best representation of the fading distributions of the two states [19]. It should be noted though that only Scenario 1 (subject behind the other) of cycling activity experience regular line of sight and

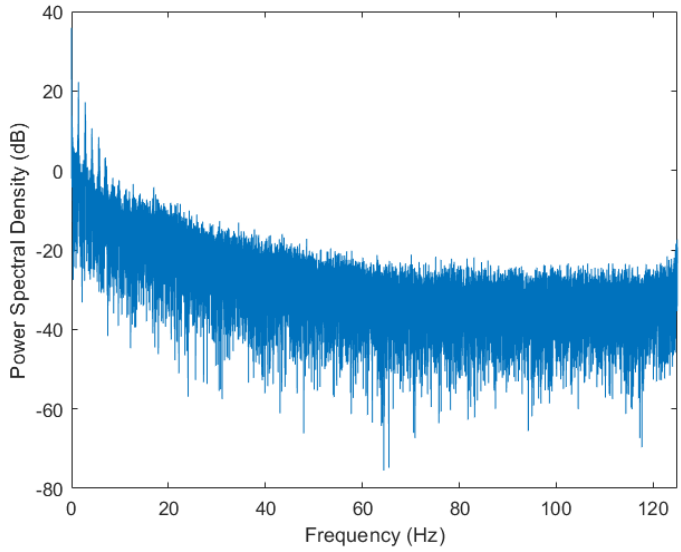

(a)

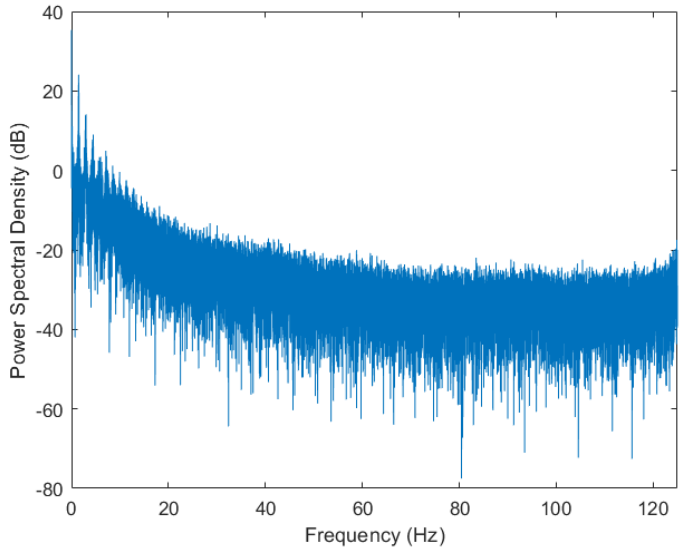

(b)

Figure 6: The PSD of running activity. (**a**) Scenario 1; (**b**) Scenario 2.

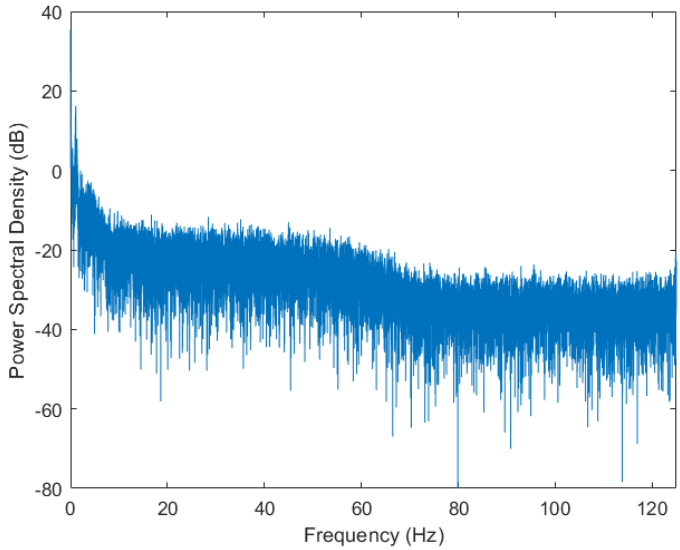

(a)

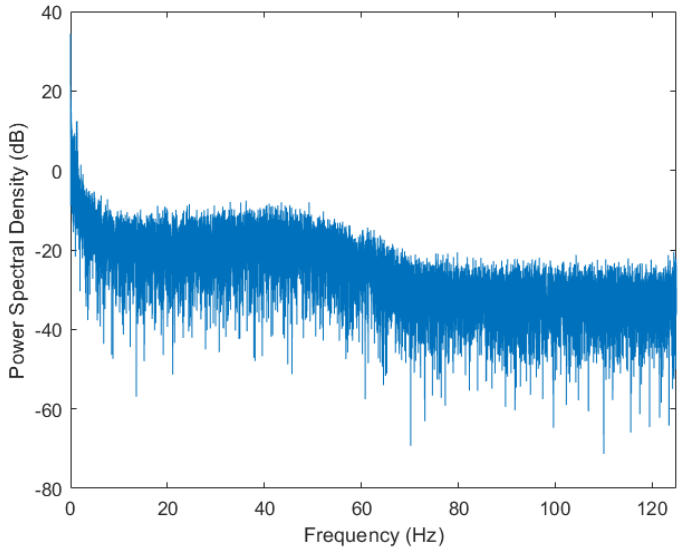

(b)

Figure 7: The PSD of cycling activity. (**a**) Scenario 1; (**b**) Scenario 2.

hence Nakagami-m given by

$$f(x|m,\omega) = \frac{2m^m}{\omega^m \Gamma(m)} x^{2m-1} e^{-\frac{mx^2}{\omega}} \tag{2}$$

gave the best representation of the fading distributions for the two states in that scenario. As the LOS path was subjected to shadowing in the other scenarios, Lognormal distribution given by

$$f(x|\mu,\sigma) = \frac{1}{x\sigma\sqrt{2\pi}} e^{-\frac{(\ln x-\mu)^2}{2\sigma^2}} \tag{3}$$

gave the best representation of the fading distributions for the two states instead.

To obtain the time period of each state, we use the obtained ACF shown in Figure 5. From the ACF, one can determine the total period of the two states, which is equal to the oscillation period of the ACF. The ratio of the time period of each state can then be obtained by using the ratio between the samples present in each state. The resulting state periods obtained, T_g and T_b, control the time spent in each state as the state machine alternates between the two states. The simulation model also included the shadowing and fading effects caused by the change in the surrounding environment as well as the changes in the relative position between the subjects (see Figures 4). Since these changes are relatively slow, they are normally considered as large scale fading effects and are modelled using Lognormal distribution [20, 21]. The parameters of the distribution were determined by performing ML from the samples of the local mean.

Lastly, to ensure the presence of the right frequency composition, the simulated envelope has to pass through an appropriate filter. The PSD of the measured data shown in Figures 6 and 7 can in general be modeled using a lowpass filter. For the case of running activity, where the PSD decreases exponentially in logarithmic scale (see Figure 6), a first-order Butterworth filter with cutoff frequency around 10 Hz gives a good approximation. For the case of cycling activity, the PSD tend to settle between 20 and 50 Hz before it start decreasing again (see Figure 7). This motivated the use of a third-order Butterworth filter instead, with cutoff frequency around the turning point (50 Hz). Figure 8 summarizes the simulation model for BBWN channels during running and cycling, and the corresponding parameters used in the simulation are given in Tables 2 and 3. In the simulation model, samples of good and bad states are generated from the corresponding D_g and D_b distributions for the specified T_g and T_b periods of time respectively. The outputs are then multiplied by $L(t)$, which is the large-scale fading component. The time series is then passed through the lowpass filter with appropriate cutoff

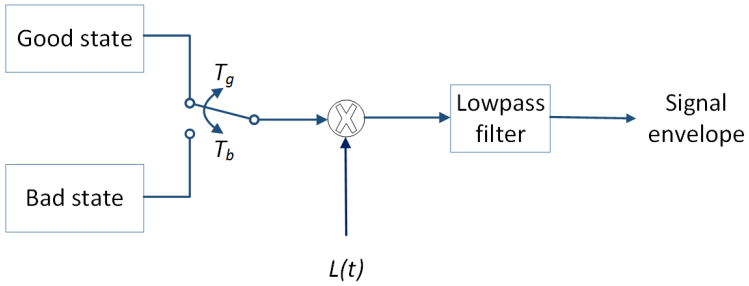

Figure 8: Channel simulator for BBWNs during running and cycling. $L(t)$ is the component of the large scale fading, T_g and T_b are the period of good and bad states, respectively.

Table 2: Parameters Used for Simulation of Running Activity

Parameters	Scenario 1	Scenario 2
Good distribution, D_g	Lognormal $\mu = 0.54, \sigma = 0.61$	Lognormal $\mu = 1.01, \sigma = 0.16$
Bad distribution, D_b	Lognormal $\mu = -1.72, \sigma = 1.32$	Lognormal $\mu = -1.42, \sigma = 0.93$
Large-scale distribution, L	Lognormal $\mu = -0.23, \sigma = 0.26$	Lognormal $\mu = -0.29, \sigma = 0.26$
Good period, T_g	312 ms	256 ms
Bad period, T_b	392 ms	432 ms
Filter order	First	First
Cutoff frequency, f_c	8 Hz	15 Hz

frequency for spectrum shaping. The output from the simulator is a signal envelope that incorporates the overall fading characteristics of body-to-body channels under sporting activities.

To validate the proposed model, TSSMM channel simulations were performed using parameters given in Tables 2 and 3, and the first and second order statistics of the received signal power were calculated from the simulation results. The resulting statistics were then compared with the statistics obtained from the measurement data. We start the comparison with the cumulative distribution function (CDF), which is the probability of a signal being below a certain value. This information is commonly used in performance evaluation of the channel with regard to the channel capacity and outage probability. Figure 9 shows a good agreement between the measurement results, and the proposed simulation model results for all scenarios and activities. For second order statistics, the level crossing rate (LCR) and the average fade duration (AFD) were used for comparison. These statist-

Table 3: Parameters Used for Simulation of Cycling Activity

Parameter	Scenario 1	Scenario 2
Good distribution, D_g	Nakagami-m $m = 5.5, \omega = 1.99$	Lognormal $\mu = 0.29, \sigma = 0.04$
Bad distribution, D_b	Nakagami-m $m = 1.79, \omega = 0.23$	Lognormal $\mu = -0.59, \sigma = 0.73$
Large-scale distribution, L	Lognormal $\mu = -0.05, \sigma = 0.15$	Lognormal $\mu = -0.14, \sigma = 0.3$
Good period, T_g	436 ms	376 ms
Bad period, T_b	460 ms	392 ms
Filter order	Third	Third
Cutoff frequency, f_c	45 Hz	50 Hz

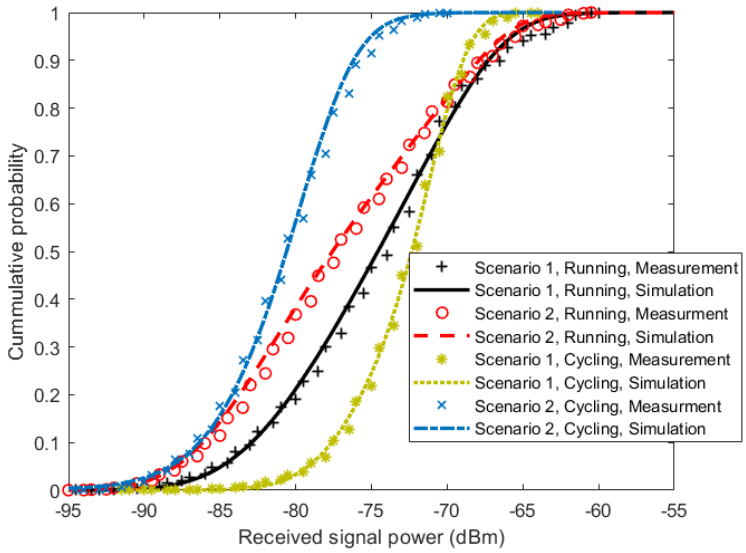

Figure 9: Comparison of CDF of the measurement results, and the developed simulated model results.

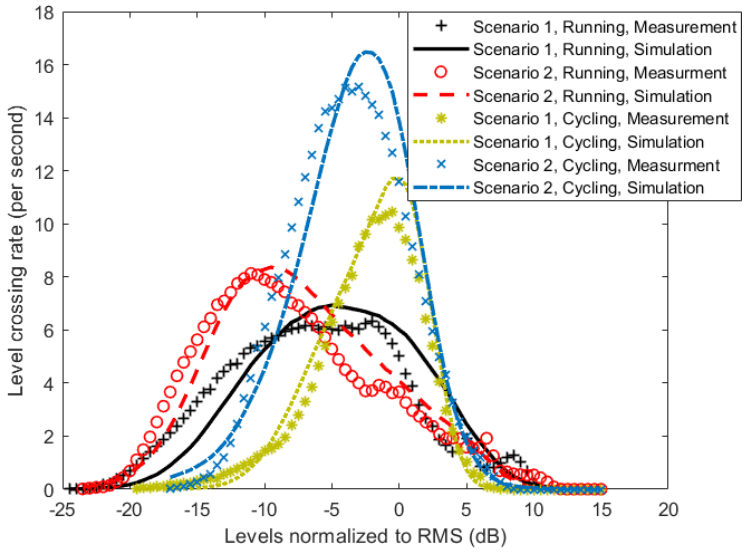

Figure 10: Comparison of LCR of the measurement results, and the developed simulated model results.

ics are important in comparing the time-varying properties of a channel, as they quantify how often the signal crosses a certain threshold and how long it stays below it. Figures 10 and 11 show the comparison of the LCR and AFD of the received signal normalized to their root mean square (RMS) values. We observe a good agreement between the measurement results and the developed simulation model results.

5 Performance Analysis

In this section, the TSSMM simulation model of Section 4 is utilized to conduct performance analysis of BBWNs. The analysis is achieved by evaluating the network performance measurement parameters for the two scenarios and the two activities, in terms of channel capacity and outage probability.

5.1 Channel Capacity

Channel capacity is the maximum rate at which information can be transmitted reliably over a communication channel. Normalized to the bandwidth, it can be expressed in bps/Hz as [22, 23]

$$C_N = \log_2(1 + SNR), \tag{4}$$

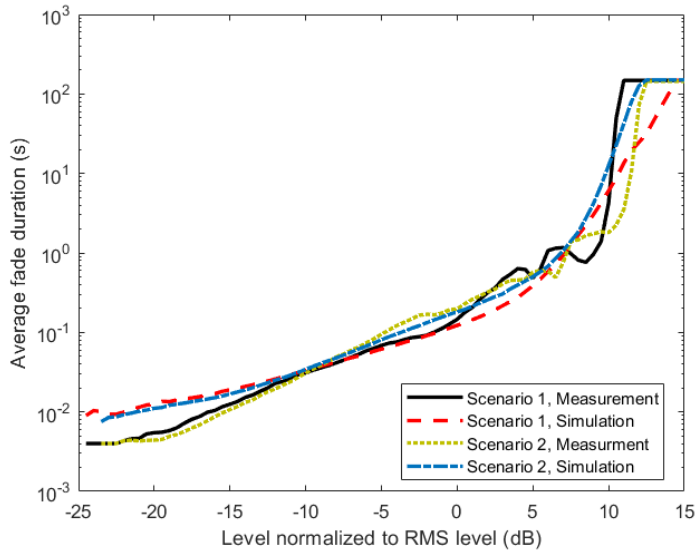

(a)

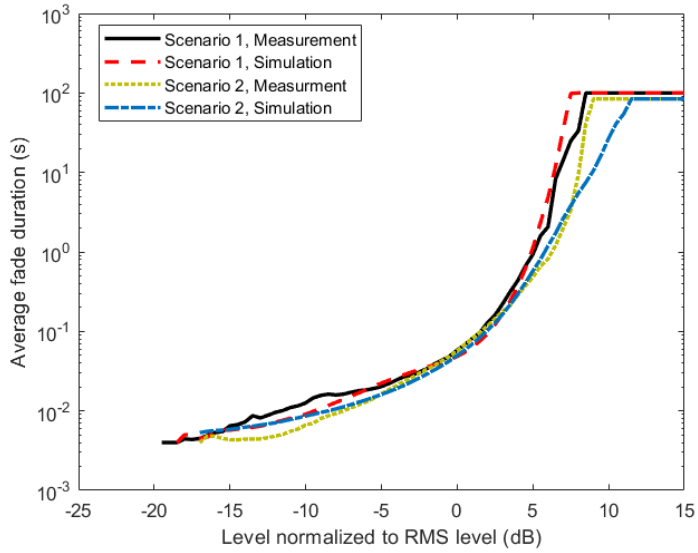

(b)

Figure 11: Comparison of AFD of the measurement results, and the developed simulated model results.(**a**) running; (**b**) cycling.

Table 4: Parameters Used in Performance Analysis Simulations

Parameter	Value
Average received power ($\overline{P}_r$)	[4 16 64] pW
Boltzmann constant (k)	1.38×10^{-23} JK^{-1}
Temperature in Kelvin (T)	290 K
Noise bandwidth (B)	300 kHz
Receiver noise figure (N_f)	6.3

where SNR is the received signal to noise ratio that can be expressed as

$$SNR = \frac{P_r}{kTBN_f}. \tag{5}$$

Here, P_r is the received power, k is the Boltzmann constant, T is the temperature in Kelvin, B is the signal bandwidth in Hz and N_f is the receiver linear noise figure. Due to the time-varying fading effects of the received signal power P_r in BBWNs, the SNR in (4) varies accordingly, making the channel capacity a random variable. Using the CDFs obtained in Section 4 from the simulation model as well as the measured results, the capacity of the channel in different scenarios and activities were simulated and analyzed. Parameters used to calculate the noise power are given in Table 4. Figure 12 shows the CDFs of the instantaneous channel capacity for different average received power $\overline{P}_r$. Considering the running activity in Figure 12(a), it can be observed that Scenario 1 (subject behind the other) gives the best instantaneous channel capacity most of the time. However, it is interesting to notice that, with equal average received power, the instantaneous channel capacity of the given two possible scenarios is almost equal for more than 25% of the time. This is indicated by the convergence of the two curves in their upper part. With relatively stable transceivers achievable during cycling activity, the instantaneous channel capacities obtained has steeper slopes as seen in Figure 12(b). Here, Scenario 1 gives the best instantaneous channel capacity most of the time due to the presence of the LOS component, while Scenario 2 (subject beside the other) gives the worst due to its absence.

The effect of the stability of the arms and hence the transceivers can be observed further in Figure 13, where CDFs of instantaneous channel capacity for all scenarios are plotted together. It can be observed that, with similar average received power, cycling where the arm is more stable, outperform running by having larger values in similar scenarios. This is regardless of the fact that the velocity of the subjects during cycling is more than 50% larger than that of running.

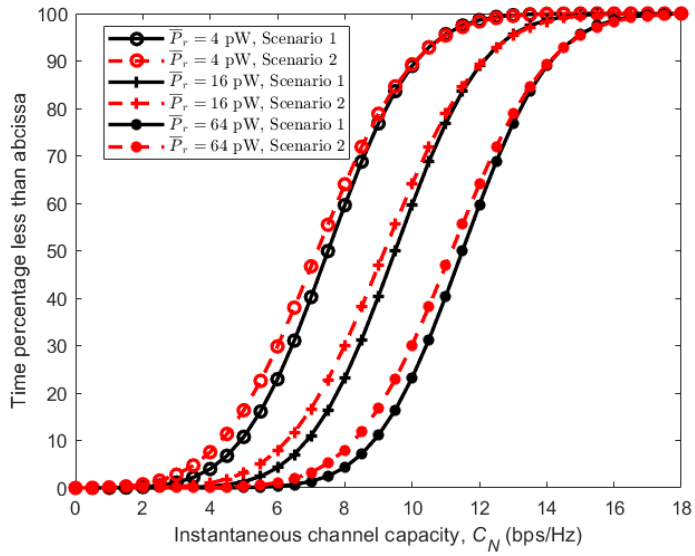

(a)

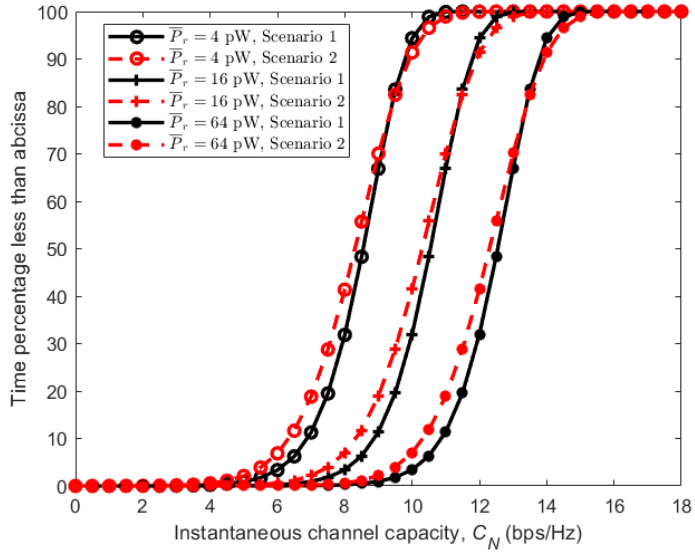

(b)

Figure 12: CDFs of channel capacity C for different average received power $\overline{P}_r$. (a) Running. (b) Cycling.

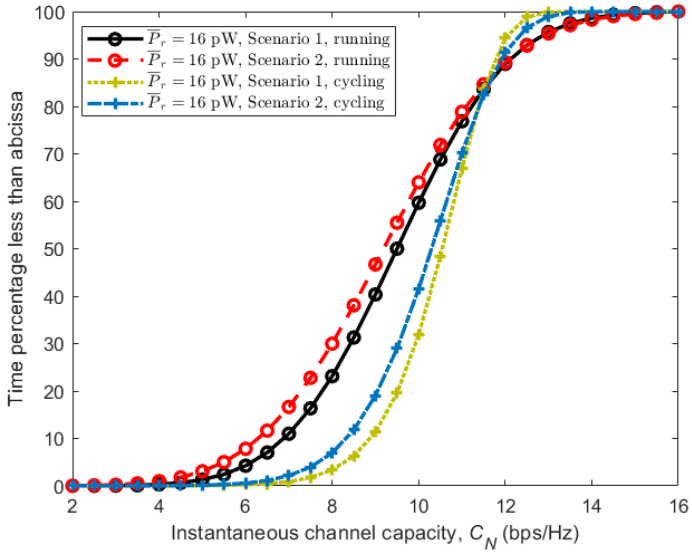

Figure 13: CDFs of channel capacity C for all scenarios during running and cycling activities with average received power $\overline{P}_r = 16$ pW.

5.2 Outage Probability

The outage probability p_{out} is defined as the probability that a receiver will not be able to decode the transmitted information correctly. This happens when the received signal has a SNR below a threshold value SNR_0, required for correct decoding, and can be expressed as [23]

$$p_{out} = \Pr(SNR \leq SNR_0). \tag{6}$$

The threshold value SNR_0, depends on the sensitivity of the receiver S_r, and can be expressed as

$$SNR_0 = \frac{S_r}{kTBN_f}. \tag{7}$$

As in channel capacity, the SNR in (6) varies with the received signal power P_r, making the outage probability p_{out}, a random variable. Again, we use the CDFs obtained in Section 4 from the simulation model as well as the measured results, and values in Table 4 to simulate and analyze the outage probability, relative to the receiver sensitivity S_r.

Figure 14 shows outage probabilities for different average received powers ($\overline{P}_r$) in relation to the receiver sensitivity. Considering the running activity in Figure 14a, we can observe the same trend as in instantaneous channel capacity with Scenario 1

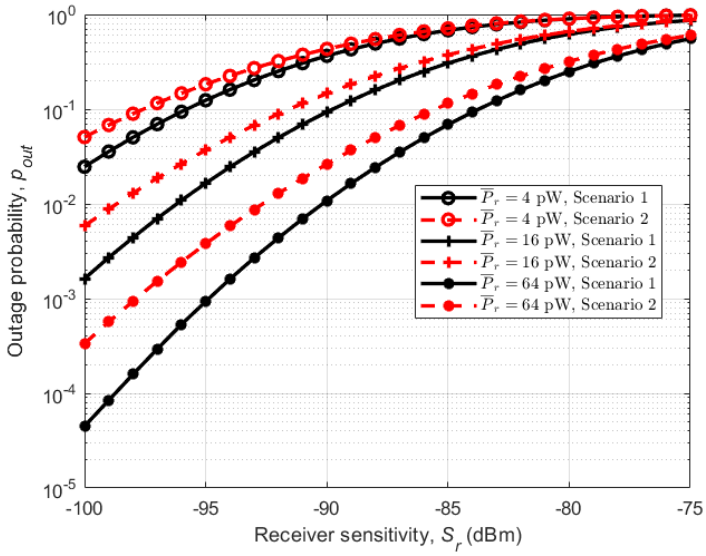

(a)

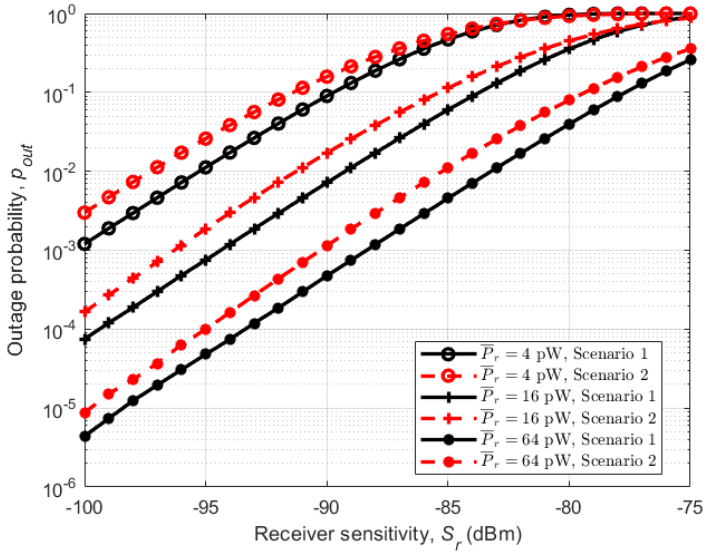

(b)

Figure 14: Outage probabilities p_{out} relative to receiver sensitivity S_r for different average received power $\overline{P}_r$. (**a**) running; (**b**) cycling.

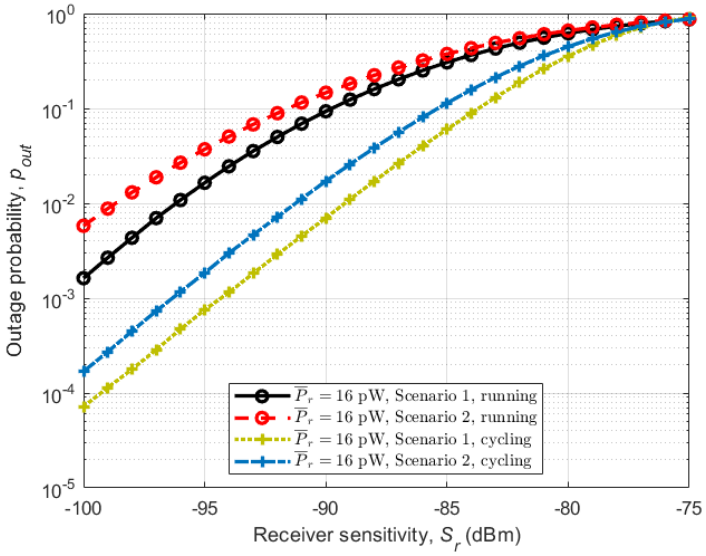

Figure 15: Outage probabilities p_{out} in relation to the receiver sensitivity S_r for all scenarios during running and cycling with average received power $\overline{P}_r = 16$ pW.

(subject behind the other) having lower outage probability than Scenario 2 (subject beside the other), with the same average received power and receiver sensitivity. This is the same for the cycling activity in which Scenario 1 (subject behind the other) has the lowest outage probability under the same conditions, Figure 14b. As with channel capacity, the effect of the stability of the arms on the performance of the channels is seen in Figure 15, where the outage probabilities of the two activities are plotted together. Cycling shows lower outage probabilities for all scenarios under the same receiver sensitivity.

6 Conclusion

This paper presents measurement results of body-to-body communication channels during sport activities. More specifically, the activities involved were running and cycling in an outdoor environment, in which two possible scenarios, which could represent the overall dynamics involved in these kinds of activities, were considered. Due to the on-off nature of the channels in hand, a TSSMM approach was used to develop a simulation model that was validated using the measured data in terms of first and second order statistics, showing good agreement.

The CDFs obtained from the simulation model, as well as the measured results, were then used to conduct performance analysis of the channels in terms of chan-

nel capacity and outage probability. Cycling activities showed better performance than running activities for having higher channel capacity and lower outage probability regardless of the speed of cycling being significantly higher. This is mainly because, during cycling, the arms where the transceivers were attached are more stable. The positive effect of the stability of the arms was also seen in LCR in which cycling showed a smaller fading variation compared to running. In general, these kinds of measurement campaigns and the analysis performed in this study are important in characterizing the transmission channel in hand. They give an aspect to the engineers on the challenges involved in communicating through such channels, and assist in deciding the appropriate solution. Furthermore, the performance analysis completed gives insight, which is important for system design.

Acknowledgments

This work was supported by the Norwegian University of Science and Technology.

Authors Contributions

Mashed Mohamed, Michael Cheffena, and Arild Moldsvor conceived and designed the measurement campaign; Marshed Mohamed made the measurement device, conducted the measurement campaign, analyzed the data, and wrote the manuscript. Michael Cheffena and Arild Moldsvor supported and supervised the research as well as proofread the manuscript.

Conflict of Interest

The authors declare no conflict of interest.

References

[1] R. Cavallari, F. Martelli, R. Rosini, C. Buratti, and R. Verdone, "A survey on wireless body area networks: Technologies and design challenges," *IEEE Communications Surveys & Tutorials*, vol. 16, no. 3, pp. 1635–1657, 2014.

[2] S. F. Heaney, W. G. Scanlon, and E. Garcia-Palacios, "Effect of environmental multipath on line of sight body to body communication at 2.45 GHz," in *Proceedings of Loughborough Antennas and Propagation Conference*, 2012, pp. 1–4.

[3] S. L. Cotton, A. McKernan, and W. G. Scanlon, "Received signal characteristics of outdoor body-to-body communications channels at 2.45 GHz," in *Proceedings of Antennas and Propagation Conference*, 2011, pp. 1–4.

[4] R. Rosini, R. Verdone, and R. D'Errico, "Body-to-body indoor channel modeling at 2.45 GHz," *IEEE Transactions on Antennas and Propagation*, vol. 62, no. 11, pp. 5807–5819, 2014.

[5] M. M. Alam, E. Ben Hamida, D. Ben Arbia, M. Maman, F. Mani, B. Denis, and R. D'Errico, "Realistic simulation for body area and body-to-body networks," *Sensors*, vol. 16, no. 4, p. 561, 2016.

[6] S. L. Cotton, "Shadowed fading in body-to-body communications channels in an outdoor environment at 2.45 GHz," in *Proceedings of IEEE-APS Topical Conference on Antennas and Propagation in Wireless Communications*, 2014, pp. 249–252.

[7] S. L. Cotton, W. G. Scanlon, and A. McKernan, "Improving signal reliability in outdoor body-to-body communications using front and back positioned

antenna diversity," in *Proceedings of 6th European Conference on Antennas and Propagation*, 2012, pp. 3393–3396.

[8] T. Kumpuniemi, M. Hamalainen, K. Y. Yazdandoost, and J. Iinatti, "Human body shadowing effect on dynamic UWB on-body radio channels," *IEEE Antennas and Wireless Propagation Letters*, 2017.

[9] T. Instruments, "CC2500 low-cost low-power 2.4 GHz RF transceiver; datasheet," 2010.

[10] D. Smith, J. Zhang, L. Hanlen, D. Miniutti, D. Rodda, and B. Gilbert, "Temporal correlation of dynamic on-body area radio channel," *Electronics Letters*, vol. 45, no. 24, pp. 1212–1213, 2009.

[11] D. B. Smith, D. Miniutti, T. A. Lamahewa, and L. W. Hanlen, "Propagation models for body-area networks: A survey and new outlook," *IEEE Antennas and Propagation Magazine*, vol. 55, no. 5, pp. 97–117, 2013.

[12] L. Hanlen, V. Chaganti, B. Gilbert, D. Rodda, T. Lamahewa, and D. Smith, "Open-source testbed for body area networks: 200 sample/sec, 12 hrs continuous measurement," in *Proceedings of IEEE 21st International Symposium on Personal, Indoor and Mobile Radio Communications Workshops*, 2010, pp. 66–71.

[13] T. S. Rappaport *et al.*, *Wireless Communications: Principles and Practice*. Upper Saddle River, NJ, USA: Prentice Hall, 1996.

[14] J. B. Andersen, J. O. Nielsen, G. F. Pedersen, G. Bauch, and G. Dietl, "Doppler spectrum from moving scatterers in a random environment," *IEEE Transactions on Wireless Communications*, vol. 8, no. 6, 2009.

[15] L. Liu, R. D'Errico, L. Ouvry, P. De Doncker, and C. Oestges, "Dynamic channel modeling at 2.4 GHz for on-body area networks," *Advances in Electronics and Telecommunications*, vol. 2, no. 4, pp. 18–27, 2011.

[16] R. D'Errico and L. Ouvry, "Doppler characteristics and correlation proprieties of on-body channels," in *Proceedings of 5th European Conference on Antennas and Propagation*, 2011, pp. 2977–2981.

[17] E. Lutz, D. Cygan, M. Dippold, F. Dolainsky, and W. Papke, "The land mobile satellite communication channel-recording, statistics, and channel model," *IEEE Transactions on Vehicular Technology*, vol. 40, no. 2, pp. 375–386, 1991.

[18] L. E. Braten and T. Tjelta, "Semi-Markov multistate modeling of the land mobile propagation channel for geostationary satellites," *IEEE Transactions on Antennas and Propagation*, vol. 50, no. 12, pp. 1795–1802, 2002.

[19] K. P. Burnham and D. R. Anderson, "Multimodel inference: Understanding AIC and BIC in model selection," *Sociological methods & research*, vol. 33, no. 2, pp. 261–304, 2004.

[20] A. Aragon-Zavala, *Antennas and Propagation for Wireless Communication Systems*. Hoboken, NJ, USA: John Wiley & Sons, 2008.

[21] F. P. Fontán and P. M. Espiñeira, *Modelling the Wireless Propagation Channel: A Simulation Approach with MATLAB*. Hoboken, NJ, USA: John Wiley & Sons, 2008.

[22] M. Cheffena, "Performance evaluation of wireless body sensors in the presence of slow and fast fading effects," *IEEE Sensors Journal*, vol. 15, no. 10, pp. 5518–5526, 2015.

[23] A. Goldsmith, *Wireless Communications*. Cambridge, UK: Cambridge University Press, 2005.

Paper IV

M. Cheffena and M. Mohamed, "The application of lognormal mixture shadowing model for B2B channels," *IEEE Sensors Letters,* vol. 2, no. 3, pp. 1-4, 2018.

Paper IV

The Application of Lognormal Mixture Shadowing Model for B2B Channels

Michael Cheffena and Marshed Mohamed

Abstract

In this article, a Lognormal mixture shadowing model based on a cluster concept is utilized in the modeling of body-to-body (B2B) channels for different running and cycling activities. The mixture model addresses the inaccuracies observed using a unimodal distribution that may not accurately represent the measurement dataset. Parameters of the mixture model are estimated using the expectation-maximization (EM) algorithm. The accuracy of the proposed mixture model is compared to other commonly utilized unimodal distributions showing significant improvement in representing the empirical dataset. The measured data, as well as the developed model, can be used for accurate planning and deployments of wireless B2B networks for use in various sporting and other related activities.

Index Terms

Body-to-body (B2B) communications, cycling, fading distributions, Lognormal mixture shadowing, running, sport, wireless body area networks (WBAN), wireless networks.

1 Introduction

In recent years, there has been a growing interest on body-centric wireless communications because of their great potential applications in various domains such as health, entertainment, sports, or any other application that requires transmission of data from the human body [1]. Among other communication scenarios, the transmission could involve between a device mounted on one person to a device situated on another person in a different physical location. This kind of communication is known as B2B communications and is subject to time-varying shadowing effects caused by the movements of the human bodies at both the ends of the communication link [2]. The successful design of such networks requires a good understanding of the propagation impairments affecting the wireless link.

The wave propagation characteristics of on-body and off-body channels have been extensively studied in the past; see [3] and [4] for review. However, body-to-body (B2B) propagation channels have not been extensively studied. Measurement data at 2.45 GHz was utilized in [2] to assess the impact of typical human body movements on the signal characteristics of outdoor B2B channels using flexible patch antennas. A modified log-distance path loss model that accounts for body shadowing and signal fading was proposed. Channel model characterization for indoor B2B scenarios based on 2.45 GHz measurements was reported in [5]. The shadowing and small-scale fading effects for line-of-sight (LOS) and non-LOS conditions were evaluated. Similar studies were also conducted in [6–8].

For B2B wireless networks, shadowing is the dominant propagation impairment causing partial or total blockage of the received signal due to environmental factors, as well as due to the random (or periodic) movements of the body components at both ends of the communication link. Existing studies utilize a unimodal distribution (usually a Lognormal or Gamma distribution) to characterize the shadowing effects of B2B channels. However, such distributions may not be based on the actual underlying physical propagation process of such channels [9]. The Lognormal distribution is a widely accepted physical-based model for modeling shadowing effects in wireless links [10]. However, our histograms of measurement data for different sports activity propagation scenarios of B2B channels show mixture and skewed distribution curves, as also observed in other similar studies such as [5] and [11]. This may suggest the existence of distinct scattering clusters for these types of channels that can be modeled utilizing mixture distributions. In addition to environmental effects, the movements of the different body components of the involved subjects at both the ends of the communication link might contribute to distinct scattering clusters. This kind of clustering behavior cannot be accurately modeled using unimodal distributions.

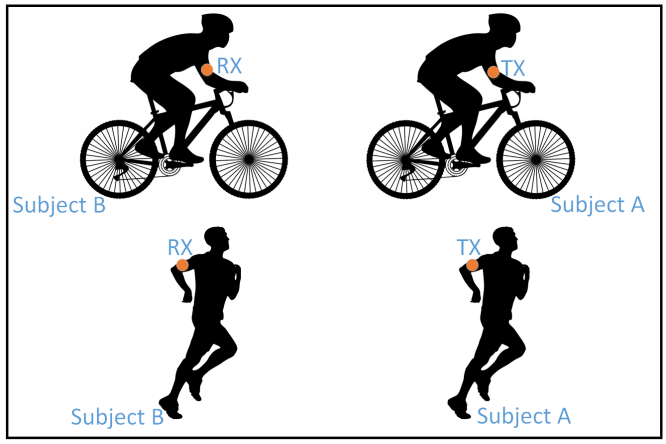

Fig. 1: Scenario 1: measurements for B2B wireless network under running and cycling activities where one subject is behind the other [12].

In this article, a Lognormal mixture shadowing was used in modeling of B2B propagation channels under different sporting activities. The letter aims to underline the potential improvement achieved by the model, over the commonly used unimodal distribution approach, in representing B2B channels. The rest of the letter is organized as follows. Section II describes the measurement campaign, presenting the practical sensor nodes used as well as the investigated B2B propagation scenarios. Measurement data analysis and the proposed Lognormal mixture shadowing model is discussed in Section III. Conclusions are given in Section IV.

2 Measurement Campaign

The measurement campaign was conducted utilizing practical sensor nodes for characterizing the B2B propagation channel under various outdoor sporting activities. A transmitting and a receiving node were attached (using a small strip of Velcro) to the upper arm of two adult males of height 1.80 m and mass 80 kg (subject A), and 1.85 m height and 75 kg mass (subject B). Two different scenarios for running (average speed of 3.33 m/s) and cycling (average speed of 5 m/s) activities were considered. *Scenario 1)* subjects behind each other as shown in Fig. 1, and *Scenario 2)* subjects beside each other as seen in Fig. 2. The experiment were conducted in 500 meter outdoor stretch, which is a common running and cycling route in Gjøvik, Norway. In all activities, the subjects tried to maintain a separation distance of 1 meter between them.

The test-bed is a programmable radio transceiver (CC2500) from Texas Instruments. The device was set to transmit a packet every 4 ms with constant transmis-

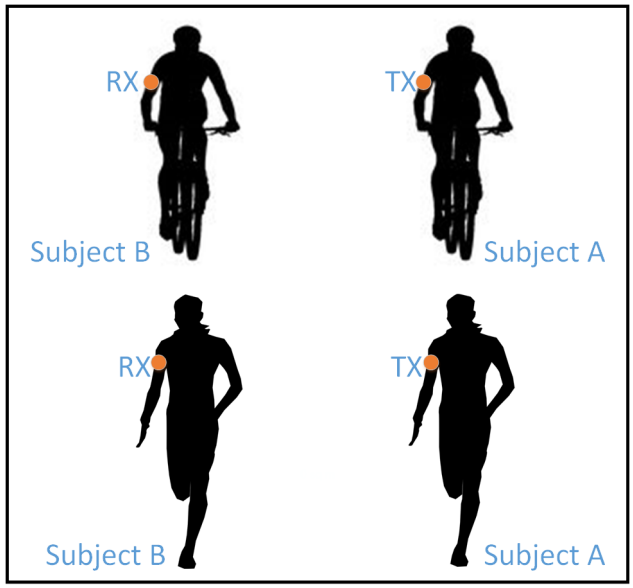

Fig. 2: Scenario 2: measurements for B2B wireless network under running and cycling activities where subjects are beside each other [12].

sion power of 1 dBm at a carrier frequency of 2.425 GHz. At the receiving end, the packet number together with its received signal strength indicator (RSSI) was stored on the MicroSD memory card. The nodes use horizontal polarized Wurth Electronik 7488910245 chip antenna. At least 25 kilo-samples for each scenario were collected, which is high enough for conducting statistical analyses. Details of the measurement campaign can be found in [12].

3 Measurement Results and Analysis

3.1 Lognormal Mixture Shadowing

The received signal power at a given separation distance, d, from the transmitter that is subject to shadowing is defined in decibel scale as [10]

$$P_{\mathrm{RX}}(d) = P_{\mathrm{TX}} - 10n\log(d) + X_\sigma \tag{1}$$

where P_{TX} is the transmitted power, n is the path loss exponent, which shows the rate at which the received signal power decreases with distance. Parameter $X_\sigma \sim \mathcal{N}(0, \sigma^2)$, denotes the shadowing fading term with Normal distribution random variable (i.e., Lognormal distribution in linear scale) with zero mean and σ^2 variance. Defining, $X_\sigma = \ln(Y_\sigma)$, the Lognormal shadow fading implies $Y_\sigma \sim \mathcal{LN}(0, \sigma^2)$ [13].

The probability density function (PDF) of Lognormal mixture distributions can be described as

$$Y \sim f_Y(y) = \sum_{k=1}^{\infty} w_k \mathcal{LN}(\mu_k, \sigma_k^2) \tag{2}$$

where μ_k and σ_k^2 are the distribution parameters of the kth mixture component (for $k = 1, 2, ...$), parameter w_k is weighting proportion of the kth component such that $\sum_{k=1}^{\infty} w_k = 1$, and the Lognormal kernel PDF of the kth mixture is then given by

$$\mathcal{LN}(\mu_k, \sigma_k^2) = \frac{1}{y\sqrt{2\pi\sigma_k^2}} \exp\left[\frac{-(\ln y - \mu_k)^2}{2\sigma_k^2}\right] \tag{3}$$

In a non-parametric estimation, the use of symmetric kernels is preferred as they provide a convergent expansion according to the Mercer's theorem [14]. The expression in (3) is not symmetric, however, since the logarithm of each observation can be described as $x_i = \ln(y_i)$ (for $i = 1, 2, ..., N$, where N is the total sample number), a univariate Gaussian distribution with mean μ_k and variance σ_k^2 can be utilized. Thus, all samples of x_i can be modeled as a mixture of Gaussian distributions as

$$X \sim f_X(x) = \sum_{k=1}^{\infty} w_k \mathcal{N}(\mu_k, \sigma_k^2) \tag{4}$$

where the corresponding kernel PDF is given by

$$\mathcal{N}(\mu_k, \sigma_k^2) = \frac{1}{\sqrt{2\pi\sigma_k^2}} \exp\left[\frac{-(x - \mu_k)^2}{2\sigma_k^2}\right] \tag{5}$$

For a given shadow fading condition, an estimate of the actual PDF (with a measurable error) can be made utilizing a finite number of K Gaussian kernels and the resulting Lognormal mixture can be expressed as [13]

$$\widehat{f}_Y(y) = \sum_{k=1}^{K} w_k \frac{1}{y\sqrt{2\pi\sigma_k^2}} \exp\left[\frac{-(\ln y - \mu_k)^2}{2\sigma_k^2}\right] \tag{6}$$

In this work, the value of K was set to 4, as higher values did not bring further improvement in the results.

3.2 Results and comparisons

Figs. 3 to 6 show the measured PDFs along with the estimated mixture of Lognormal distribution (6) with $K = 4$ (Lognormal-4). The expectation-maximization (EM) algorithm [13] was utilized to estimate the mixture model parameters and are given in Tables 1 and 2. Also shown are comparisons with unimodal distributions (Lognormal, Gamma, and Nakagami). We can observe that the measured PDFs (in all scenarios) exhibit mixture and skewed distribution curves especially those of running activity as shown in Fig. 3 and Fig. 5. Such characteristics has also been observed in other similar studies e.g., [5, 11]. With relatively stable transceivers achievable during cycling activity, the distinction between clusters is less pronounced as seen in Fig. 4 and Fig. 6. Tables 1 and 2 also show the mean error, standard deviation of error, and the root mean square error of the corresponding distributions compared to measured PDFs. The weighted mean relative difference (WMRD) expressed as a percentage was also included for easier comparison

$$\text{WMRD} = \frac{\sum_{t=1}^{n} |F_t - A_t|}{\sum_{t=1}^{n} (F_t + A_t)} \times 100 \tag{7}$$

where A_t is the measured PDF, F_t is the estimated PDF, t is the fitted point and n is the total number of fitted points. In all cases, we can observe that the best estimation is achieved utilizing the mixture model. Naturally, the mixture model will give better results due to a large number of involved parameters. However, the improvements achieved here, especially for the case of running activity is significantly large and hence, suggest the existence of distinct scattering clusters for B2B propagation channels where in addition to the environment, the movements of the different body components of each person at both ends of the communication link contribute to distinct scattering clusters. Thus, utilizing a unimodal distribution may not describe the underlying propagation process or give a good approximation of the channel in the B2B communication under sporting or other related activities.

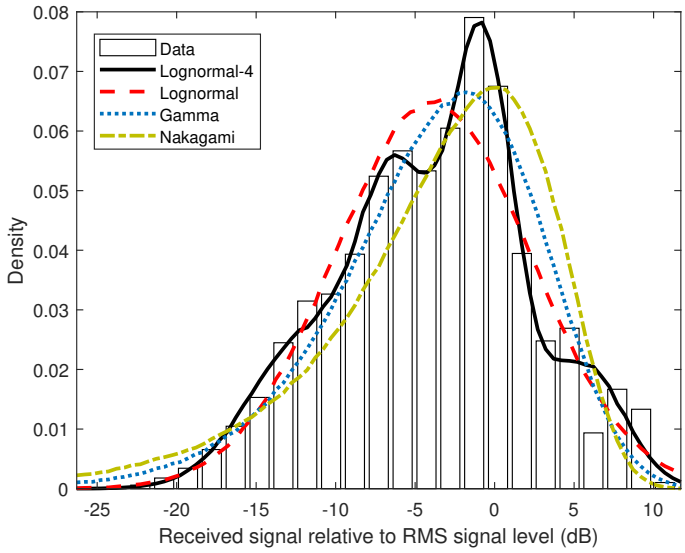

Fig. 3: Measured histogram and estimated PDFs for Scenario 1 running.

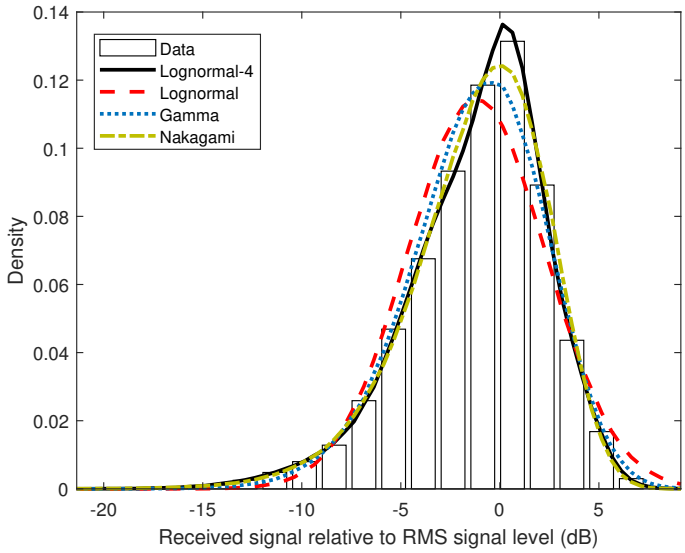

Fig. 4: Measured histogram and estimated PDFs for Scenario 1 cycling.

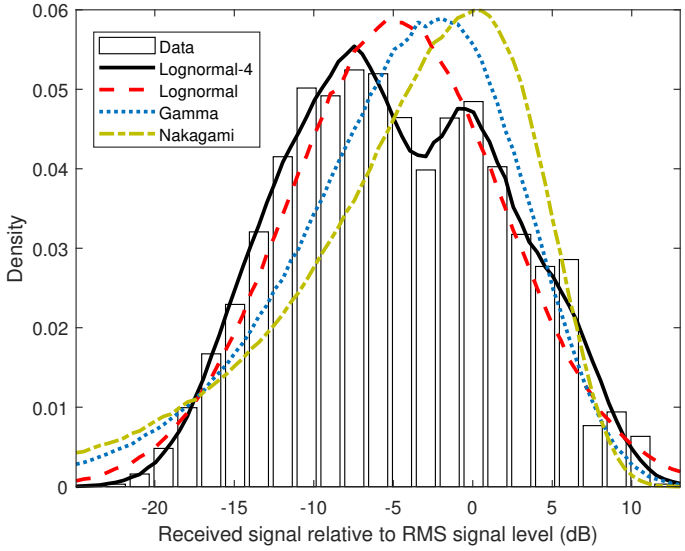

Fig. 5: Measured histogram and estimated PDFs for Scenario 2 running.

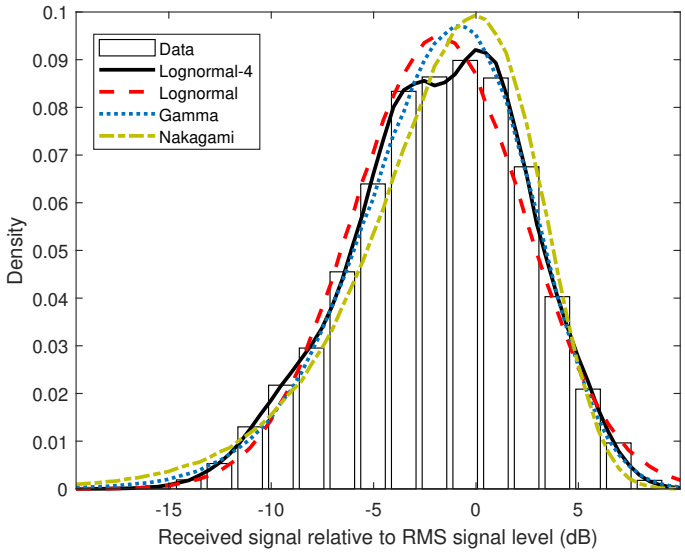

Fig. 6: Measured histogram and estimated PDFs for Scenario 2 cycling.

Table 1: Scenario 1: Distribution Parameters and Error Eetrics for PDF Estimation

Activity	Model	Parameters			Error mean	Error STD	RMSE	WMRD
Running	Lognormal-4	$\mu_1 = -0.0769$	$\sigma_1^2 = 0.0537$	$w_1 = 0.3531$	0.0001	0.0063	0.0062	3.60%
		$\mu_2 = -1.3645$	$\sigma_2^2 = 0.1563$	$w_2 = 0.2245$				
		$\mu_3 = 0.6879$	$\sigma_3^2 = 0.0920$	$w_3 = 0.2921$				
		$\mu_4 = -0.6476$	$\sigma_4^2 = 0.0793$	$w_4 = 0.1303$				
	Lognormal	$\mu = -0.4501$	$\sigma^2 = 0.5030$	-	0.0003	0.0143	0.0143	9.53%
	Gamma	$\alpha = 2.2387$	$\beta = 0.3619$	-	0.0002	0.0141	0.0138	9.88%
	Nakagami	$\mu = 0.6749$	$\omega = 1$	-	0.0005	0.0218	0.0214	9.88%
Cycling	Lognormal-4	$\mu_1 = -0.3353$	$\sigma_1^2 = 0.0663$	$w_1 = 0.3485$	8.4×10^{-6}	0.0017	0.0017	0.74%
		$\mu_2 = -0.6487$	$\sigma_2^2 = 0.2319$	$w_2 = 0.1273$				
		$\mu_3 = 0.0372$	$\sigma_3^2 = 0.0300$	$w_3 = 0.3690$				
		$\mu_4 = 0.3266$	$\sigma_4^2 = 0.0350$	$w_4 = 0.1551$				
	Lognormal	$\mu = -0.1350$	$\sigma^2 = 0.1607$	-	0.0002	0.0205	0.0200	9.49%
	Gamma	$\alpha = 7.0029$	$\beta = 0.1342$	-	3.9×10^{-5}	0.0118	0.0115	4.88%
	Nakagami	$\mu = 2.0019$	$\omega = 1$	-	1.5×10^{-6}	0.0062	0.0061	4.88%

Table 2: Scenario 2: Distribution Parameters and Error Metrics for PDF Estimation

Activity	Model	Parameters			Error mean	Error STD	RMSE	WMRD
Running	Lognormal-4	$\mu_1 = -1.5353$	$\sigma_1^2 = 0.1391$	$w_1 = 0.2063$	4.6×10^{-5}	0.0051	0.0050	3.21%
		$\mu_2 = -0.9126$	$\sigma_2^2 = 0.1086$	$w_2 = 0.3216$				
		$\mu_3 = 0.4865$	$\sigma_3^2 = 0.1337$	$w_3 = 0.1964$				
		$\mu_4 = -0.1630$	$\sigma_4^2 = 0.1129$	$w_4 = 0.2757$				
	Lognormal	$\mu = -0.5596$	$\sigma^2 = 0.6158$	-	0.0003	0.0124	0.0122	8.60%
	Gamma	$\alpha = 1.8033$	$\beta = 0.4287$	-	0.0006	0.0183	0.0179	13.65%
	Nakagami	$\mu = 0.5581$	$\omega = 1$	-	0.0011	0.0262	0.0257	13.65%
Cycling	Lognormal-4	$\mu_1 = 0.4655$	$\sigma_1^2 = 0.0452$	$w_1 = 0.1297$	1.1×10^{-5}	0.0021	0.0021	1.06%
		$\mu_2 = -0.8142$	$\sigma_2^2 = 0.1180$	$w_2 = 0.2189$				
		$\mu_3 = 0.0993$	$\sigma_3^2 = 0.0356$	$w_3 = 0.2914$				
		$\mu_4 = -0.3385$	$\sigma_4^2 = 0.0552$	$w_4 = 0.3600$				
	Lognormal	$\mu = -0.2108$	$\sigma^2 = 0.2348$	-	0.0003	0.0105	0.0102	5.37%
	Gamma	$\alpha = 4.6427$	$\beta = 0.1950$	-	7.1×10^{-5}	0.0058	0.0057	2.98%
	Nakagami	$\mu = 1.3281$	$\omega = 1$	-	0.0001	0.0123	0.0119	2.98%

4 Conclusions

B2B wireless networks can support applications in various domains such as health, entertainment, sports, or any other application that requires the exchange of data among different persons. The design and reliable operations of such networks require accurate characterization of the propagation channel utilizing practical sensor devices. Inaccurate channel models may lead to poor decision making in the deployment of such networks resulting in unreliable communications. Inaccurate models may also result in poor energy efficiency of the wireless network.

In this article, the shadowing effects of B2B communications under various sporting activities are investigated using extensive measurements at 2.425 GHz. Running and cycling activities where the subjects are behind and beside each other are considered. Our histograms of measurement data for the different propagation scenarios show mixture and skewed distribution curves, as also observed in other reported similar studies. This suggests the existence of distinct scattering clusters for B2B propagation channels where in addition to the environment, the movements of the body components of the persons involved at both ends of the communication link contribute to distinct scattering clusters. A Lognormal mixture shadowing model for B2B channels under different running and cycling activities based on a cluster concept is proposed. The mixture model addresses the inaccuracies observed using a unimodal distribution that may not accurately represent the measurement dataset. Parameters of the mixture model are estimated using the EM algorithm. The accuracy of the proposed model is compared to other commonly utilized unimodal distributions showing significant improvement in representing the empirical dataset.

The measured data, as well as the developed Lognormal mixture shadowing model, can be used for accurate planning and deployments of wireless B2B networks for use in various sporting and other related activities. Future works include conducting measurement campaign and analysis for varying distances between subjects.

5 Acknowledgment

This work was supported by the Norwegian University of Science and Technology (NTNU).

References

[1] M. Cheffena, "Time-varying on-body wireless channel model during walking," *EURASIP Journal on Wireless Communications and Networking*, vol. 2014, no. 1, p. 29, 2014.

[2] S. L. Cotton, A. McKernan, and W. G. Scanlon, "Received signal characteristics of outdoor body-to-body communications channels at 2.45 GHz," in *Proceedings of Loughborough Antennas and Propagation Conference*, 2011, pp. 1–4.

[3] D. B. Smith, D. Miniutti, T. A. Lamahewa, and L. W. Hanlen, "Propagation models for body-area networks: A survey and new outlook," *IEEE Antennas and Propagation Magazine*, vol. 55, no. 5, pp. 97–117, 2013.

[4] S. L. Cotton, R. D'Errico, and C. Oestges, "A review of radio channel models for body centric communications," *Radio Science*, vol. 49, no. 6, pp. 371–388, June 2014.

[5] R. Rosini, R. Verdone, and R. D'Errico, "Body-to-body indoor channel modeling at 2.45 GHz," *IEEE Transactions on Antennas and Propagation*, vol. 62, no. 11, pp. 5807–5819, November 2014.

[6] F. Mani and R. D'Errico, "A spatially aware channel model for body-to-body communications," *IEEE Transactions on Antennas and Propagation*, vol. 64, no. 8, pp. 3611–3618, August 2016.

[7] S. L. Cotton and W. G. Scanlon, "Channel characterization for single-and multiple-antenna wearable systems used for indoor body-to-body communications," *IEEE Transactions on Antennas and Propagation*, vol. 57, no. 4, pp. 980–990, April 2009.

[8] Z. H. Hu, Y. Nechayev, and P. Hall, "Measurements and statistical analysis of the transmission channel between two wireless body area networks at 2.45 GHz and 5.8 GHz," in *Proceedings of 20th International Conference on Applied Electromagnetics and Communications*, September 2010, pp. 1–4.

[9] J. Salo, L. Vuokko, H. M. El-Sallabi, and P. Vainikainen, "An additive model as a physical basis for shadow fading," *IEEE Transactions on Vehicular Technology*, vol. 56, no. 1, pp. 13–26, January 2007.

[10] T. S. Rappaport *et al.*, *Wireless Communications: Principles and Practice*. Upper Saddle River, NJ, USA: Prentice Hall, 1996.

[11] T. Kumpuniemi, M. Hämäläinen, K. Y. Yazdandoost, and J. Iinatti, "Human body shadowing effect on dynamic UWB on-body radio channels," *IEEE Antennas and Wireless Propagation Letters*, vol. 16, pp. 1871–1874, 2017.

[12] M. Mohamed, M. Cheffena, and A. Moldsvor, "Characterization of the body-to-body propagation channel for subjects during sports activities," *Sensors*, vol. 18, no. 2, p. 620, 2018.

[13] S. Büyükçorak, M. Vural, and G. K. Kurt, "Lognormal mixture shadowing," *IEEE Transactions on Vehicular Technology*, vol. 64, no. 10, pp. 4386–4398, October 2015.

[14] "XVI. functions of positive and negative type, and their connection with the theory of integral equations," *Philosophical Transactions of the Royal Society of London A: Mathematical, Physical and Engineering Sciences*, vol. 209, no. 441-458, pp. 415–446, 1909.

Paper V

M. Mohamed and M. Cheffena, "Received signal strength based gait authentication," *IEEE Sensors Journal,* vol. 18, no. 16, pp. 6727-6734, 2018.

Paper V

Received Signal Strength Based Gait Authentication

Marshed Mohamed and Michael Cheffena

Abstract

Expansion of wireless body area networks (WBANs) applications such as healthcare, m-banking, and others has lead to vulnerability of privacy and personal data. An effective and unobtrusive natural method of authentication is therefore a necessity in such applications. Accelerometer-based gait recognition has become an attractive solution, however, continuous sampling of accelerometer data reduces the battery life of wearables. This paper investigates the usage of received signal strength indicator (RSSI) as a source of gait recognition. Unlike the accelerometer-based method, the RSSI approach does not require additional sensors (hardware) or sampling of them, but uses the RSSI values already available in all radio devices. Three radio channel features namely, the time series, auto-correlation function, and level crossing rate were extracted from unique signature of the RSSI in relation to the corresponding subject. The extracted features were then used together with 4 different classification learners namely decision tree, support vector machine, k-nearest neighbours, and artificial neural network, to evaluate the method. The best performance was achieved utilizing artificial neural network with 95% accuracy when the features were extracted from 1 on-body radio channel (right wrist to waist), and 98% when the features were extracted from 2 on-body radio channels (right wrist to waist, and left wrist to waist). The developed RSSI-based gait authentication approach can complement high-level authentication methods for increased privacy and security, without additional hardware, or high energy

consumption existing in accelerometer based solutions.

Keywords

Wireless body area networks, physical layer security, wireless channel characteristics, biometrics authentication, human gait.

1 Introduction

THE advances in microelectronics and wireless communications have led to the availability of lightweight devices with wireless communication capabilities that can be used to monitor the human body functions and its surrounding environment. Networks made of such devices are known as Wireless Body Area Networks (WBANs) and have found significant applications in health monitoring [1]. In such applications, WBAN sensors collect vital physiological parameters of a subject, which serve as a reference in medical diagnosis, treatment and health indicator in industry service as well. Due to the sensitivity of the data involved, security and privacy measures are vital to the success of the WBANs [2].

Due to the difficulty for biometrics counterfeit, biometrics authentication has been proposed as a solution to improve security in the communication of such personal data [3]. One of the biometric traits which is attractive in health monitoring applications security is gait. Studies in medicine and psychology have shown that each individual has a distinctive walking style that allows his recognition. Unlike other biometrics traits such as voice, fingerprints, and facial recognition, gait is noninvasive and can be measured without subject intervention. This makes it more user-friendly especially in continuous identity re-verification [4].

Although the first gait recognition systems used video, the current trend is to use accelerometers included in wearables or portable smart devices [5]. In [6] a real-time gait recognition system using the wavelet transform was presented. The simulation results showed that the proposed method has reliable recognition accuracy both in the real-time and in the long-term cases. Machine learning algorithms were used in [7] to train the classifiers and authenticate the subjects. More specifically their work concentrates on methods of segmentation of the accelerometer data and compares between the fixed length and fixed cycle approach in which fixed length showed better results. Further research was conducted in [8] on the influence of walking speeds and surfaces on gait recognition. Different parameter settings in dynamic time warping were evaluated to optimize the cycle extraction process. Since most methods on accelerometer-based gait recognition suffer from cycle detection failures, [4] proposed a novel algorithm which uses a multiscale signature point extraction method, and has shown significant improvements.

accelerometer-based gait recognition systems have a lot of positive traits, however, they suffer from high energy consumption due to continuous accelerometer data sampling. Researcher in [9] tried to solve this problem by proposing a kinetic energy harvesting device and used its output voltage signal as the source of gait recognition. In [10] capacitive coupled human body communication was presented as a biometric authentication method instead. The method requires S-parameters over wide range of frequencies to be able to function. With the use of current available devices, [11–13] attempts to exploit propagation characteristics or wireless channel to obtain behavioral fingerprint and use it in authentication. They make use of the channel state information (CSI) of Wi-Fi signal to extract features that identify individuals by their intrinsic body movement during walking without attachments to the body. It requires a multiple antenna transmitter and receiver fixed in a certain environment.

In this work a received signal strength indicator (RSSI) based gait authentication method is proposed. Arm movement during walking has been chosen as the gait identification feature as the body mounted sensors on the arm wrists (smartwatches) are already popular. The method does not require hardware upgrades as it only relies on regular communication between body mounted sensors (e.g. smartwatch) and body mounted access node (e.g. smartphone). This makes the system mobile and not bounded to a specific location, contrary to Wi-Fi-based gait recognition systems. Unlike accelerometer-based gait recognition systems, it does not require sampling of sensor data, making it more energy efficient. Moreover, it does not require any additional packet transmission but instead, make use of the RSSI values available in regular communications.

The paper begins in Section II by discussing the radio features that are applicable in gait detection. In Section III, 4 different classification learners are presented for use in RSSI based gait authentication. Experimental data and performance analysis is presented in Section IV. Finally, the conclusion is given in Section V.

2 Gait Radio Features

The most common architecture of WBANs consist of body mounted sensors known as nodes, and an access node such as smartphone also mounted on the body, known as central coordinator as shown in Fig. 1 [14]. The nodes have sensors that measure various physiological conditions, or other types of data and transmit it wirelessly to the coordinator. The coordinator acts as an access point by collecting data from the nodes, and transmit them to the data center through an off-body node acting as a communication access point. It is in the radio channel between the nodes and the coordinator that the gait information is available and could be extracted, processed and used for authentication by the coordinator. If processing power is a

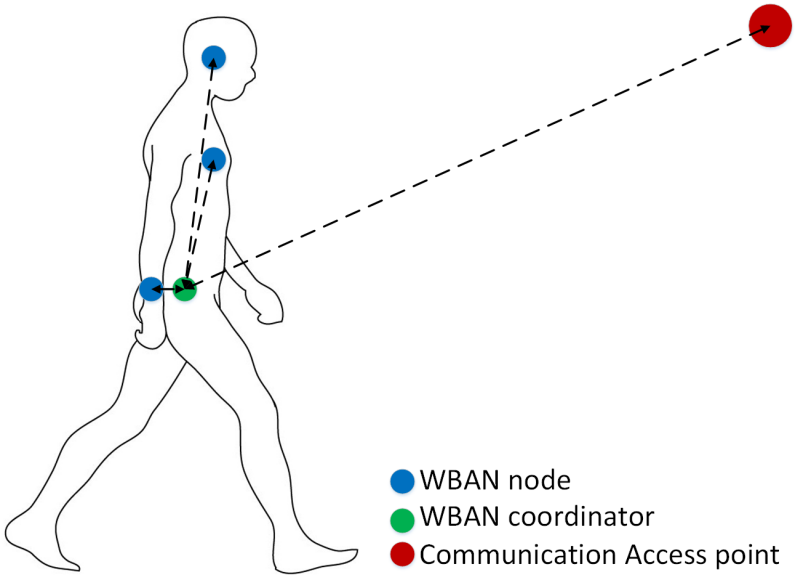

Fig. 1: Example of WBAN with 3 nodes and 1 coordinator. The off-body node act as communication access point.

concern at the coordinator, the raw gait information could simply be forwarded to the server together with the rest of the data, and the authentication process could be performed there. This kind of authentication will ensure that the data uploaded to the server are indeed from the intended subject and will prevent impersonation attacks. It could be used together with other authentication methods, to add another security layer for applications in which one-time validation of the user's identity is insufficient. Since it can be measured without subject intervention, it could be used as a continuous authentication method and set to trigger other security measures whenever it fails.

The gait information available in the radio channels can be extracted from the measurement of the power present in the received signal. This measurement is already being conducted by wireless radio transceivers and is indicated by their RSSI values [15]. This gives the RSSI method an edge over the accelerometer-based systems, which needs sampling of sensor data specifically for gait recognition purpose. The most commonly available accelerometers have been shown to consume current of more than 130μA [16] as shown in Fig 2, and that the sampling process consumes around 3 mW for low power processors [9] and 370 mW for smart phones [17]. The proposed method eliminates the sensor, and all the power consumption related to it by relying on measurement which are already

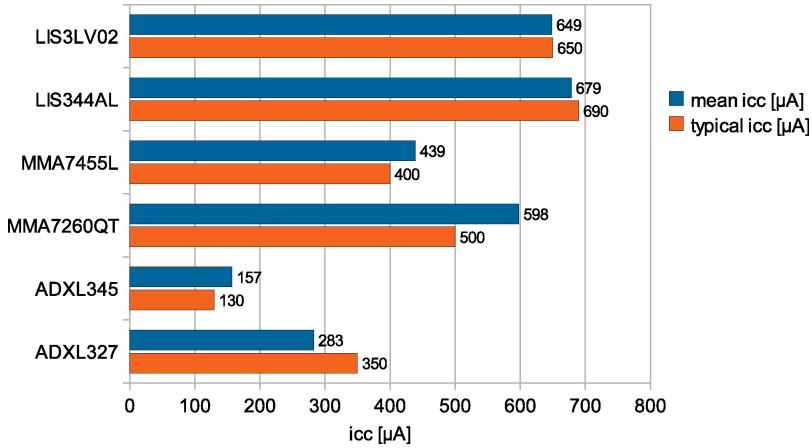

Fig. 2: Mean current consummation of common accelerometers connected to 3.3 V power supply together with typical values given in their respective data sheets [16].

conducted by transceivers and are available for processing. This means the power consumption on the sensor node (e.g., smartwatch) due to RSSI based method is zero. The RSSI values are used to obtain radio features such as variation of power received with time (time series), the measure of degree of time dependency (auto-correlation function), and how often does the signal crosses a certain threshold (level crossing rate). It is through these radio features that one subject can be differentiated from the other. The considered radio features are discussed in the following.

2.1 The Time Series

It has been shown that the power received in a WBANs is related to the dynamics involved with the specific activity of the subject . For the case of walking, the power received is periodic to the relative movement of the body parts where the nodes are attached to. The period of the signal tends to correspond to the period of the limb swinging, and the amplitude variation depends on the size of the limbs, distance from its rest position, and the amount of shadowing the body provide during walking [18]. This is normally different enough from one person to another to a point that it could be used for individual identification.

Fig. 3 shows the time series of the received signal power of 3 subjects during walking for the duration of 3 seconds. The transceivers were placed at the right wrist and the right side of the waist, and the received signal power was smoothed using a sliding window of length of 0.15 seconds. The time series of all 3 subjects are periodic with a period of around 1 second, consistent with the oscillatory move-

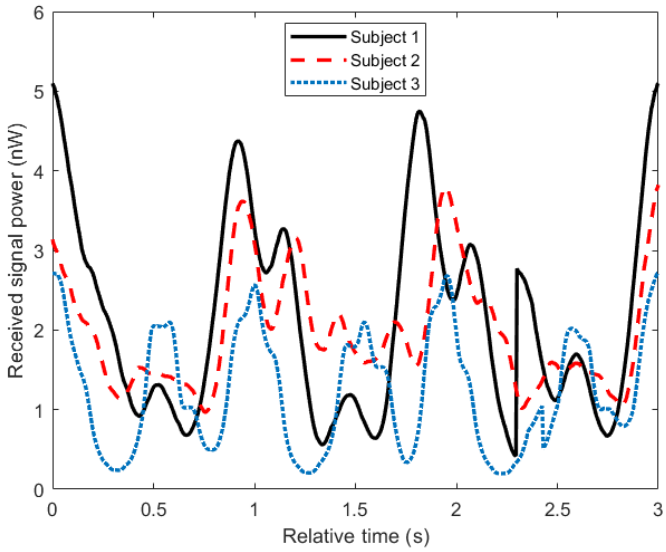

Fig. 3: Example of time series of the received signal power of WBANs of 3 different subjects during walking. The transmitter was attached to the waist, and the receiver was attached to the right wrist.

ment of the corresponding arms. However, the series also show that the received signal power is different between the subjects and hence, the overall patterns have enough features to distinguish them from one another. More discussions on the measurement campaign and the subjects involved are provided in Section IV.

2.2 The Auto-Correlation Function

The Auto-correlation function (ACF) is a measure of the degree of time dependency among the observations of signals. It is used to characterize the periodicity in a fading signal envelope. For real discrete sampled data $x(t)$, it can be calculated using [19, 20]:

$$r_{xx}(\tau) = \sum_{t=1}^{N-\tau} (x(t) - \mu)(x(t-\tau) - \mu) \tag{1}$$

where τ is the time delay, N is the length and μ is the mean of the sampled data. The normalized ACF can then be obtained by using (2) to give an output with a maximum value of 1 at $\tau = 0$

$$\rho_{xx}(\tau) = \frac{r_{xx}(\tau)}{r_{xx}(0)} \tag{2}$$

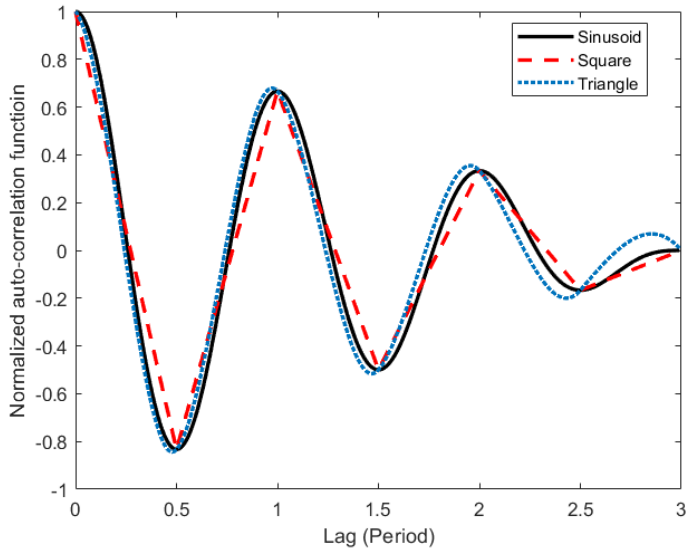

Fig. 4: Example of normalized ACF of periodic signals of length of 3 periods. The ACF of all the signals have peaks at $\tau = 1$ of $\frac{2}{3}$, and at $\tau = 2$ of $\frac{1}{3}$

For a perfect periodic signal, the normalized ACF oscillates with its period corresponding to the period of the signal. If the signal is limited to a specific number of periods (it does not go to infinity), the envelope of the normalized ACF tends to decay exponentially. Take for example the normalize ACF of periodic signal limited to 3 periods will have a peak of 1 at $\tau = 0$, a peak of $\frac{2}{3}$ at $\tau = 1$ period, and a peak of $\frac{1}{3}$ at $\tau = 2$ periods as shown in Fig. 4.2 for sinusoid, square, and triangle signals. These peaks values tend to decrease as the noise in the periodic signal increase and hence can be used as an indicator of change in activity. Take for example if a walking subject stops in the middle of sampling, the peak value at $\tau = 1$ period will be significantly smaller than the expected value and hence the change in activity could be detected.

In addition to that, since the received signal power is different from one subject to the other during walking, the normalized ACF has the potential of being different. Fig. 5 shows the normalized ACF of the signals shown in Fig. 3. The ACF of the 3 subjects show properties of a signal composed from a number of periodic signals, with the main envelope having a period of around 1s (0.92 s for Subject 1, 1.02 s for Subject 2, and 0.96 s for Subject 3), consistent with the oscillatory movement of the corresponding arms. However, the composition of these periodic signals are different from one subject to the other, making the overall pattern of the ACF

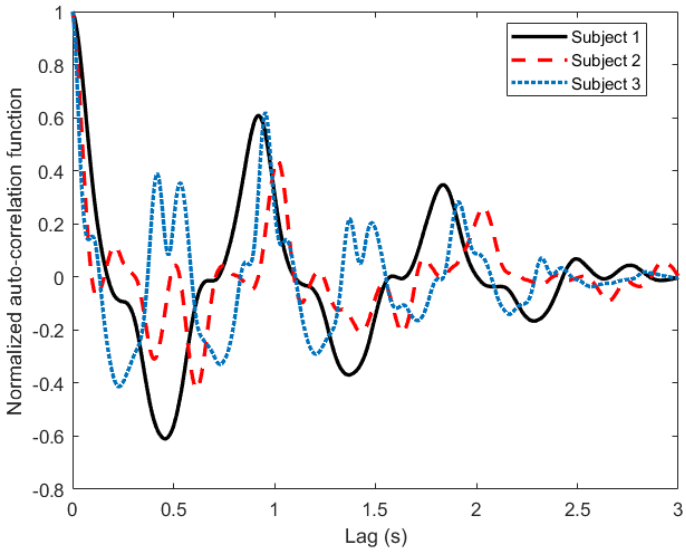

Fig. 5: The normalized ACF of the signals shown in Fig.3. The ACFs show properties of periodic signals with significantly different patterns.

significantly different and hence could be used in gait recognition.

2.3 The Level Crossing Rate

Another manner of quantifying periodic signals is using the level crossing rate (LCR), which is the measure of how often a signal crosses a certain threshold going in a positive direction [20]. LCR represent signals in such a way that the primary focus is on power levels and frequency of crossing them. It clearly shows the signal range, and emphasizes the location of the high-frequency component of the signal. Fig. 6 shows the LCR representation of the signals shown in Fig. 3. As expected the LCR of the 3 subjects are different due to the difference in the subjects' gait, and the size of their bodies. The LCR shows clearly the minimum and the maximum power level received by each subject. LCR could be too simple as a differentiating factor on its own, however, it could have good contribution as an additional feature.

3 Classification Learners

Four different classification learners were considered for distinguishing from the walking pattern of one person to the other based on extracted radio features discussed in Section II. The radio features are presented by a vector with a length L, taken from a period of 3 seconds. The vector length L, varies with the feature in

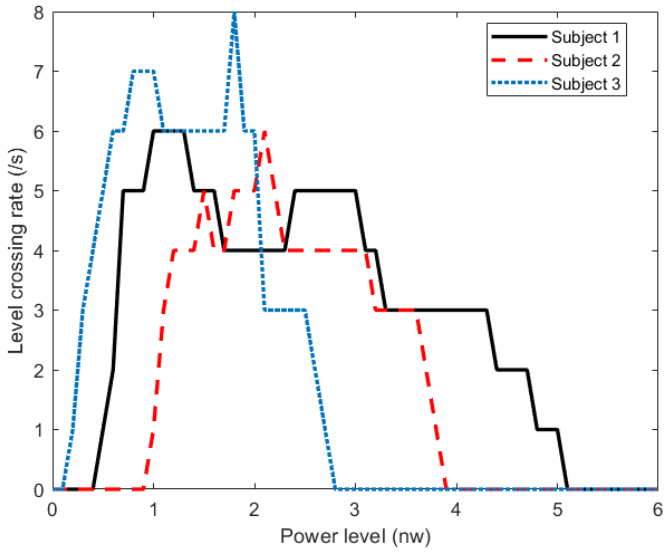

Fig. 6: LCR representation of signals shown in Fig. 3.

hand where for time series $L = 600$, for ACF $L = 300$, and for LCR $L = 60$. All the classification learners are implemented in MATLAB environment with a brief introduction of each following in this section.

3.1 Decision Trees

Decision tree learners comprise a series of logical decisions taken at decision nodes, in which each possible decision's choice results in a tree branch. The tree is terminated by the leaf nodes that denote the result of following a combination of decisions. Data that is to be classified begin at the root node, where it is passed through the various decisions in the tree according to the values of its features, until it reaches a leaf node, which assigns it a predicted class [21]. To identify which feature to split upon at the decision nodes, Gini's diversity index was used as a split criterion. For a data set S, Gini index G is defined as follows [22]:

$$G(S) = 1 - \sum_{i=0}^{C-1} \left(\frac{s_i}{S}\right)^2 \tag{3}$$

where C is the number of predefined classes, and s_i is the number of samples belonging to class c_i. The quality of a split on a feature into h subsets S_j is then

computed as the weighted sum of the Gini indices of the resulting subsets:

$$G_{split} = \sum_{j=0}^{h-1} \frac{n_j}{n} G(S_j) \tag{4}$$

where n_j is the number of samples in subset S_j after splitting, and n is the total number of samples in the given decision node. Thus, G_{split} is calculated for all possible features, and the feature with minimum value is selected as a split point. To limit the growth of the tree, so that the model does not get over-fitted to the training data, the maximum number of splits was set to 100. Detailed description of the decision tree classification learner is found in [21, 22].

3.2 Support Vector Machine

Support vector machine (SVM) is a type of machine learning algorithm in which the classification of the outputs depend on explicit generalization, obtained from analyses of the training data. In this algorithm, the training data items are put in a P-dimensional space, and classification is performed by finding the hyper-planes that differentiate the required number of classes very well. The obtained hyper-planes are then used in the classification of test data. The hyper-planes are obtained by maximizing functional margin which is the distances between the nearest data point and the hyper-plane. This can be achieved by [23]:

$$\min_{u,b} H(u) = \frac{||u||^2}{2} \text{ subject to } c_l(u^T p_l + b) \geq 1 \quad \text{for } l = 1, ..., P \tag{5}$$

where p_l is the training example, c_l represents the labels of the training examples, P is the total number of features to be compared, u is the weight vector and b is the bias of the optimal hyper-plane. The SVM can be extended to non-linear classification by the usage of kernel method to map the inputs into high-dimensional feature space. In this work, a quadratic kernel function was used in the application of SVM. See [23] for more details on the SVM classification learner.

3.3 K-Nearest Neighbors Classifier

k-nearest Neighbors (k-NN) algorithm is a type of machine learning algorithm in which the classification of the output does not depend on explicit generalization, but instead compares new problem instances with instances seen in training. More specifically, it compares the new problem with k nearest neighbors, and assign it to the class most common among them [24]. It is among the simplest of all machine learning algorithms especially in its simplest form where $k = 1$. The

nearest neighbors are identified by calculating the Euclidean distance d between a training data p_l and the test data q_l as

$$d = \sqrt{\sum_{l=1}^{l=P} (p_l - q_l)^2} \tag{6}$$

Since (6) is dependent on how features are measured, the features values were re-scaled so that each one contributes relatively equally to the distance formula [25]. The algorithm was implemented with $k = 10$, in which weight v were assigned to the contributions of the neighbors using,

$$v = \frac{1}{d^2} \tag{7}$$

so that the nearer neighbors contribute more to the decision. A detailed description of the k-NN classification learner is found in [24, 25].

3.4 Artificial Neural Network

An Artificial Neural Network (ANN) models the relationship between a set of input data and the output class by the use of network of nodes known as artificial neurons to solve learning problems. Each node takes M inputs of r_m, weight them with w_m according to their importance, and then the summation is passed on according to an activation function $f(g)$. Mathematically the processes can be represented by the formula [21]:

$$y(x) = f\left(\sum_{m=1}^{M} w_m r_m\right) \tag{8}$$

with a sigmoid activation function defined as:

$$f(g) = \frac{1}{1 + e^{-g}} \tag{9}$$

The nodes were grouped into 2 layers, hidden layer, and output layer. The hidden layer processes the input data prior to reaching the output layer which does further processing and generates a final prediction. The number of nodes in the output layer is predetermined by the number of classes in the outcome, however, in the hidden layer, there is no reliable rule to determine the number of nodes needed. In this work, 25 nodes were used in the hidden layer as the addition of more nodes in this layer did not give significant improvement in performance. The weights w_m were adjusted in the training process using scaled conjugate gradient back-propagation algorithm. In this algorithm, the gradient of activation function is used to determine which weight should be adjusted in order to reduce the error between the actual and predicted class. See [21, 25] for more details on the ANN classification learner.

Table 1: Volunteers Details

#	Gender	Age	Height (cm)	Weight (kg)
1	Female	35	168	63
2	Female	23	174	69
3	Female	25	159	53
4	Female	29	171	66
5	Female	24	167	61
6	Male	29	180	83
7	Male	35	185	75
8	Male	25	178	67
9	Male	23	173	80
10	Male	27	168	65
11	Male	28	183	105
12	Male	26	165	66
13	Male	30	160	53
14	Male	21	175	80
15	Male	30	181	75
16	Male	26	175	83
17	Male	26	167	79
18	Male	49	178	75
19	Male	40	170	78
20	Female	60	170	75

4 Experimental Data and Analysis

4.1 Measurement Data

The experiments conducted in this study are preliminary towards the validation of the proposed method. The dataset used to evaluate the RSSI-based gait recognition consist of 20 healthy subjects (14 males and 6 females), with different age, height, and weight detailed in Table 1. During the data collection phase, 3 transceivers were attached on the participants, a transmitter on the right side of the waist representing devices such as smartphones, and a receiver on the wrist of the right and left arms representing devices such as smartwatches. The transceivers were attached in such a way that the antennas were vertically polarized. The participants were asked to walk at their normal speed in both outdoor and indoor environments in order to capture the influence of different environment. The outdoor environment was a parking lot with an asphalt surface, while the indoor environment was a cafeteria with a tiled surface. Each participant walked for approximately 4 minutes

Fig. 7: Wearable radio transceiver. The device is approximately 50 mm x 20 mm x 20 mm.

outdoors followed by 4 minutes indoors to include natural gait changes over time and environments. The experiments were limited to single trial per subject, with no donning/doffing of the transceivers. The transceivers (see Fig. 7) were made using programmable radio CC2500 from Texas Instruments [26]. The transmitter was set to transmit a packet every 5 ms with constant transmission power of 1 dBm at the 2.425 GHz carrier frequency. The receiver was used to store the packet number together with RSSI on its MicroSD memory card. The data were later exported from the memory card to a computer running MATLAB software for analysis.

In MATLAB, the collected data was split into segments of 3 seconds giving us a total of 150 segments from each subject. In each segment, 3 radio channel features (time series, ACF, and LCR) discussed in Section II were extracted. The radio features were later used with classification learners discussed in Section III for testing the performance of the RSSI-based gait authentication system. For the case of time series, the signal was shifted on time axis so that all the segments have their peaks at $t = 0$ as in Fig 3. Whenever ACF was used as a radio feature, an additional process of eliminating segments with periodicity noise was used. The process was set to eliminate any segment in which its ACF does not have a peak greater than 0.3 at $\tau = 1$ period.

4.2 Performance Metric Index

A reliable gait authentication algorithm has to make a decision whether the gait measured is of the genuine user or an imposter. The following 3 success criteria could be used to measure its performance [9].

- **True positive rate (TPR)**: Also know as sensitivity, is the probability that the authentication system correctly accepts the access request from the genuine users. If TP and FN represents the number of times the genuine user's access request is accepted and rejected respectively, then TPR can be calculated as follows

$$\text{TPR} = \frac{\text{TP}}{\text{TP} + \text{FN}} \times 100 \tag{10}$$

- **True negative rate (TNR)**: Also known as specificity, is the probability that the authentication system correctly rejects the access request from an imposter. If TN and FP represents the number of times an imposter's access request is rejected and accepted respectively, then TNR can be calculated as follows

$$\text{TNR} = \frac{\text{TN}}{\text{TN} + \text{FP}} \times 100 \tag{11}$$

- **Recognition accuracy**: It represents the percentage of correct classifications which is simply the number of true classifications (acceptance from genuine users and rejection from imposter) over the total number of tests. It can be calculated as follows

$$\text{Accuracy} = \frac{\text{TP} + \text{TN}}{\text{TP} + \text{FN} + \text{TN} + \text{FP}} \times 100 \tag{12}$$

In general, the system should minimize the FPs and FNs, however, greater emphasis could be set on minimizing FPs so that the imposter's access request is rejected all the times.

4.3 Results and Discussions

The objective of the analysis is to investigate which radio channel feature and which classification learner are suitable for RSSI-based gait authentication system. For each radio channel feature obtained from the channel between the right wrist and the waist, the performance of each classification learner in terms of TPR, TNR, and accuracy is evaluated independently, and in combination with each other. The same analysis were repeated when additional radio features were extracted from the channel between the left wrist and the waist, and used together with those from the channel between the right wrist and the waist. From our experimental data, 150 of 3-second segments were extracted from each user, giving us a total of 2550 segments for testing. To protect the algorithm against over-fitting, a 10 folds cross-validation method was employed. In this method, the data set is partitioned into 10 fold, in which 9 are used for training and 1 is used for validation purposes. The training and testing process is repeated 10 times so that each of the 10 partition

Table 2: Performance Results Using Data From One Radio Channel: Right Wrist to Waist

Radio feature	Performance metric	Decision tree	Quadratic SVM	Weighted k-NN	ANN
TS	TPR	67%	86%	83%	68%
	TNR	67%	88%	85%	71%
	Accuracy	70%	88%	85%	74%
ACF	TPR	63%	81%	72%	85%
	TNR	64%	84%	77%	86%
	Accuracy	66%	83%	75%	86%
LCR	TPR	57%	70%	64%	73%
	TNR	56%	72%	67%	74%
	Accuracy	61%	74%	67%	76%
TS+ACF	TPR	77%	92%	87%	90%
	TNR	76%	93%	89%	91%
	Accuracy	78%	93%	89%	91%
TS+LCR	TPR	71%	89%	86%	85%
	TNR	71%	89%	88%	85%
	Accuracy	73%	89%	88%	87%
ACF+LCR	TPR	72%	88%	81%	93%
	TNR	72%	90%	85%	94%
	Accuracy	73%	90%	84%	94%
TS+ACF+LCR	TPR	76%	92%	89%	94%
	TNR	76%	93%	91%	95%
	Accuracy	78%	93%	91%	95%

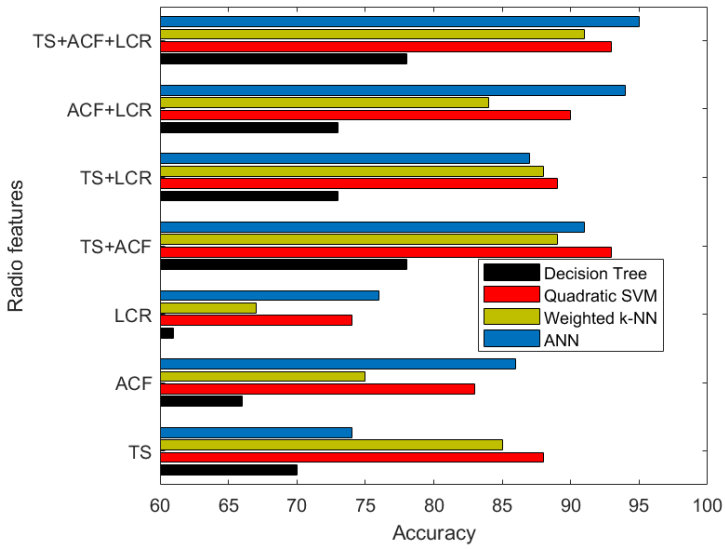

Fig. 8: Performance results using data from one radio channel: Right wrist to waist.

is used exactly once as the testing data. The results are then averaged over the 10 validations to yield the average performance.

Table 2 and Fig. 8 show the performance of the different classifiers using time series (TS), ACF, LCR, and different combination of those features, obtained from radio channel between the right wrist and the waist. For all the radio features, the worst performance is shown by decision tree algorithm, with maximum accuracy of 78% obtained when all the radio features are used together. When only a single radio feature is used, LCR has shown to give the worst results, and TS the best results for all classification learners except ANN, in which TS gave the worst results and ACF gave the best results. When the radio features are used in pairs, ACF+LCR pair gives the best results when ANN is used, while TS+ACF pair gives the best results for the remaining classification learners. The combination of all 3 features archives an accuracy of 95% using ANN as the classification learner. It is also interesting to notice that, moving from the use of a single radio feature (TS with SVM as classification learner) to radio features in pair (ACF+LCR pair with ANN as a classification learner) improves accuracy by 6%, while from the pair to the combination of all 3 radio features (TS+ACF+LCR with ANN as the classification learner) the improvement is only 1%.

When additional radio features are extracted from the channel between the left wrist and the waist, and are used together with those from the channel between

Table 3: Performance Results Using Data From Two Radio Channels: Right Wrist to Waist, and Left Wrist to Waist

Radio feature	Performance metric	Decision tree	Quadratic SVM	Weighted k-NN	ANN
TS	TPR	69%	88%	81%	81%
	TNR	69%	89%	83%	83%
	Accuracy	73%	89%	84%	84%
ACF	TPR	66%	82%	75%	90%
	TNR	66%	85%	82%	91%
	Accuracy	69%	85%	79%	91%
LCR	TPR	62%	78%	64%	81%
	TNR	63%	81%	69%	81%
	Accuracy	66%	81%	69%	83%
TS+ACF	TPR	78%	93%	90%	95%
	TNR	78%	94%	92%	96%
	Accuracy	81%	94%	92%	96%
TS+LCR	TPR	75%	89%	84%	93%
	TNR	75%	90%	87%	93%
	Accuracy	77%	91%	86%	94%
ACF+LCR	TPR	72%	88%	83%	96%
	TNR	72%	90%	86%	96%
	Accuracy	74%	90%	85%	97%
TS+ACF+LCR	TPR	79%	94%	90%	98%
	TNR	79%	94%	92%	98%
	Accuracy	82%	95%	92%	98%

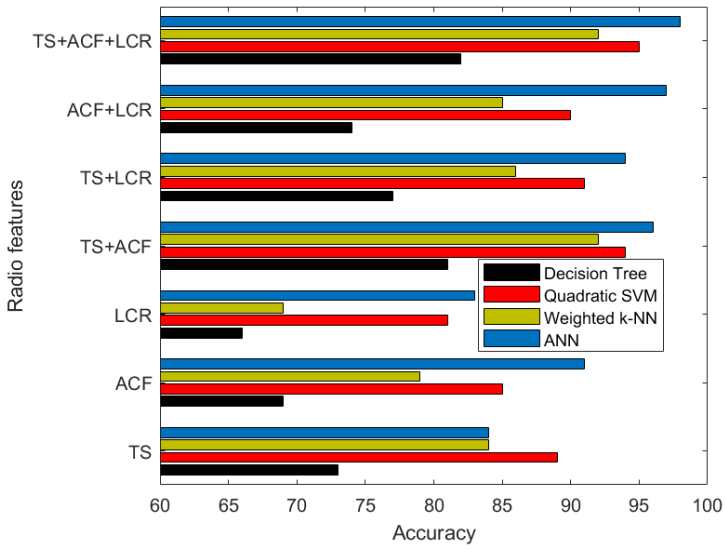

Fig. 9: Performance results using data from two radio channels: Right wrist to waist, and left wrist to waist.

the right wrist and the waist, we notice improvement in all performance metric (see Table 3 and Fig. 9), with the most improvement in accuracy of 7% achieved when LCR is used as a single radio feature, and the least of 1% achieved when TS is used as a single radio feature. We also notice a similar trend in which moving from the use of a single radio feature (ACF with ANN as classification learner) to a pair of features (ACF+LCR pair with ANN as classification learner) accuracy improves by 6%, while from the pair to the combination of all 3 radio features (TS+ACF+LCR with ANN as classification learner) only 1% of improvement is achieved. Here the accuracy reaches 98%.

Based on the above results, the use of ACF+LCR pair, extracted from a single radio channel, with ANN as the classification learner is suggested for practical implementations. This is due to the level of accuracy achieved (94%), despite the number of predictors being 67% less than those used to achieve the best performance. Its confusion matrix is shown in Fig. 10 with positive predictive values in green, and the false discovery rates highlighted in red.

5 Conclusion

In this study, an RSSI-based gait authentication algorithm was proposed. The system is applicable when unobtrusive, natural method of authentication, with low

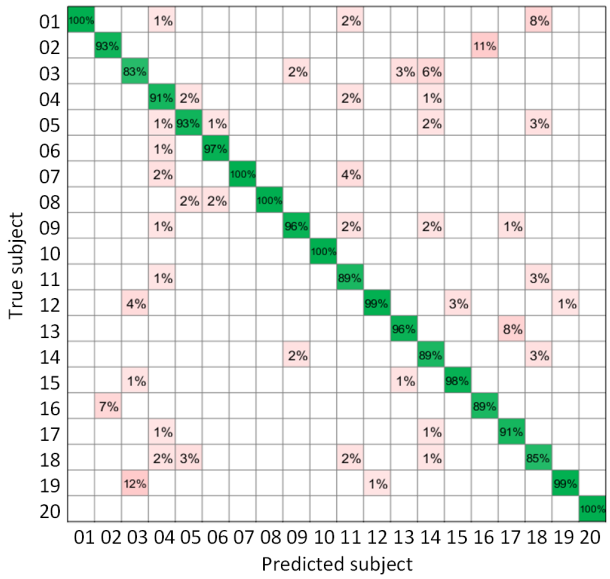

Fig. 10: Confusion matrix showing positive predictive values in green, and false discovery rates in red. The radio features used were ACF+LCR with ANN as the classification learner.

hardware cost and power demands is needed. The system was based on extracting features from the radio channels between the wrists and the waist, through RSSI present in all wireless devices. The features extracted were time series, ACF, and LCR from 20 subjects walking in outdoor and indoor environment. Four different classification learners namely decision tree, SVM, k-NN, and ANN were used for testing of the algorithm.

The overall best performance was achieved using all the radio features together (TS+ACF+LCR), extracted from 2 radio channels, right wrist to waist, and left wrist to waist, and using ANN as the classification learner. All the performance metric namely TPR, TNR, and accuracy were above 97%, see Table 3. In a more practical approach, where the radio features were extracted from just 1 radio channel (right wrist to waist), the best performance achieved was above 95% for all performance metric, while using all the radio features, with ANN as the classification learner. This suggests that RSSI-based authentication system could be based on just 2 devices, (for example a smartwatch and a smartphone) especially when the system is used as a complementary to other security features.

In general the RSSI-based authentication method, using a pair of ACF+LCR extracted from a single radio channel, with ANN as the classification learner, achieved

a good level of accuracy (94%), with comparatively small number of predictors (67% less than the best performer), and hence has a good potential for practical implementation.

References

[1] R. Cavallari, F. Martelli, R. Rosini, C. Buratti, and R. Verdone, "A survey on wireless body area networks: Technologies and design challenges," *IEEE Communications Surveys & Tutorials*, vol. 16, no. 3, pp. 1635–1657, 2014.

[2] N. Zhao, A. Ren, M. U. Rehman, Z. Zhang, X. Yang, and F. Hu, "Biometric behavior authentication exploiting propagation characteristics of wireless channel," *IEEE Access*, vol. 4, pp. 4789–4796, 2016.

[3] J. Andreu-Perez, D. R. Leff, H. M. Ip, and G.-Z. Yang, "From wearable sensors to smart implants—Toward pervasive and personalized healthcare," *IEEE Transactions on Biomedical Engineering*, vol. 62, no. 12, pp. 2750–2762, 2015.

[4] Y. Zhang, G. Pan, K. Jia, M. Lu, Y. Wang, and Z. Wu, "Accelerometer-based gait recognition by sparse representation of signature points with clusters," *IEEE Transactions on Cybernetics*, vol. 45, no. 9, pp. 1864–1875, 2015.

[5] R. Ferrero, F. Gandino, B. Montrucchio, M. Rebaudengo, A. Velasco, and I. Benkhelifa, "On gait recognition with smartphone accelerometer," in *Proceedings of 4th Mediterranean Conference on Embedded Computing*, 2015, pp. 368–373.

[6] J.-H. Wang, J.-J. Ding, Y. Chen, and H.-H. Chen, "Real time accelerometer-based gait recognition using adaptive windowed wavelet transforms," in *Proceedings of IEEE Asia Pacific Conference on Circuits and Systems*, 2012, pp. 591–594.

[7] C. Nickel and C. Busch, "Does a cycle-based segmentation improve accelerometer-based biometric gait recognition?" in *Proceedings of 11th In-*

ternational Conference on Information Science, Signal Processing and their Applications, 2012, pp. 746–751.

[8] M. Muaaz and C. Nickel, "Influence of different walking speeds and surfaces on accelerometer-based biometric gait recognition," in *Proceedings of 35th International Conference on Telecommunications and Signal Processing*, 2012, pp. 508–512.

[9] W. Xu, G. Lan, Q. Lin, S. Khalifa, N. Bergmann, M. Hassan, and W. Hu, "KEH-Gait: Towards a mobile healthcare user authentication system by kinetic energy harvesting," in *Proceedings of Network and Distributed System Security Syposium*, 2017.

[10] Z. Nie, Y. Liu, C. Duan, Z. Ruan, J. Li, and L. Wang, "Wearable biometric authentication based on human body communication," in *Proceedings of IEEE 12th International Conference on Wearable and Implantable Body Sensor Networks*, 2015, pp. 1–5.

[11] Y. Li and T. Zhu, "Using Wi-Fi signals to characterize human gait for identification and activity monitoring," in *Proceedings of IEEE First International Conference on Connected Health: Applications, Systems and Engineering Technologies*, 2016, pp. 238–247.

[12] Q. Xu, Y. Chen, B. Wang, and K. R. Liu, "Radio biometrics: Human recognition through a wall," *IEEE Transactions on Information Forensics and Security*, vol. 12, no. 5, pp. 1141–1155, 2017.

[13] C. Shi, J. Liu, H. Liu, and Y. Chen, "Smart user authentication through actuation of daily activities leveraging WiFi-enabled IoT," in *Proceedings of 18th ACM International Symposium on Mobile Ad Hoc Networking and Computing*, 2017, p. 5.

[14] S. Ullah, H. Higgins, B. Braem, B. Latre, C. Blondia, I. Moerman, S. Saleem, Z. Rahman, and K. S. Kwak, "A comprehensive survey of wireless body area networks," *Journal of Medical Systems*, vol. 36, no. 3, pp. 1065–1094, 2012.

[15] S. A. Salehi, M. Razzaque, I. Tomeo-Reyes, and N. Hussain, "IEEE 802.15.6 standard in wireless body area networks from a healthcare point of view," in *Proceedings of 22nd Asia-Pacific Conference on Communications*, 2016, pp. 523–528.

[16] F. Büsching, U. Kulau, M. Gietzelt, and L. Wolf, "Comparison and validation of capacitive accelerometers for health care applications," *Computer Methods and Programs in Biomedicine*, vol. 106, no. 2, pp. 79–88, 2012.

[17] B. Priyantha, D. Lymberopoulos, and J. Liu, "Littlerock: Enabling energy-efficient continuous sensing on mobile phones," *IEEE Pervasive Computing*, vol. 10, no. 2, pp. 12–15, 2011.

[18] S. Van Roy, F. Quitin, L. Liu, C. Oestges, F. Horlin, J.-M. Dricot, and P. De Doncker, "Dynamic channel modeling for multi-sensor body area networks," *IEEE Transactions on Antennas and Propagation*, vol. 61, no. 4, pp. 2200–2208, 2013.

[19] L. Hanlen, V. Chaganti, B. Gilbert, D. Rodda, T. Lamahewa, and D. Smith, "Open-source testbed for body area networks: 200 sample/sec, 12 hrs continuous measurement," in *Proceedings of IEEE 21st International Symposium on Personal, Indoor and Mobile Radio Communications Workshops*, 2010, pp. 66–71.

[20] T. S. Rappaport *et al.*, *Wireless Communications: Principles and Practice*. Upper Saddle River, NJ, USA: Prentice Hall, 1996, vol. 2.

[21] B. Lantz, *Machine Learning with R*. Birmingham, UK: Packt Publishing Ltd, 2015.

[22] M. Kantardzic, *Data Mining: Concepts, Models, Methods, and Algorithms*. Hoboken, NJ, USA: John Wiley & Sons, 2011.

[23] N. Cristianini and J. Shawe-Taylor, *An Introduction to Support Vector Machines and Other Kernel-based Learning Methods*. Cambridge, UK: Cambridge University Press, 2000.

[24] N. S. Altman, "An introduction to kernel and nearest-neighbor nonparametric regression," *The American Statistician*, vol. 46, no. 3, pp. 175–185, 1992.

[25] M. N. Murty and V. S. Devi, *Pattern Recognition: An Algorithmic Approach*. Berlin, Germany: Springer Science & Business Media, 2011.

[26] T. Instruments, "CC2500 low-cost low-power 2.4 GHz RF transceiver; datasheet," 2010.

Paper VI

M. Mohamed, W. Joseph, G. Vermeeren, E. Tanghe, and M. Cheffena, "Characterization of dynamic wireless body area network channels during walking," *Submitted to EURASIP Journal on Wireless Communications and Networking,* 2018.

Is not included due to copyright